Stochastic Surface Growth

Dissertation der Fakultät für Physik

der Ludwig-Maximilians-Universität

vorgelegt von

Michael Prähofer

aus München

München 2003

Tag der mündlichen Prüfung: 10. Juli 2003

Erstgutachter:	Prof. Dr. Herbert Spohn
Zweitgutachter:	Prof. Dr. Wilhelm Zwerger

Zusammenfassung

Wachstumsphänomene stellen ein wichtiges Teilgebiet in der statistischen Mechanik des Nichtgleichgewichts dar. Einerseits sind sie überall in der Natur anzutreffen, andererseits stellt ihr theoretisches Verständnis eine Herausforderung an die Methoden der theoretischen Physik dar. Typischerweise führen Wachstumsprozesse zu statistisch skaleninvarianten Strukturen. Für nichtlokales Wachstum bilden sich selbstähnliche Cluster in Form von Fraktalen, man denke an Schneeflocken oder Eisblumen. Oberflächenwachstum, bei dem das Wachstum ausschließlich lokal bestimmt ist, führt dagegen zur Bildung eines kompakten Objekts, das durch eine wohldefinierte Oberfläche von seiner Umgebung getrennt ist, wie zum Beispiel bei Kristallwachstum aus einer Lösung. Die Komplexität liegt in diesem Fall in der selbstaffinen Rauhigkeit der Oberfläche, die durch Fluktuationen bei der zufälligen Anlagerung bewirkt wird.

Für solches stochastisches Oberflächenwachstum schlugen Kardar, Parisi und Zhang (KPZ) im Jahre 1986 eine Kontinuumstheorie vor, die durch die KPZ-Gleichung, eine nichtlineare stochastische partielle Differentialgleichung definiert wird. Sie ist die wohl einfachstmögliche Bewegungsgleichung für die Dynamik einer Grenzfläche, die alle wesentlichen Zutaten für nichttriviales Wachstum beinhaltet, nämlich Irreversibilität, Nichtlinearität, Stochastizität und Lokalität. Wegen ihrer grundlegenden Bedeutung für die Physik des Nichtgleichgewichts war und ist die KPZ-Theorie Gegenstand intensiver Forschung mittels Simulationen, feldtheoretischer und anderer, überwiegend approximativer Methoden.

In dieser Arbeit wird ein besonders einfaches halbdiskretes Modell, das polynuclear growth (PNG)-Modell, betrachtet, das in der KPZ-Universalitätsklasse liegt. Daher ergeben alle im Skalenlimes für dieses Modell gewonnenen Ergebnisse direkte Vorhersagen für die entsprechenden Größen in der KPZ-Theorie und somit für alle Wachstumsmodelle in der gleichen Universalitätsklasse. Für Wachstum auf einem eindimensionalen Substrat ist das PNG-Modell exakt lösbar. Durch Umformulierung zu einem last-passage-Perkolationsproblem werden die von der $(1 + 1)$-dimensionalen KPZ-Theorie vorhergesagten Skalenexponenten rigoros hergeleitet und zum ersten mal Grenzverteilungen der Oberflächenfluktuationen für verschiedene Wachstumsgeometrien bestimmt. Darüber hinaus wird die dynamische KPZ-Zweipunktfunktion durch die Lösung des Riemann-Hilbert Problems für die Painlevé-II-Gleichung ausgedrückt und mit nicht unerheblichem Aufwand numerisch bestimmt.

Durch die Erweiterung zu einem Multi-layer-Modell kann die Wahrscheinlichkeitsverteilung zu einem festen Zeitpunkt durch eine Theorie freier Fermionen auf einem eindimensionalen Gitter in euklidischer Zeit beschrieben werden. In dieser Formulierung ist der Kontinuumslimes durchführbar. Die Fluktuationen bei Wachstum mit mittlerer Krümmung werden im Skalenlimes durch den hierzu eingeführten Airy-Prozess [102] beschrieben, der grob gesagt der Trajektorie des letzten Teilchens in Dysons Version sich nicht überschneidender Brownscher Bewegungen entspricht.

Eng verwandt mit dem Multi-layer-PNG-Modell ist das Gates-Westcott-Modell einer relativ zu einer Hochsymmetrie-Ebene leicht angeschrägten wachsenden Kristalloberfläche. Die Vorhersagen der zugehörigen anisotropen KPZ-Theorie werden durch eine exakte Lösung auch dieses Modells bestätigt. Schließlich werden noch Monte-Carlo-Simulationen für das PNG-Modell in höheren Dimensionen präsentiert.

Abstract

Growth phenomena constitute an important field in nonequilibrium statistical mechanics. On the one hand, they are ubiquitous in nature, on the other hand, their theoretical understanding poses a challenging problem for the methods of theoretical physics. Typically, growth processes lead to statistically scale invariant structures. For nonlocal growth, self-similar clusters are generated in the form of fractals, as for example snowflakes or patterns on a frosted window. In contrast, surface growth with strictly local rules leads to the formation of a compact body separated by a well-defined surface from its surrounding. In this case the complexity lies in the roughness of the surface generated by the fluctuations of the random attachment.

For this type of surface growth, in 1986 Kardar, Parisi, and Zhang (KPZ) proposed a continuum theory, which is defined by the KPZ equation, a nonlinear stochastic partial differential equation. It is arguably the simplest possible equation of motion for the dynamics of an interface, which comprises all the ingredients for nontrivial growth: irreversibility, nonlinearity, stochasticity, and locality. Because of its fundamental importance for nonequilibrium physics the KPZ theory has been and still is the subject of intensive research by means of simulations, field theoretic and other, predominantly approximative methods.

In this work an especially simple semi-discrete model, the polynuclear growth (PNG) model, is considered, which lies in the KPZ universality class. Therefore all results for this model obtained in the scaling limit provide direct predictions for the corresponding quantities in KPZ theory and thereby for all models belonging to the same universality class. For growth on a one-dimensional substrate the PNG model is exactly solvable. Through reformulation as a last-passage percolation problem the scaling exponents, predicted by $(1 + 1)$-dimensional KPZ theory are rigorously derived and for the first time limiting distributions of the surface fluctuations are determined for different growth geometries. Moreover the dynamical KPZ two-point function is expressed by means of the solution to the Riemann-Hilbert problem for the Painlevé II equation and solved numerically, which requires some effort.

By means of the extension to a multi-layer model the probability distribution at a given point in time is described by a theory of free fermions on a one-dimensional lattice in Euclidean time. In this formulation the continuum limit is feasible. The fluctuations for curved growth are described by the Airy process [102], introduced for this purpose. Roughly speaking the Airy process corresponds to the trajectory of the last particle in Dyson's Brownian motion.

Closely related to the multi-layer PNG model is the Gates-Westcott model of a vicinal growing surface. The predictions of the corresponding anisotropic KPZ theory are confirmed by an exact solution of the model. Finally Monte-Carlo simulations of the PNG model in higher dimensions are presented.

CONTENTS

CHAPTER 1

Introduction

Matter in its solid state has been formed originally always by some sort of growth process. Therefore the theoretical understanding of growth phenomena has at all times been a challenging problem. In the framework of statistical mechanics one tries to discover and explain macroscopic or mesoscopic laws from systems which have a simple microscopic description. Nonequilibrium statistical mechanics deals with the properties of nonreversible processes where thermodynamical notions like entropy and temperature are not directly available. One of the most common types of processes which are out of thermodynamical equilibrium are growth processes.

Patterns originating from growth processes have been always fascinating to curious observers. The faceted shape of naturally formed crystals, the ramified structure of snowflakes and other frost patterns, the rough surface of amorphously growing solids, raise the question for a deeper understanding of the underlying mechanisms which could explain structural similarities and differences of the results of growth processes. Since the advent of semiconductor technology about half a century ago it has become more and more important to be able to quantitatively control the growth of crystals. Modern techniques like molecular beam epitaxy allow to engineer solid state devices with a precision ranging up to single atomic layers. On the other hand surface structures can be probed by scanning tunneling or atomic force microscopy with a resolution distinguishing individual atoms or molecules, which allows for testing theoretical predictions with spectacular precision.

Apart from the eminent technological relevance growth phenomena are of considerable fundamental interest, since they provide examples for the emergence of complex structures out of interacting simple agents. A very powerful concept which originally was developed in the context of equilibrium statistical mechanics is scale invariance. At the critical point of a second order phase transition an infinite system has no distinguished length scale. Therefore the system looks statistically the same on every length scale. Correlation functions have to decay as a power law, and the corresponding scaling exponents are characteristic for the system in question. Microscopic models always have some sort of short distance cut-off. Scale invariance thus can hold only in the limit of arbitrary large scales. The phenomenon that the large scale limit does not depend on the details of the

underlying model but only on qualitative properties like conservation laws and symmetries is called universality.

A very spectacular realization of scale invariance is encountered in fractal geometry. Random fractals show scale invariance in the form of statistical self-similarity characterized by the fractal dimension. Another instance of scale invariance is self-affinity, where one has to rescale the axes of the observation frame differently. The simplest example for scale invariance is Brownian motion. The image of a d-dimensional Brownian path is perfectly self-similar, whereas the graph of a Brownian motion as a whole is only self-affine. Upon rescaling space by a factor ℓ, time has to be rescaled by ℓ^2 in order to recover the same law of Brownian motion characterized by its variance. Universality expresses itself in this context by the simple fact that any discrete random walk model with weakly dependent increments of finite variance converges to Brownian motion in the large scale limit.

It is remarkable that there are not so many mechanisms known which generically produce scale invariance of nonequilibrium systems. Among these are clusters created by Brownian motion, like the outer boundary of a planar Brownian path and related processes like Schramm-Loewner evolutions in two dimensions [128]. More directly related to physics is nonlocal growth, where the driving force is a Laplacian field, as for diffusion limited aggregation (DLA) [129] or front propagation in Hele-Shaw cells [109]. The resulting structures are statistically self-similar objects with characteristic fractal dimensions. Slowly driven noisy systems which exhibit self-organized criticality [15] typically produce avalanche-like events, which look similar on every length scale. Finally local surface growth is characterized by a well-defined interface between the growing cluster and its environment. The attachment of new material takes place according to rules depending only on the local surface configuration. In this case the growing cluster is not fractal. It acquires a definite macroscopic shape. The randomness of the growth process manifests itself in the fluctuations around the mean shape. The dynamical fluctuations lead to self-affine surface roughness.

1.1 KPZ theory

There are numerous books about growth phenomena and scale invariance in general [43, 126, 16, 88]. In this thesis we focus on stochastic surface growth which is dominated by local dynamical rules. In 1986 Kardar, Parisi, and Zhang proposed a continuum description of stochastic surface growth, the famous KPZ equation [70]. Together with its equivalent formulations as stochastic Burgers equation and as directed polymers in random media, it is probably the most extensively studied theory of nonequilibrium physics. All the above mentioned books devote a consid-

erable part to KPZ theory. In addition a number of review articles have appeared over the time which give thorough accounts of the KPZ theory [78, 87, 59, 75, 80].

The $(d+1)$-dimensional KPZ equation describes the stochastic dynamics of an interface parameterized by a height function $h(x,t)$ relative to a d-dimensional substrate, $x \in \mathbb{R}^d$, which is driven by some noise $\eta(x,t)$ random in space and time,

$$\partial_t h(x,t) = v_0 + \nu\Delta h(x,t) + \tfrac{1}{2}\lambda\big(\nabla h(x,r)\big)^2 + \eta(x,t). \tag{1.1}$$

This equation is believed to capture the essential ingredients of stochastic surface growth, irreversibility, nonlinearity, stochasticity, and locality, which lead to the phenomenon of kinetically enhanced surface roughness.

Without the noise term $\eta(x,t)$ (1.1) describes deterministic growth of an interface. Hills grow upward if $v_0 > 0$ and extend laterally for $\lambda > 0$. v_0 can be absorbed by using a co-moving frame, but $\lambda \neq 0$ generates an intrinsic nonlinearity, which can not be removed by any simple transformation. The Laplace term represents surface tension which prevents the formation of cusps in the valleys. The noise term mimics the stochastic nature of the growth process. If $\eta(x,t)$ is chosen as white noise in space and time the equation has no intrinsic length scale and produces scale invariant fluctuations of its solutions. Without the nonlinear term, if $\lambda = 0$, (1.1) becomes a linear stochastic partial differential equation, known as the Edwards-Wilkinson equation [42]. In this case, since white noise has a Gaussian distribution, the solutions to the linear equation are Gaussian, too, with a simple covariance matrix. The fluctuations show scale invariance. Since they are Gaussian the corresponding scaling exponents are easily extracted from the covariance matrix. The associated field theory is a free massless scalar field [93, 92], which is well understood. In particular with the nonlinearity vanishing, the equation is reversible and therefore can be interpreted as a model of equilibrium surface dynamics.

Kardar, Parisi, and Zhang recognized the importance of the quadratic term in order to describe isotropic growth. Other possible non-linear terms turn out to be always negligible in the presence of the KPZ nonlinearity. Although the KPZ equation with white noise is ill-defined as it stands, a perturbative renormalization group treatment shows already that the nonlinearity is always relevant in 1 and 2 substrate dimensions, whereas in higher dimensions for small enough λ the large-scale behavior of solutions to (1.1) is characterized by the linear theory with $\lambda = 0$, called the weak coupling regime. For $d \geq 2$ a natural generalization of the KPZ equation is to allow λ to be a quadratic form represented by a $d \times d$ matrix. Wolf argued [130] that if λ is not strictly positive (or negative) definite (the anisotropic case) again the nonlinear term is irrelevant. On the other hand if all eigenvalues of λ have the same sign the large scale behavior is the same as in the isotropic case.

From the beginning the great challenge was to extract information in the strong coupling case, when the nonlinearity is relevant. The corresponding field theory is non-Lagrangian, reflecting irreversibility, and non-perturbative, a consequence of nonlinearity. Renormalized perturbation theory, which treats the nonlinearity as a small perturbation, fails to approximate the strong coupling fixed point [46, 48, 79]. Several other approaches have been developed. A mode-coupling approximation [18, 49, 34, 35], an approximate real space renormalization scheme [29], a soliton approximation treating the noise as perturbation [44, 45], a non-perturbative operator product expansions technique [80] and of course numerous Monte-Carlo simulations of discretized models believed to belong to the KPZ universality class, e.g. [77, 120, 3, 4, 71, 85, 86].

Despite these considerable efforts there is no consistent answer to the properties of the strong coupling phase in dimensions $d \geq 2$. There are several distinct predictions for the scaling exponents and even the existence of an upper critical dimension at $d_c = 4$ is under dispute. For $d = 1$ the situation is somewhat better. A formal fluctuation-dissipation theorem allows to determine the values of the critical exponents exactly and the KPZ equation has always been regarded as exactly solvable in some sense. Nevertheless scaling functions have been calculated only by some sort of uncontrolled approximations [119, 49, 35, 44]. Limiting distributions and their universal moment ratios have been studied only by means of Monte-Carlo simulations [72, 7, 77, 86].

1.2 Exactly solvable models

From very early on the one-dimensional KPZ model was regarded as being exactly solvable. The Bethe ansatz solution for the ASEP chain, formulated as a six-vertex model, provides a semi-rigorous derivation of the scaling exponents [40, 57, 56]. Also exact large deviation functions for finite systems could be obtained [39, 38].

Exactly solvable models provide arguably the greatest insight into a physical theory. For example, the $2d$-Ising model can be viewed as a discretization of the Ginzburg-Landau scalar ϕ^4-theory. To extract information beyond the values of critical exponents seems to be feasible only by using exact expressions of the finite Ising system and identifying their asymptotics in the infinite volume limit as has been achieved by Wu et al [131] for critical and close to critical scaling functions. By universality one has obtained the corresponding scaling functions of the ϕ^4-theory which provide a prediction for the scaling functions fo any model believed to be in the ϕ^4 universality class.

This approach to scale invariance and universality has its restrictions. Firstly, the universality class in question has to contain at least one model which is exactly solvable. In equilibrium statistical mechanics for critical phenomena this is

believed to be restricted to one or two spatial dimensions. In nonequilibrium one usually hopes for exactly solvable models only in one spatial dimension. Roughly speaking the non-reversible dynamics, lacking detailed balance, requires to take into account the two-dimensional space-time. Secondly by solving a special model one obtains no direct information on the universality of the results. Although there is usually no doubt about its validity, to actually prove universality is a different issue. Even for slight modifications of the solvable model which apparently do not affect its physical properties but renders it non-solvable, there are only very few examples where some kind of universality is proven rigorously, as has been achieved for the $2d$-Ising model with local perturbations [115].

In this thesis we provide a similar approach to the study of the $(1+1)$-dimensional KPZ field. We mainly deal with a class of very simple growth models, the polynuclear growth (PNG) model and its fully discretized version whose space-time trajectory we call the Bernoulli cone. Originally it was introduced by Rajesh and Dhar as an anisotropic directed percolation model [106]. The Bernoulli cone might be regarded as the "Ising" model of nonequilibrium physics. It contains the PNG model and the celebrated (totally) asymmetric simple exclusion process (ASEP) as limiting cases.

The connection to longest increasing subsequence problems, which only recently has gained fast-growing attention through the already seminal work of Baik, Deift, and Johansson [10], allows us not only to confirm the $1d$ KPZ scaling exponents rigorously for the PNG model, but also, for the first time, to identify limiting distributions of the height fluctuations. Furthermore the scaling form of the stationary two-point function for the PNG model can be obtained. By universality it determines the two-point function of the stationary KPZ field.

There is a deep connection of curved nonstationary KPZ growth with random matrices [68, 99]. The reason is that both theories can be formulated as free fermion theories with determinantal correlation functions. The PNG model can be extended in a very natural way to a multi-layer version consisting of many height lines, where the last line describes the original PNG cluster. Like the eigenvalues of a stochastically evolving random matrix they form a non-intersecting, otherwise non-interacting line ensemble. Therefore it is not too surprising that the statistics of the last line in the growth model has the same scaling limit as the trajectory of the largest eigenvalue in the matrix model. This limiting process, the Airy process, roughly looks like Brownian motion in a confining potential, but it has only slow decay of correlations.

The results in this thesis yield very detailed information on the properties of the one-dimensional KPZ field theory. For example, the rather intricate definition of the stationary two-point function, which is obtained by taking the scaling limit of the PNG correlations, should be derivable from the KPZ equation directly in an appropriate field theoretic formulation. It is not at all clear how this could be

achieved. The Airy process as the limiting process of curved KPZ growth shows that there must be non-stationary but nevertheless scale invariant "solutions" to the KPZ equation which are essentially different from the stationary KPZ field.

For a full understanding of the KPZ field one needs to know arbitrary n-point correlation functions. For a Gaussian field they are given in a simple and direct way by means of the two-point correlation function. For a non-Gaussian theory like KPZ there should be a way to generate them in a systematic way. The Airy process, although not very explicit, provides such a tool for the curved KPZ field, but only for single-time correlations. It remains an open problem to extend this to dynamical n-point correlation functions evaluated at different times.

1.3 Outline

In Chapter 2 we introduce the description of macroscopic self-similar growth in some detail, leading to the Wulff construction. Small perturbations around the self-similar solutions are discussed qualitatively, implying already two different modes of stochastic growth, convex and saddlelike. The scaling theory for stationary stochastic growth, is reviewed briefly and then extended to curved surface growth.

Chapter 3 deals with the one-dimensional polynuclear growth (PNG) model as an especially simple model for stochastic surface growth. It is exactly solvable and confirms validity of the scaling theory, at least in one substrate dimension. In the simplest geometry with droplet initial conditions it can be mapped to Ulam's problem about longest increasing subsequences in random permutations. We show how this leads by means of the orthogonal polynomial method to a recursive expression for the height distribution above the origin. In the scaling limit they become differential equations and the limiting distribution can be identified as the GUE Tracy-Widom distribution known from random matrix theory. Similar results for other deterministic initial and boundary conditions are reported. A special type of random boundary conditions corresponds to exact sampling of the stationary PNG model. We use this fact to determine the exact stationary two-point function, and analyze its scaling limit.

In Chapter 4 we introduce the Bernoulli cone, a discrete version of the PNG model, interpreted as a random set in space-time. We describe several stochastic models, some of them well-known, which, with appropriate initial and boundary conditions, are all equivalent to the Bernoulli cone. Two different continuum limits let us recover the PNG model and the (continuous-time) totally asymmetric simple exclusion process (TASEP). We determine the family of stationary states in an especially simple geometry and sketch, how this allows to predict quantitatively the scaling behavior of all the described models.

In Chapter 5, to go beyond one- (or two-) point distributions, we extend the PNG model to a multi-layer version, with the statistics of the last line being unchanged. To describe the fluctuations of the last line in the scaling limit, we introduce the Airy process, which roughly speaking behaves as the last particle in Dyson's Brownian motion. By means of the determinantal correlations of the multi-layer process it is shown (in the sense of finite-dimensional joint distributions) that the height of the PNG droplet in a region above the origin converges to the Airy process when scaled appropriately.

Chapter 6 is devoted to anisotropic growth on a two-dimensional substrate. We introduce the Gates-Westcott model which mimics a vicinal growing surface, being closely related to multilayer PNG growth. Its steady state on a finite substrate is very simple, and we determine the growth velocity and height-height fluctuations in the thermodynamic limit of infinite substrate area and show agreement with the prediction by a thermodynamical equilibrium argument.

Finally, in Chapter 7 we introduce simple higher dimensional generalizations of the PNG model. The Monte-Carlo simulations performed for some of these models lead to estimates of the KPZ exponents which in two dimensions are in accord with previous Monte-Carlo studies, but differ considerably from the theoretical prediction of Lässig. In three dimensions they are closer to the theoretical prediction. The analogue of the GUE Tracy-Widom distribution for curved stochastic growth on a two-dimensional substrate is determined from the Monte-Carlo data.

Appendix A collects some useful identities for orthogonal polynomials on the circle and Appendix B describes the numerical method we used to determine the solution of the Riemann-Hilbert problem for Painlevé II.

Parts of the results presented in this thesis have been already published in articles co-authored by Herbert Spohn [97, 98, 99, 100, 102, 101].

Acknowledgments

I would like to express my special thanks to my supervisor Herbert Spohn for introducing me to this fascinating topic, for his invaluable guidance, his inexhaustible patience an his continuous support throughout the period of this work. His profound insights, critical thinking, and insistence on clarity have been most fruitful and inspiring.

Many people contributed to this work by sharing their insights with me and/or providing me their results, sometimes prior to publication. Especially I would like to thank Jinho Baik, Deepak Dhar, Erwin Frey, Mike Moore, Lei-Han Tang, and Craig Tracy. Among the countless people to whom I am very grateful for fruitful discussions are Alexei Borodin, Patrik Ferrari, Johannes Hager, Rudolf

Haussmann, Frank Hövermann, Kurt Johansson, Joachim Krug, Michael Lässig, Andrei Okounkov, Martin Rost, and many others. Special thanks to Patrik Ferrari for helping to reduce the number of mistakes in the final version of the manuscript.

Finally I would like to thank Eva Prähofer for teaching me some time management and Sibina Šukman for sharing all the burdens with me I took upon me.

This work has been supported by a "Graduiertenstipendium des Freistaates Bayern zur Förderung des wissenschaftlichen und künstlerischen Nachwuchses", by the "Graduiertenkolleg Mathematik im Bereich ihrer Wechselwirkung mit der Physik", and by the "Technische Universität München".

CHAPTER 2

Self-similar surface growth

2.1 Deterministic dynamics

On a macroscopic level the dynamics of an interface between two thermodynamical phases at a first order transition follows the steepest energy gradient determined by the sum of bulk and surface energies. For simplicity we imagine one phase being a solid and the other the corresponding gas phase. If the chemical potential is slightly in favor of the solid phase both bulk phases away from the interface are very close to equilibrium and the dynamics is determined by physical (or chemical) processes at the interface alone (reaction limited aggregation, RLA). This is in contrast to, for example, diffusion limited aggregation (DLA), where the supply of material is subject to transport properties of the bulk. In RLA the solid, described by a subset of $(d+1)$-dimensional space evolving in time, grows at the expense of the gas phase with a growth velocity depending on the local interface configuration. Let us represent the interface by the graph of a smooth single-valued height function $h(x,t)$, $x \in \mathbb{R}^d$, $t \geq 0$, with respect to an appropriate reference frame, which excludes the existence of small scale overhangs or cavities. For a global description several frames might have to be glued together. In a deterministic continuum description of RLA the growth velocity is a functional of the local height configuration, or, assuming enough regularity, a function of derivatives of the height function,

$$\partial_t h(x,t) = v\big(\partial_x h(x,t), \partial_x^2 h(x,t), \dots\big). \tag{2.1}$$

We focus here on scale invariant growth properties, i.e. properties, which pertain on large length scales, where curvature and higher derivatives of the height function become arbitrarily small. Therefore we neglect higher derivatives in (2.1) and are left with the deterministic large-scale equation of motion for the height function

$$\partial_t h(x,t) = v\big(\partial_x h(x,t)\big). \tag{2.2}$$

The main focus will be on self-similar solutions, i.e. solutions $h(x,t)$ to (2.2) with

$$l h(x,t) = h(lx, lt), \quad \text{for } l > 0. \tag{2.3}$$

The macroscopic shape

$$H(c) = h(c, 1) \tag{2.4}$$

allows to recover the self-similar solution as $h(x,t) = tH(x/t)$. In geometric terms self-similarity means that the region occupied by the solid phase at time t, $C_t \subset \mathbb{R}^{d+1}$ forms a cone in $(d+2)$-dimensional space-time, i.e. for $C = \{(C_t, t); t > 0\}$ one has

$$lC = C, \quad \text{for } l > 0. \tag{2.5}$$

Certains of these macroscopic shapes $H(c)$ are attractors in the space of solutions to (2.1) and (2.2) (parameterized by their initial conditions). Thus if $h(x,t)$ is a solution to (2.1) or (2.2) with $h(x,0) = h_0(x)$, there is a macroscopic shape $H(c)$, such that

$$\lim_{l\to\infty} l^{-1} h(lx, lt) = tH(x/t). \tag{2.6}$$

Clearly the $t \to 0$ limit of a self-similar solution $h(x,t)$, if it exists, is self-similar itself,

$$lh(x,0) = h(lx,0). \tag{2.7}$$

Generically it will have a cusp at the origin. We will argue that for physically relevant self-similar solutions there is even a one-to-one relation between self-similar initial conditions and macroscopic shapes.

To facilitate coordinate transformations one can define a homogeneous scalar function $F(x,t,h)$, whose set of zeros coincides with the boundary of the self-similar cluster, and which has nonzero gradients along this set. F is clearly not unique, for example one can choose

$$F(x,t,h) = h^\gamma - (h(x,t))^\gamma, \quad \gamma > 0, \tag{2.8}$$

such that F is homogeneous of degree γ. To fully specify a convex cluster one has to use several height functions in different coordinate systems to describe the full circonference of the cluster. F can be defined for the whole cluster boundary, which makes it easy to recover the form of the height function for any choice of coordinates (x', t', h') just by solving $F'(x', t', h')$ for h', where $F'(x', t', h') = F(x, t, h)$, since F transforms as a scalar under change of coordinates. This property will be very useful, as described in Section 2.5 where a special choice of F will allow us to encode the size of fluctuations around the deterministic cluster shape in the gradient of F at the cluster boundary.

For illustration we look at the fully isotropic case. The normal velocity v_0 is independent of the interface slope, which implies in Cartesian coordinates the growth velocity

$$v(u) = v_0\sqrt{1+|u|^2}, \tag{2.9}$$

where $u \in \mathbb{R}^d$ is the surface slope. For simplicity we set $v_0 = 1$. Obviously the semi-spherical cluster $H(c) = \sqrt{1-|c|^2}$ for $|c| \le 1$, $H(c) = -\infty$, otherwise, is a possible macroscopic shape. The corresponding self-similar initial configuration is $h_0(x) = 0$ for $x = 0$, $h_0(x) = -\infty$ otherwise. The homogeneous function $F(x,t,h) = h^2 + x^2 - t^2$ obviously encodes the full spherical cluster shape also for negative values of x.

Different initial conditions lead to further self-similar shapes. Another possible macroscopic shape, for example, is $H(c) = \sqrt{1-|c|^2}$ for $|c| \le \frac{1}{\sqrt{2}}$, $H(c) = \sqrt{2} - |c|$ otherwise, leading to the self-similar solution

$$h(x,t) = \begin{cases} \sqrt{t^2-|x|^2} & \text{for } |x| \le \frac{1}{\sqrt{2}}t, \\ -|x| + \sqrt{2}t & \text{otherwise.} \end{cases} \tag{2.10}$$

The initial configuration to (2.10) is $h_0(x) = -|x|$. But also $h(x,t) = -|x| + \sqrt{2}t$ provides a self-similar solution to (2.2) with this initial conditions, besides for the persisting cusp at $x = 0$. The latter self-similar solution is very unstable with respect to small perturbations of the initial conditions, whereas the first is generically stable. The cusp itself is not an indicator for instability per se, as can be seen from the initial conditions $h_0(x) = |x|$. A self-similar solution with this initial conditions is

$$h(x,t) = \sqrt{2}t + |x|. \tag{2.11}$$

Although there is a cusp at $x = 0$, (2.11) is the only almost everywhere solution to (2.2) and it is very stable with respect to perturbations of the initial conditions.

The question arises how stable self-similar solutions may be characterized. For convex cluster growth, i.e. when a convex cluster grows from a single seed, self-similar solutions are obtained from the initial conditions by the Wulff construction, which is explained in the next section and we will reformulate it as a deterministic last passage percolation problem. In Section 2.1.2, for non-convex self-similar growth we give an analytic characterization of self-similar shapes, which requires enough regularity of the growth velocity $v(u)$.

2.1.1 Convex growth, last passage percolation

If the growth velocity is a convex function of the slope, or at least has a convex envelope, the fundamental growth mode is a cluster growing from a single small

seed at the origin in $(d+1)$-dimensional space. For simplicity we assume the growth velocity to be positive for all slopes. To obtain the cluster shape at later times, one employs the Wulff construction. A crystal filling the half-space on one side of a perfect plane evolves in time by moving the boundary plane parallely with its characteristic growth velocity. Imagine now a collection of these plane interfaces at all possible slopes intersecting the initial seed and moving independently. The actual cluster then arises as the intersection of all these extending half spaces.

This geometrical construction of the cluster shape, the Wulff construction, has been known for a long time in crystallography [132]. In the substrate geometry one has

$$h(x,t) = \inf_u tv(u) + u \cdot x. \tag{2.12}$$

Mathematically the macroscopic shape $H(c) = h(c,1)$ is the Legendre transform of the growth velocity

$$H(c) = \inf_u v(u) + u \cdot c. \tag{2.13}$$

By construction the droplet shape is a concave function. The region $D_t = \{(x,h); h \le h(x,t)\}$ is a convex set in $\mathbb{R}^{d+1}$. As is well-known for the Legendre transformation nonconvex parts of the growth velocity $v(u)$ are irrelevant, $v(u)$ could be replaced by its convex hull [78].

The droplet cluster D_t grows according to Huygen's principle. The cluster at time t, D_t, arises from the cluster at time s, D_s, as the superposition of droplets growing for a time $t-s$ from each point in the cluster D_s,

$$D_t = D_s + D_{t-s}, \tag{2.14}$$

with the common notation $A + B = \{x+y;\ x \in A \text{ and } y \in B\}$. For the height function this reads

$$h(x,t) = \sup_y h(y,s) + (t-s)H\Big(\frac{x-y}{t-s}\Big) \tag{2.15}$$

Iterating this splitting we can write $h(x,t)$ as a functional of paths,

$$h(x,t) = \sup_{y,\gamma_y} h(y,0) + \int_0^t H\big(\dot\gamma_y(s)\big)ds, \tag{2.16}$$

where the supremum runs through all continuous, piecewise differentiable paths $\gamma_y : [0,t] \to \mathbb{R}^d$ with $\gamma_y(0) = y$ and $\gamma_y(t) = x$. Eq. (2.16) is valid for arbitrary initial conditions $h(x,0) = h_0(x)$.

The desired one-to-one mapping from self-similar initial conditions to stable self-similar solutions is given by Huygen's construction. If C_0 is a cone in $\mathbb{R}^{d+1}$ the corresponding macroscopic shape is given by $C_1 = C_0 + D_1$.

In eq. (2.16) $h(x,t)$ might be interpreted as a deterministic last passage percolation problem. For this we interpret the height variable h as time and the time variable t as an additional spatial dimension. $H(c)$ is regarded as a passage velocity of, say, a fluid which depends on the direction c. The passage time along a directed path γ from $(y,0)$ to (x,t) is given by

$$L(\gamma) = \int_0^t H\big(\dot\gamma(s)\big)ds. \tag{2.17}$$

In these terms $h(x,t)$ arising from initial conditions $y \mapsto h(y,0)$ is the last passage time of the fluid which origins from the line $t = 0$ with starting times $h(y,0)$ at $(y,0)$, subjected to the anisotropic passage velocity $H(c)$. $tH(x/t)$ itself can be thought of as the point-to-point last passage time for paths starting at $(0,0)$ and ending at (x,t)

2.1.2 Saddle-like growth

When the growth velocity depends smoothly on the slope we can give an local analytic characterization for the macroscopic shape.

One plugs the homogeneity ansatz inspired by (2.3), $h(x,t) = tH(x/t)$, directly into the evolution equation (2.2) yielding the condition

$$H(c) - c\nabla H(c) = v\big(\nabla H(c)\big). \tag{2.18}$$

Differentiating with respect to $c \in \mathbb{R}^d$, at a point where $\nabla H(c) = u$, yields the linear equation

$$0 = (\partial^2 H)(c)\big(c + \nabla v(u)\big), \tag{2.19}$$

which is a sufficient local condition for a self-similar shape. The trivial solution $\partial^2 H = 0$ everywhere leads to the family of plane solutions $h(x,t) = t\,v(u) + x \cdot u$. Assuming $\partial^2 H$ to be invertible, enforces $c = -\nabla v(u)$, or equivalently $\partial^2 H(c) = -\left(\partial^2 v(u)\right)^{-1}$. Thus if the vector field $\nabla v(u)$ is differentiable and invertible in some open set one recovers the differential version of the Legendre transformation,

$$H(c) = v\big(u(c)\big) + c \cdot u(c), \tag{2.20}$$

with $u(c)$ the inverse vector field of $-\nabla v(u)$.

In the case that $\partial^2 v$ is positive (if negative, flip from v to $-v$) definite we are led back to the Legendre transform (2.13) for a concave macroscopic shape. When $\partial^2 v$ has eigenvalues of different sign, but nevertheless is invertible, (2.20) defines H only locally. Initial conditions enforcing such a nonconvex self-similar shape have to form a nonconvex cone. As an explicit example in $2+1$ dimensions, the growth velocity for the multi-layer PNG (or Gates-Westcott) model [50, 97] is

$$v(u) = \pi^{-1}\sqrt{(2\sin u_1\pi)^2 + (u_2\pi)^2}, \tag{2.21}$$

defined for $u = (u_1, u_2) \in [0,1] \times \mathbb{R}$. A simple but tedious calculation yields for the macroscopic shape

$$h(x,y,t) = \begin{cases} \pi^{-1}\big(\sqrt{4(t^2-y^2)-x^2} + x \arccos\big(x/\sqrt{4(t^2-y^2)}\,\big)\big) & \\ \qquad\qquad \text{for} \quad x^2/4 + y^2 \le t^2, & \\ \max\{0,x\} \quad \text{for} \quad y^2 \le t^2 < x^2/4 + y^2, & \\ 0 \qquad\qquad \text{otherwise.} & \end{cases} \tag{2.22}$$

In this case the initial conditions are $h(x,y,0) = \max\{0,x\}$ for $y = 0$ and $h(x,y,0) = 0$ otherwise. The set initially occupied by the crystal, $\{(x,y,h) \in \mathbb{R}^3;\, h \le h(x,y,0)\} = \mathbb{R}^2 \times \mathbb{R}_0^- \cup \{(x,0,z); z \le x\}$ is a nonconvex cone in $\mathbb{R}^3$.

2.2 Perturbations around the deterministic shape

We give a rough argument concerning the stability of a self-similar solution $h(x,t)$ to (2.2) with respect to small localized deviations. The argument is independent of the macroscopic curvature, since the support of the perturbation can be made arbitrary small. Therefore we take as unperturbed height $h(x,t) = v(0)t$ for the sake of simplicity and, by a suitable Gallilean transformation in x and t, one can arrange $v(0) = 0$, $\nabla v(0) = 0$, leaving unchanged the second derivative $\partial^2 v(0)$. In one substrate dimension, $x \in \mathbb{R}$, if the growth velocity has nonzero curvature we take it to be positive. Otherwise one has to flip the height coordinate. A positive perturbation of initial excess height, Δh, and small compact support, denoted a bump, spreads in the course of time and quickly adopts the approximate shape of a parabola with decreasing curvature , $(v''(0)t)^{-1}$ at its maximum, which itself does not move in time. Higher derivatives of the growth velocity only result in a diminishing deviation from this parabolic shape. The excess height stays constant and the lateral extension increases with the square root of the time passed since the formation of the bump, compare with Fig. 2.1(a). Conversely a negative perturbation, a dent, develops a cusp at its center after some finite time. The further evolution is approximately described by the right and left branch of two parabolas,

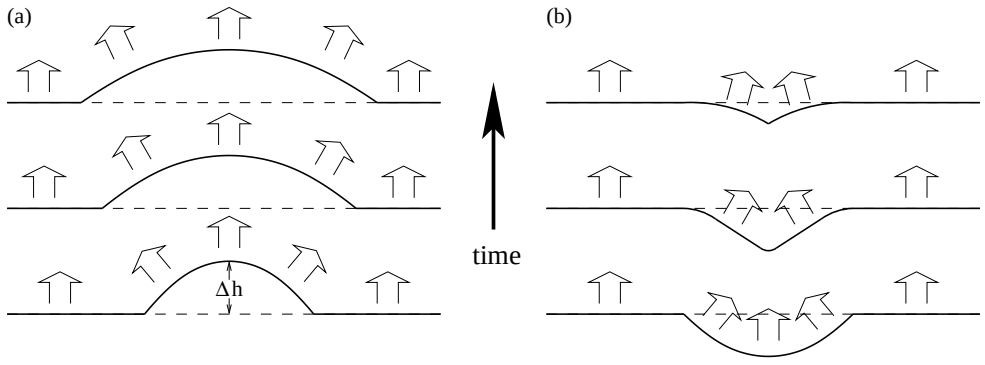

Figure 2.1: *A bump, (a), and a dent, (b), with the same initial excess height Δh, evolving in time for positive curvature of the growth velocity.*

having their maxima fixed at the left, resp. right, edge of the initial dent. Since the curvature of these parabolas has the same behavior as for a bump, the cusp in the middle flattens asymptotically, and the excess height vanishes as t^{-1}, compare with Fig. 2.1(b). Thus if bumps and dents are added at random in space and time to the self-similar solution, only the bumps effectively contribute to the time evolution of the surface line. Since new bumps can be added on already existing ones, the net effect is an enhancement, or renormalization, of the mean growth velocity. Furthermore the surface line becomes roughened by such a persistent stochastic perturbation.

In higher dimensions, if the curvature of the growth velocity is convex (resp. concave) the above picture remains unchanged. Bumps spread laterally into all directions, adopting a paraboloidal shape, and dents do not extend laterally and there excess height vanishes very fast.

In contrast if the curvature is indefinite, a bump spreads in the directions of positive curvature but shrinks in the direction of negative curvature, and from the latter its excess height vanishes inevitably. The same holds for dents with the subspaces of positive and negative curvature interchanging their role. This behavior indicates that in the convex case dynamically added perturbations around the deterministic shape generically enhance the growth velocity and the roughness, whereas for a saddle-like growth velocity the effect is suppressed by a qualitatively different behavior.

This naïve argument is corroborated by Wolf's analysis [130] of the Kardar-Parisi-Zhang equation, a stochastic continuum model for surface growth explained in detail in Section 2.4. Furthermore in Chapter 6 we present a microscopic growth model where we determine explicitly the growth velocity and show that at its is behavior conforms with the anisotropic scenario established by Wolf.

2.3 Stochastic surface growth

The macroscopic laws for a compactly growing cluster described in Section 2.1 emerge phenomenologically from the underlying physical solidification process. On a classical level growth processes can be described as random dynamics of the microscopic particles. Mathematically a macroscopic mean growth velocity and correspondingly a deterministic shape of the self-similarly growing cluster arise as a law of large numbers for an underlying stochastic process. For simplicity we assume that the stochastic growth process can be parameterized by a single-valued height function $h(x,t)$ relative to a d-dimensional substrate, $x \in \mathbb{R}^d$. Vaguely this can be achieved by some coarse graining procedure, which gets rid of cavities and overhangs. We think of $h(x,t)$ as a function valued stochastic process in t with local time- and space-homogeneous update rules and some, yet unspecified, initial and/or boundary conditions. Expectation values will be denoted by $\mathbb{E}(\cdot)$.

2.3.1 Stationary growth

In general one expects to have a family of space-time stationary solutions $h_u(x,t)$ which is parameterized by the mean slope $u = \mathbb{E}\big(\nabla h_u(0,0)\big) \in \mathbb{R}^d$. A standard way to obtain these stationary processes is to start with a finite substrate and to impose suitable boundary conditions fixing the desired mean slope u. The simplest choice, for example, is to take chiral boundary conditions in a rectangular substrate, which means that opposite borders are identified only after an appropriate vertical shift. In finite volume the height process is required to be ergodic. It relaxes to a unique stationary state, which depends only on the boundary conditions. In the thermodynamic limit of infinite substrate area at given slope u one expects to have a unique limiting process, $h_u(x,t)$, whose gradient is stationary in space and time [117]. To be precise at this point, one obtains a limiting measure on space-time height configurations which is invariant under vertical shifts, $h_u(x,t) \mapsto h_u(x,t) + const$, and thus can not be normalized. The probability measure of the height process has to be defined on equivalence classes of height functions differing only by a constant. Consequently expectations are well defined only for height differences.

If the thermodynamical limit exists and is unique, one can define the mean growth velocity $v(u)$ corresponding to the slope u, as the infinite substrate limit of the finite stationary growth velocities. A priori there is no reason why the pointwise defined growth velocity should have any regularity properties. Nevertheless, since fluctuations cause to probe also neighboring slopes, one expects a smooth dependence on u, at least generically. In the following we describe the situation at slopes u where $\lambda = v''(u)$ is a well-defined matrix, as it is suggested by renormalization group studies of the corresponding continuum theory, the Kardar-

Parisi-Zhang equation [70, 130].

Since the growth rule is local there is only one intrinsic length scale, x_m, given by the underlying lattice structure or the effective correlation length of the deposition dynamics. For length scales much larger than x_m one expects scale invariance of the surface fluctuations, as it is familiar for an order parameter in equilibrium thermodynamics at criticality, because of the absence of any distinguished length scale. For example height differences relative to the mean slope should increase algebraically with the distance,

$$\mathbb{E}\left((h_u(x,0) - h_u(0,0) - x\cdot u)^2\right) \propto |x|^{2\alpha}, \quad \text{for large } |x| \tag{2.23}$$

with the static roughness exponent $\alpha < 1$. If $\alpha = 0$, the marginal case, the surface may be logarithmically rough, if $\alpha < 0$ the surface is microscopically flat with very small deviations from the mean shape.

This asymptotic scale invariance extends to dynamical fluctuations. We perform a Gallilean transformation which absorbs the constant and the linear part of the growth velocity,

$$\xi_u(x,t) = h_u(tc + x, t) - t(v(u) + c\cdot u) - x\cdot u, \tag{2.24}$$

with $c = -v'(u) \in \mathbb{R}^d$. The mean slope of $\xi_u(x,t)$ is zero and the transformed growth velocity $w(u)$ reads

$$w(u) = \tfrac{1}{2}\langle u, \lambda u\rangle + \mathcal{O}(|u|^3). \tag{2.25}$$

$\xi_u(x,t)$ represents the fluctuations of h_u around its mean along the characteristic trajectory $x = ct$. In this new coordinates

$$\mathbb{E}\left((\xi_u(0,t) - \xi_u^{\text{stat}}(0,0))^2\right) \propto |t|^{2\beta}, \tag{2.26}$$

where the dynamical roughness exponent β turns out to be smaller than α in general. The scaling hypothesis states that not only the two-point correlation has the scaling properties explained above, but that the stationary height process as a whole is statistically self-affine at large scales.

Scaling Hypothesis. If $\alpha, \beta > 0$ the fluctuation process $\xi_u(x,t)$ converges under proper scaling to a scale invariant limiting process $H(x,t)$,

$$\ell^{-\beta}\xi_u(\ell^{1/z}x, \ell t) \to H(x,t), \quad \text{as } \ell \to \infty, \tag{2.27}$$

with $z = \alpha/\beta$. Obviously (2.27) reproduces (2.23) and (2.26). The scale invariance of $H(x,t)$ is expressed by

$$H(\ell^{1/z}, \ell t) = \ell^{\beta} H(x,t) \tag{2.28}$$

in distribution.

The renormalization group analysis suggests that α and β are universal in the sense that they depend only on qualitative properties of the underlying microscopic model like the substrate dimension and the signature of λ. More precisely, one has to distinguish three cases:

Universality Hypothesis.

1. **(Anisotropic KPZ)** If λ is not positive or negative definite, i.e. if λ has one eigenvalue equal to 0 or two eigenvalues of opposite sign, then $H(x,t)$ is the solution of a linear partial differential equation, the Edwards-Wilkinson equation

$$\partial_t H(x,t) = \langle \partial_x, C\partial_x \rangle H(x,t) + \eta(x,t) \tag{2.29}$$

   with $\eta(x,t)$ space-time white noise of strength D, for some $D > 0$, with covariance $\mathbb{E}\big(\eta(x,t)\eta(x',t')\big) = D\delta(x'-x)\delta(t'-t)$, and C some positive definite $d \times d$-matrix.

2. **(Isotropic KPZ, strong coupling)** If λ is positive definite (if $\lambda < 0$ we switch from H to $-H$), and if for $d > 2$ the microscopic noise is strong enough, then the scaling relation

$$\alpha + z = 2 \tag{2.30}$$

   holds. The variance of height differences is given by

$$\mathbb{E}\left(\big(H(x,0) - H(0,0)\big)^2\right) = a\left(\langle x, \lambda^{-1}x\rangle\right)^{\alpha}, \tag{2.31}$$

   with the roughness parameter a, and

$$H_d^{\text{KPZ}}(x,t) = (c_d/a)^{1/2} H(\lambda^{1/2}x, t) \tag{2.32}$$

   is a space-time stationary, isotropic, and scale invariant process. It is completely independent of the underlying microscopic model and the slope one is looking at. $c_d > 0$ is an arbitrary constant fixing the static two-point function as $\mathbb{E}\big((H_d^{\text{KPZ}}(x,0) - H_d^{\text{KPZ}}(0,0))^2\big) = c_d|x|^{2\alpha}$.

3. **(Isotropic KPZ, weak coupling)** If $\lambda > 0$, $d > 2$, and the noise produced by the microscopic dynamics is weak enough, $H(x,t)$ is again a solution of the Edward-Wilkinson equation (2.29).

Remarks:

- The anisotropic KPZ case is motivated by the renormalization group treatment of Wolf [130]. For $d = 2$ we give convincing support for the conjecture in Chapter 6 by showing that the stationary distribution of a particular anisotropic growth model is consistent with (2.29).

- The scaling relation (2.30) in the strong coupling regime is well established on a nonrigorous level independently of the substrate dimension. There are more or less formal derivations of its validity, e.g. [78] and references therein. We will present another heuristic argument based on the extended self-affinity conjecture at the end of Section 2.3.2. The analysis of the continuum theory confirms (2.30) to all orders in perturbation theory [79], and simulations agree with it very well within statistical errors. Nevertheless only for $d = 1$, where $\alpha = 1/2$ there have been rigorous results confirming $z = 3/2$ indirectly for special models [40, 56]. But only the limiting theorems of Johansson [68] and the ones presented in Chapters 3 and 5 of the present work go beyond the mere determination of the exponents and thus verify (2.30) explicitely for some special models. For 2 or more substrate dimensions nobody doubts the validity of (2.30), but the convincing support is at most indirect and far from rigorous.

- $H_d^{\mathrm{KPZ}}(x,t)$ arises from the model dependent $H(x,t)$ by rescaling the substrate coordinates in a way to make the two point function isotropic. By the scale invariance (2.28) and isotropy the universal two-point scaling-function

$$g_d^{\mathrm{dyn}}(|x|) \stackrel{\mathrm{def}}{=} t^{-2\beta}\mathbb{E}\left(\left(H_d^{\mathrm{KPZ}}(t^{1/z}x,t) - H_d^{\mathrm{KPZ}}(0,0)\right)^2\right) \tag{2.33}$$

  is well defined since the rhs is independent of $t > 0$ and $x/|x|$. One has $g_d^{\mathrm{dyn}}(y) \sim c_d y^{2\alpha}$ for large y. In Section 3.3 we determine $g_1^{\mathrm{dyn}}(y)$. The analytical expressions suggest to set $c_1 = 2$. Therefore we propose to set $c_d = 2$ for higher dimensions as well.

- For $d = 1$ and $c_1 = 2$ the formulas simplify considerably. In this case $x \in \mathbb{R}$, $\lambda = v''(u)$ is a number and the exponents $\alpha = \frac{1}{2}$, $\beta = \frac{1}{3}$ are known exactly. It is natural to define the roughness amplitude as

$$A = \lim_{x\to\infty} x^{-1}\mathbb{E}\left((h_u(x,0) - h_u(0,0) - xu)^2\right), \tag{2.34}$$

  thus $a = A\lambda^{1/2}$. With these settings one has for the fluctuations (2.24) directly the limit

$$\frac{\xi_u\left((2\ell^2\lambda^2 A)^{1/3}x, \ell t\right)}{\mathrm{sign}(\lambda)(\frac{1}{2}\ell|\lambda|A^2)^{1/3}} \stackrel{\ell\to\infty}{\longrightarrow} H_1^{\mathrm{KPZ}}(x,t) \tag{2.35}$$

as a universal relation for any growth model in the KPZ universality class with nonlinearity $\lambda(u) \neq 0$ and roughness amplitude $A(u)$, for all possible slopes u. Although the equal-time distribution of the KPZ field, $x \mapsto H_1^{\mathrm{KPZ}}(x,0)$ is Brownian motion which is symmetric under the transformation $H \mapsto -H$, dynamical correlations do depend on the sign of λ as indicated in (2.35). This can be seen already in the two-point probability distribution, which is identified in Section 3.3. In higher substrate dimensions even the up/down symmetry of the equal-time distribution seems to be broken [80, 32].

- The weak-coupling/strong-coupling transition for $d > 2$ is indicated by perturbative renormalization of the KPZ theory [70]. Existence of the weak coupling phase is confirmed for $d \geq 3$ by rigorous results for directed polymer models [64, 23, 95]. Existence of the strong-coupling phase in substrate dimensions $d \geq 4$ is a controversially discussed question [81, 2, 21, 34, 86].

2.3.2 Extended self-affinity

The macroscopic growth velocity $v(u)$ arises from the stationary processes at given slope u. If we start with arbitrary initial conditions $h(x,0)$, the surface roughens on a microscopic scale. But, assuming appropriate regularity of $v(u)$, on a larger scale fluctuations will be around a mean shape. One area of interest is to derive the macroscopic evolution equation (2.2) from the microscopic dynamics in the sense of a law of large numbers. In general one takes a sequence of initial conditions $h_n(x,0)$ approximating the smooth function $h(x)$ in the macroscopic limit $\frac{1}{n}h(nx,0) \to h(x)$ as $n \to \infty$. The aim is to show that the rescaled processes converge to a (weak) solution $h(x,t)$ of (2.2) with initial data $h(x,0) = h(0)$, i.e.

$$\tfrac{1}{n}h_n(nx,nt) \to h(x,t) \quad \text{in probability as } n \to \infty, \tag{2.36}$$

uniformly in x and $t \in [0,T]$, $T > 0$. There is a huge literature on these hydrodynamic limit type results, e.g. [36, 116, 112, 73] and references therein.

We focus here on a simpler setting. We take just one process, whose initial condition $h(x,0)$ itself is macroscopically self-similar,

$$\lim_{\ell \to \infty} \ell^{-1} h(\ell x, 0) = h_0(x), \tag{2.37}$$

where necessarily $h_0(\ell x) = \ell h_0(x)$. If $h(x,0)$ is random (2.37) has to be understood as convergence in probability.

Macroscopic Self-similar Shape Conjecture. On macroscopic scales $h(x,t)$

converges to a self-similar deterministic solution $H(x,t)$ of (2.2) with initial condition $H(x,0) = h_0(x)$. One has $\ell^{-1}H(\ell x, \ell t) = H(x,1) \stackrel{\text{def}}{=} H(x)$, where $H(x)$ is the Wulff shape (2.13) or (2.20) with respect to the growth velocity $v(u)$. Then

$$\lim_{\ell\to\infty} \ell^{-1} h(\ell x, \ell t) = H(x) \tag{2.38}$$

in probability.

Closely related to the macroscopic shape is the

Local Stationarity Hypothesis. Relative to a ray $x = ct$ of constant and well defined mean slope, $u = H'(c) \in \mathbb{R}^d$, the fluctuations of $h(x,t)$,

$$\xi_{c,T}(x,t) = h\big((T+t)\,c + x, T+t\big) - (T+t)(v(u) + c\cdot u) - x\cdot u, \tag{2.39}$$

locally converge to the stationary fluctuations (2.24) at slope u, i.e.

$$\lim_{T\to\infty} \xi_{c,T}(x,t) = \xi_u^{\text{stat}}(x,t) \tag{2.40}$$

in distribution for x, t restricted to a bounded set.

The plausible assumption that local stationarity holds not only on the microscopic scale but does extend maximally to regions in which the systematic curvature of $h(x,t)$ is still negligible leads to the

Extended Self-Affinity Conjecture. If for some $c \in \mathbb{R}^d$ the macroscopic shape is smooth and concave, $H''(c) < 0$, then, setting $u = H'(c)$, we know that the curvature of the growth velocity is $\lambda = v''(u) = -\big(H''(c)\big)^{-1}$. If in addition $\alpha > 0$, then $\alpha + z = 2$, or equivalently $\beta = \alpha/(2-\alpha)$. In this case the fluctuations converge to a unique limit

$$\lim_{T\to\infty} 2^{\beta} (\tfrac{c_d}{a})^{1/z} T^{-\beta} \xi_{c,T}\big(2^{1/z}(\tfrac{a}{c_d})^{1/2z} T^{1/z} \lambda^{1/2} x, 0\big) = H_d^{\text{curved}}(x) - |x|^2, \tag{2.41}$$

where a is the static roughness parameter from the stationary process (2.31). $H_d^{\text{curved}}(x)$ is stationary in x and isotropic.

Remarks:

- By the local stationarity hypothesis one recovers the stationary KPZ distribution in the small scale limit

$$\lim_{\ell\to 0} \ell^{-\beta} H_d^{\text{curved}}(\ell^{1/z} x) = H_d^{\text{KPZ}}(x,0). \tag{2.42}$$

- The distribution of the universal random variable $\chi_d^{\text{curved}} \stackrel{\text{def}}{=} H_d^{\text{curved}}(0)$ depends only on the substrate dimension d. For $d = 1$ it is the GUE Tracy-Widom distribution as derived in the following chapter. In Chapter 7 Monte-Carlo results for $d = 2$ are presented.

- For $d = 1$ with the roughness amplitude (2.34) the scaling form (2.41) simplifies to

$$\frac{\xi_{c,T}\big((2\lambda^2 AT^2)^{1/3}x, 0\big)}{\text{sign}(\lambda)(\frac{1}{2}|\lambda|A^2T)^{1/3}} \stackrel{T\to\infty}{\longrightarrow} H_1^{\text{curved}}(x) - x^2, \tag{2.43}$$

  with λ and A evaluated at $u = H'(0)$. In chapter 5 the process $x \mapsto H_1^{\text{curved}}(x)$ is identified as the Airy process [102].

- For $|x|$ large $H_d^{\text{curved}}(x)$ and $H_d^{\text{curved}}(0)$ become independent. The correlations define another universal scaling function

$$g_d^{\text{curved}}(|x|) = \mathbb{E}\big((H_d^{\text{curved}}(x) - H_d^{\text{curved}}(0))^2\big). \tag{2.44}$$

  By definition $g_d^{\text{curved}}(y) \simeq y$ for small y and by the postulated independence $g_d^{\text{curved}}(y) \simeq 2\text{Var}(\chi_d^{\text{curved}})$.

The scaling form (2.41) is trivial in the case of zero substrate dimensions. The "cluster" being a single column of increasing height by the random attachment of material. If these increments are independent or only weakly dependent in time, the law of large numbers tells us that indeed $h(T)/T \to v$ in probability, v being the macroscopic growth velocity. Furthermore by the central limit theorem we know, that $\beta = 1/2$, and the limiting distribution χ_0 is Gaussian, its width being determined by the first and second moments of the increments alone. Since $x \in \mathbb{R}^0 = \{0\}$ the definition of the static roughness is void.

For higher substrate dimensions the following picture arises. At a given time T the surface fluctuates around its deterministic shape, as if it were confined in a potential well along h^{det}, whose width scales as T^β, and whose shape is given by the logarithm of the probability density of χ_d^{curved}. Thus at finite T local stationarity has to be violated above a length scale, where the static roughness is of the same order as the global surface width implied by the width of the distribution of $H_d^{\text{curved}}(0)$. This happens at a time-dependent typical correlation length $\xi(T)$ and suggests that for $|x| \gg \xi(T)$ the random variables $h(cT, T)$ and $h(cT + x, T)$ are essentially independent. We have $\xi(T)^\alpha \approx T^\beta$, or $\xi(T) \approx T^{1/z}$. On the other hand, if the macroscopic shape is convex, $\partial^2 h^{det}(cT, T) < 0$, the mean deviation from the tangent at $(cT + x, T)$ is $\frac{1}{2}(x, \partial^2 h^{det}(cT, T)x) \propto x^2/T$, which at a distance $\xi(T)$ is estimated to be of the same order as the surface width of order T^β. Thus we obtain $\xi(T)^2 \approx T^\beta$, or $2/z = \beta$. Multiplying by α one recovers by this simple heuristical argument the celebrated scaling relation (2.30), valid for all substrate dimensions d [78, 74, 89].

2.4 Universality

It is widely accepted that the roughness exponents α and β are the same for all microscopic models of reaction limited aggregation (RLA), i.e. where the growth process depends only on the local interface configuration, and vary only for different substrate dimension d. For $d = 1$ the static roughness exponent is fixed by a fluctuation-dissipation relation as $\alpha = \frac{1}{2}$, the interface line has the static roughness of a fluctuating string, as in equilibrium [78]. Thus by the scaling relation (2.30), the dynamical roughness scales with $\beta = \frac{1}{3}$. For $d = 2$ the value of the exponents is still controversial. Numerical investigations [120] indicate $\beta = 0.240(1)$, but theoretical predictions, based on an operator product expansion [80], or on a self-consistent real space renormalization [30], are $\beta = \frac{1}{4}$ and $\beta = 0.22$, respectively. For $d > 2$ there is a weak coupling regime, predicted already by the renormalization group flow of the KPZ equation [70] with $\alpha = \beta = 0$. For strong coupling in $d = 3$ the predictions for β range from 0.1655 [30] over $\frac{1}{6}$ [80] to $0.180(2)$ [120, 3]. For $d \geq 4$ even the nature of the strong coupling fixed point is under dispute. There are theoretical arguments which predict that $d_c = 4$ is the upper critical dimension with $\alpha = \beta = 0$ for $d \geq d_c$ even in the strong coupling regime [81]. But numerical investigations, though restricted to moderate system sizes, especially in higher dimensions, notoriously indicate $\alpha, \beta > 0$ even for large d [3, 71] and a self consistent expansion in $1/d$ predicts $\beta \propto 1/d$ asymptotically [29].

The universality hypothesis comprises not only the exponents but also the shape of the distributions whose width scales with the roughness exponents, like the Gaussian normal distribution does in the central limit theorem. The distributions arising are generically non-Gaussian. The properly rescaled (truncated) moments have universal ratios corresponding to the moments of the limiting distribution, sometimes called universal amplitude ratios [72, 58, 77, 7].

In Section 2.3 we presented a formulation of the universality hypothesis which emphasizes the uniqueness of the fluctuation fields in the proper scaling limit. For convex growth, i.e. $\partial^2 v(u) > 0$ or $\partial^2 v(u) < 0$, we assumed that after a linear transformation of the local substrate coordinates such that $\partial^2 v(u)$ becomes the identity matrix, the stationary fluctuation field is rotationally invariant, and indeed is up to a normalizing prefactor *the* stationary KPZ fluctuation process $H_d^{\mathrm{KPZ}}(x,t)$ of (2.32).

The stochastic field $H_d^{\mathrm{KPZ}}(x,t)$ is usually thought of as a spatio-temporally stationary solution to the KPZ equation [70]

$$\partial_t h = \nu \Delta h + \tfrac{\lambda}{2} (\nabla h)^2 + \eta(x,t), \tag{2.45}$$

with space-time white noise $\eta(x,t)$ of zero mean and correlations

$$\langle \eta(x,t)\eta(x',t')\rangle = 2D\delta(t-t')\delta(x-x'). \tag{2.46}$$

The nonlinear term arises from a second order Taylor expansion of the growth velocity with respect to the slope, lower order terms being absorbed by a suitable affine transformation, higher orders being irrelevant by naïve power counting. The Laplace operator is added to represent surface tension, being necessary to control the singular noise term. The stochastic partial differential equation (2.45) is ill-defined as it stands and much effort has been made to extract physical information by means of renormalization group (RG) analysis in the field theoretical context [70, 48, 79, 80], which unfortunately can not reliably access the strong coupling fixed point. In principle eq. (2.45) has to be regularized with some kind of ultra-violet cut-off, and then studied in the large scale limit.

Let us mention that there are two formally equivalent formulations of the KPZ equation. We set

$$Z(x,t) = \exp\big(-\tfrac{\lambda}{2\nu}h(x,t)\big), \tag{2.47}$$

which is called the Cole-Hopf transformation of $h(x,t)$. $Z(x,t)$ is governed by the linear diffusion equation

$$\partial_t Z = \nu\Delta Z - \tfrac{\lambda}{2\nu}\eta(x,t)Z. \tag{2.48}$$

The price for obtaining a linear equation is paid by introducing multiplicative noise. Formally $Z(x,t)$ can be written as a path integral over Brownian paths, B_s, with $B_0 = 0$ and $B_t = x$, weighted by the Boltzmann factor

$$\exp\Big(-(2\nu)^{-1}\int_0^t \eta(B(s),s)ds\Big). \tag{2.49}$$

Thus, if we call such a Brownian path with fixed endpoints a directed polymer, $Z(x,t)$ has an interpretation as the partition sum for a directed polymer in a random environment. The temperature corresponds to 2ν and the KPZ height is proportional to the free energy $-\ln Z$. Of course one still has to regularize the noise in order to give meaning to eq. (2.48). The growth models we are presenting in the following chapters all have the property that once mass is attached to the growing cluster it can never detach. We will see that these property allows to formulate naturally a corresponding directed polymer problem at zero temperature.

If we take the gradient on both sides of the KPZ equation and substitute h through the gradient vector field $u = \nabla h$, we obtain the noisy Burgers equation

$$\partial_t u = \nu\Delta u + \lambda(u\cdot\nabla)u + \nabla\eta \tag{2.50}$$

driven by conserved noise. For $d = 1$ it can be interpreted as the flow of a fluid with conserved mass. All the 1-dimensional growth models which will be described in this work have a fairly obvious interpretation as a driven particle model which are possible discretizations of the noisy Burgers equation.

Let us describe the nonrigorous results about the KPZ equation obtained from renormalization theory in some detail. The RG approach supplies a sophisticated framework to obtain flow equations for the parameters ν, λ, and D, in a perturbative approximation. Roughly described, the KPZ equation is regularized by introducing an ultraviolet cut-off Λ in Fourier space. One tries to match the parameters of the KPZ equation for different values of the cut-off parameter. Integrating out high frequency modes results in an effective lowering of Λ and at the same time changing the effective values for λ, ν, and D. The resulting equation with effective parameters is rescaled, such that the noise strength D and the surface tension ν is unchanged. The dimension d becomes a parameter in this formulation which naturally extends to real values. One expands around $\lambda = 0$ and obtains for fixed d a differential equation for λ under the continuous coarse-graining and rescaling procedure, called renormalization group flow. If λ converges to zero under this flow, the nonlinearity in (2.45) is irrelevant, and the large scale behaviour should be governed by the linear equation with $\lambda = 0$, called the Edwards-Wilkinson equation [42], which is well-defined mathematically and can be analyzed thoroughly [92]. λ diverging under the RG flow, however, indicates a strong coupling fixed point at $\lambda = \infty$.

For $d \leq 2$ the fixed point $\lambda = 0$ is unstable, which implies that under renormalization the rescaling after coarse-graining should be done in a way to leave λ invariant. Doing this the parameters D and ν tend to zero, and the limiting equation is deterministic, reflecting only the quadratic nonlinearity in (2.2). In this sense perturbative renormalization is not able to predict properties of the strong coupling phase beyond the macroscopic shape. Above the lower critical dimension 2 the fixed point $\lambda = 0$ becomes stable. Thus for small values of λ the large scale behavior should be governed by the Edwards-Wilkinson equation. A refined analysis around $d = 2$ exhibits a bifurcation. For $d > 2$ a second fixed point emerges with a square root singularity, which is unstable, compare with Figure 2.2. Thus for a large enough nonlinearity, also in dimensions $d > 2$ one still expects the existence of a strong coupling phase. Using higher orders in the perturbation theory and extrapolating along the unstable fixed point seems to indicate that at $d = 4$ a further singularity develops, leading to the claim that $d = 4$ is the upper critical dimension for the KPZ equation [81].

A closer inspection of the KPZ equation (2.45) exhibits that the nonlinear term should be replaced by a quadratic form, $\frac{1}{2}(\nabla h, \lambda \nabla h)$, where λ is the Hesse matrix of the slope dependent growth velocity. In coordinates where the $d \times d$ matrix is diagonal one has d nonlinear terms, $\frac{\lambda_i}{2}(\partial_i h)^2$, $i = 1, \ldots, d$ where the eigenvalues

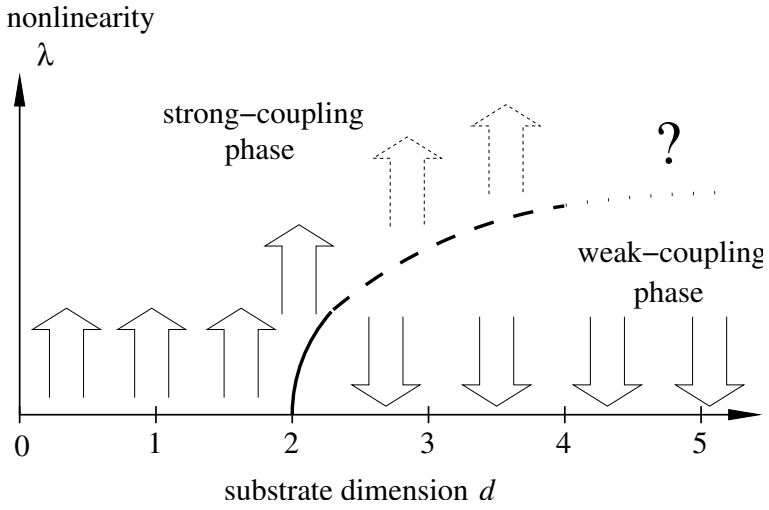

Figure 2.2: *The phase diagram for the KPZ equation.*

λ_i can take arbitrary values. For $d = 2$ Wolf [130] analyses the RG flow for arbitrary values of λ_1, λ_2. For $\lambda_1\lambda_2 > 0$ he obtains qualitatively the same result as in the isotropic case. If the two eigenvalues have different sign or one of them is zero, $\lambda_1 = \lambda_2 = 0$ is the only stable fixed point indicating the weak coupling regime.

All these methods start with regularizing the ill-defined KPZ equation. In the renormalization group approach one regularizes by introducing an ultraviolet cut-off in Fourier space. One can also discretize the KPZ equation by introducing a lattice constant, which can be viewed as an ultraviolet cut-off in real space.

A somewhat different approach is to take a definite model with a specified small scale dynamics, to determine the model dependent parameters and then *define* the KPZ field as the appropriately scaled limit of the well defined growth process. Believing in universality the limiting process does not depend on the choice of the model. This has to be thought of in much the same way as Brownian motion could be defined as the diffusive limit of any well-behaved random walk model. Since Wiener it is known that there are more elegant ways to define Brownian motion explicitely. For KPZ although there are abstract approaches [20, 8], they do not seem to be able to extract any non trivial properties of the KPZ field, so far.

We mention here two ways to extract all the model parameters for a given microscopic model. The first possibility is to take a growing droplet, whose macroscopic shape has encoded via the Legendre transform the full slope dependence of the growth velocity $v(u)$. The scaling of the height distribution along a ray in

space-time $x = ct$ can be written in the form

$$h(cT, T) = H(c)T + C(c)\, T^{\beta} \chi_d^{\text{curved}}, \tag{2.51}$$

with $\chi_d^{\text{curved}} = H_d^{\text{curved}}(0)$ the dimensionless universal random variable for curved KPZ growth. The knowledge of of $H''(c)$ and $C(c)$ allows to fix all model dependent quantities needed to determine the parameters in (2.41) at fixed macroscopic slope $H'(c)$.

The second possibility is to start with the steady state of the height process for mean slope u, $h_u(x)$, at a given time. To determine the growth velocity $v(u) = \partial_t \mathbb{E}\big(h(x)\big)$ one only needs to apply the generator of the dynamics onto the steady state, and thus requires no knowledge of dynamical correlations. If one can determine the roughness amplitude $A(u, n)$, $n \in \mathbb{R}^d$ a unit vector, defined as

$$\mathbb{E}\big((h(x) - h(0) - u \cdot x)^2\big) \simeq A(u, x/|x|)|x|^{2\alpha}, \tag{2.52}$$

the KPZ theory predicts that $x \mapsto \big(A(u, x/|x|)\big)^{1/\alpha}|x|^2$ is a positive quadratic form, and actually is a multiple of $\big(v''(u)\big)^{-1}$. The proportionality factor is given as $a(u)^{1/\alpha}$ by (2.31) with the roughness parameter $a(u)$. Again the knowledge of $v(u)$ up to second derivatives and $a(u)$ at a given slope u is enough to write down the correct scaling form (2.41) along a space-time trajectory $x = -v'(u)\, t$.

2.5 Space-time description

A convenient way to emphasize universality in stochastic growth is to regard the growing cluster as a random set C in a $d + 2$ dimensional space made up of the d substrate dimensions and an extra dimension for the height and time coordinate, each. If the cluster grows macroscopically self-similar, C has a deterministic shape in the macroscopic scaling limit,

$$\ell^{-1} C \to C_\infty, \quad \text{in probablity, for } \ell \to \infty. \tag{2.53}$$

The boundary of the cone C_∞ can be characterized by the set of zeros of a suitable homogenous function $G(x, t, h)$, as described briefly at the end of Section 2.1.2. For example one can take $G(x, t, h) = h^2 - h^{\text{det}}(x, t)^2$, where $h^{\text{det}}(x, t) = tH(x/t)$ and $H(c)$ is the Wulff shape of the cluster (2.38).

Shape fluctuations of C, i.e. the deviations from the exact limiting shape C_∞, are described by the scaling form

$$h(x, t) \simeq h^{\text{det}}(x, t) + C(x, t)\chi_d^{\text{curved}}, \tag{2.54}$$

where $C(x,t)$ is homogeneous of degree β. Comparing with the scaling form (2.41) one finds $C(ct,t) = 2^{-\beta}(\frac{a}{c_d})^{\beta/\alpha}\, t^{\beta}$, where the roughness parameter a in general depends on c. This motivates the definition of the generator of asymptotics

$$F(x,t,h) = \frac{G(x,t,h)}{C(x,t)\partial_h G(x,t,h)}, \tag{2.55}$$

which is homogeneous of order $1-\beta$. The definition of F is not unique, only its set of zeros, ∂C, the gradient at ∂C, and its degree of homogeneity are relevant. The knowledge of F, at least in a neighborhood of its set of zeros, allows to recover easily the scaling form (2.54). One solves $F(x,t,h) = 0$ for h, obtaining $h^{\text{det}}(x,t)$. Then

$$h(x,t) \simeq h^{\text{det}}(x,t) + \left(\partial_h F(x,t,h^{\text{det}}(x,t)\right)^{-1} \chi_d^{\text{curved}}. \tag{2.56}$$

F is by construction a dimensionless scalar. Under coordinate transformations it is invariant. Thus eq. (2.56) has the advantage, that it is valid for an arbitrary choice of coordinate axes (x',t',h'). One simply has to express $F(x,t,h)$ in terms of the new coordinates (x',t',h'). As long as one can solve for h' locally, (2.56) gives the scaling form in the primed coordinates. Not that by the scaling theory of Section 2.3.2 one can also determine the lateral scaling needed to have convergence to the curved KPZ field $H_d^{\text{curved}}(x)$.

2.6 The driven 2d Ising corner – a simple application

Let us illustrate the determination of the generator of asymptotics in a simple example We define a Glauber dynamics for the Ising spins on a two-dimensional square lattice with the initial conditions that in one quadrant of the plane all spins are up, all other spins are down. A spin can flip, only if exactly two of its four nearest neighbor spins are up. Under this conditions spin flips occur independently with rate r from up to down and with rate $r+\epsilon$ from down to up, driven by some chemical potential in favor of up-spins. The special initial conditions ensure that the solid-on-solid (SOS) condition is not violated, i.e. no overhangs occur, and the boundary between up-spins and down-spins can be parameterized by a time-dependent height function. If the initial borderline between ups and downs is a non-increasing or non-decreasing step-line, this property is conserved by the stochastic dynamics. The height function obtained with respect to the coordinate system spanned by the two diagonals of the lattice is known as the single-step model [120]. It is well known that the steady state of the single-step model with the above continuous-time update rule is particularly simple, the

height differences of adjacent sites are independently geometrically distributed [96]. The density, ρ, of up-steps in the steady state is related to the mean slope, $u = \langle h(x+1,t) - h(x,t)\rangle$, as $u = 2\rho - 1$. The mean growth velocity is by the absence of correlations easily obtained as

$$v(u) = 2\rho(1-\rho)(r+\epsilon-r) = \frac{\epsilon}{2}(1-u^2). \tag{2.57}$$

The critical direction being $c = -v'(u) = \epsilon u$, the macroscopic shape of the height profile is given by the Legendre transform of (2.57),

$$h^{\text{det}}(x,t) = (v(u)+cu)t = \frac{(\epsilon t)^2 + x^2}{2\epsilon t}. \tag{2.58}$$

With the same ease we calculate the roughness amplitude as

$$A(u) = \langle (h(x+1,t) - h(x,t))^2\rangle - u^2 = 1 - u^2, \tag{2.59}$$

yielding the complete asymptotic scaling form for the model as

$$\begin{aligned} h(x,t) &\simeq h^{\text{det}}(x,t) - \left(\tfrac{1}{2}|v''(u)|A(u)^2\right)^{1/3} \chi_1^{\text{curved}} \\ &= \frac{(\epsilon t)^2 + x^2}{2\epsilon t} - \left(\frac{\left((\epsilon t)^2 - x^2\right)^2}{2(\epsilon t)^3}\right)^{1/3} \chi_1^{\text{curved}}. \end{aligned} \tag{2.60}$$

Finally the generator of asymptotics for the continuous-time single-step model reads

$$G(x,t,h) = \frac{\epsilon^2 t^2 + x^2 - 2\epsilon t\, h}{2^{2/3}(\epsilon^2 t^2 - x^2)^{2/3}}. \tag{2.61}$$

Note that the generator of asymptotics depends only on the difference in the deposition and evaporation rates. The value of the evaporation rate r itself is completely irrelevant for the KPZ asymptotics of the process. Furthermore upon a simple rescaling of time we can chose $\epsilon = 1$, thereby excluding only the symmetric case. This fortunate coincidence sheds some light on the meaning of the asymptotic scaling form.

For a given value of r (2.60) tells us that for c fixed, $|c| < \epsilon$, and for a time t large enough, the distribution of $-(t(\epsilon^2 - c^2)^2/2)^{-1/3}(h(ct,t) - (\epsilon^2 + c^2)t/2\epsilon)$ is arbitrary close to the universal distribution of χ_1^{curved}. On the other hand for a given time t and location x we can always take large enough values for r such that the asymmetry in the flipping rate can be neglected and the height distribution is approximately the same as for symmetric flipping rates. This model might serve as a prototype to study the finite size corrections to the scaling form (2.43) since

by varying the flipping rate r one can control the cross-over region from purely diffusive behavior to KPZ scaling.

Only as a side remark we mention that Tang et al use an alternating parallel-update scheme in [120] (with a checker board coloring of the Ising lattice. Spins on black sites can only flip at even times and spins on a white site only at odd times). In this case, instead of rates, there are two transition probabilities, $p^{\pm} \in [0,1]$, for evaporation and deposition. This model still has a simple steady state which allows for the determination of the growth velocity and the roughness amplitude. In terms of the bias $b = p^+ - p^-$ and the product $r = (1-p^+)(1-p^-)$ one has [120]

$$v(u) = \frac{2b(1-u^2)}{\sqrt{4r+b^2} + \sqrt{4r+b^2u^2}} \tag{2.62}$$

and

$$A(u) = \frac{2(1-u^2)\sqrt{4r+b^2u^2}}{\sqrt{4r+b^2} + \sqrt{4r+b^2u^2}}. \tag{2.63}$$

Some simple but tedious algebra then yields for the scaling form

$$\begin{aligned} h(x,t) \;=\; & \frac{sr\,tx^2 + b\sqrt{4t^2-x^2}t^2}{4t^2-(1-rd^2)x^2 + sd\sqrt{4t^2-x^2}t} \\ & - \frac{2^{2/3}(4t^2-(1+4r^2)x^2)^{2/3}t^{4/3}}{(4t^2-x^2)^{5/6}(4rb\,t + s\sqrt{4t^2-x^2})^{2/3}}\chi_1^{\text{curved}} \end{aligned} \tag{2.64}$$

with the additional abbreviation $s = (1-p^+) + (1-p^-)$. The corresponding generator of asymptotics for this discrete-time single-step model (which we do not write down here because of its length) can serve, for example, to express the scaling form in the original coordinates of the Ising lattice.

CHAPTER 3

The (1+1)-dimensional Polynuclear Growth model

The polynuclear growth (PNG) model is an idealized model for surface growth [52, 47]. The discrete crystalline structure of the solid is retained only in one spatial direction. As a model for layer-by-layer growth it mimics a crystal interface along a high symmetry direction. Within the $(1+1)$-dimensional PNG model the interface is described by an integer-valued height function $h(x,t)$ on a one-dimensional substrate $x \in \mathbb{R}$. Thus the interface consists of terraces bordered by steps of unit height. The steps are at arbitrary positions in $\mathbb{R}$, cf. Fig. 3.1.

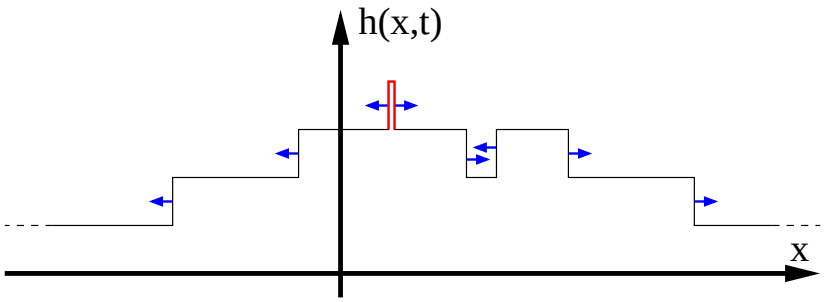

Figure 3.1: *A possible configuration of the height function $h(x,t)$ at time t.*

The dynamics has a deterministic and a stochastic part. Terraces grow deterministically in the lateral direction. Up-steps move to the left with velocity $-w$ and down-steps move to the right with velocity w. Two adjacent terraces on the same level eventually coalesce into a single one, which means that an up/down step pair, where the down step is to the immediate right of the up-step, disappears upon collision.

The stochastic part of the dynamics comes from the nucleation of spikes of unit height forming new terraces upon already existing ones. Independently with space-time density ξ up/down step pairs are generated together at one position and immediately move apart into opposite directions.

In order to identify the one-dimensional PNG model as a member of the 1d KPZ universality class we first study the stationary growth velocity and the static

roughness. Let $x \mapsto h(x,0)$ be a two sided random walk of mean slope u, $h(0,0) = 0$. This means that the positions of up-steps and down-steps are drawn from two independent Poisson point processes on $\mathbb{R}$ with densities p_+ and p_-, respectively, $p_+ - p_- = u$. During an infinitesimal time interval dt, inside an interval of length L the mean production of new up/down step pairs, $\xi L\, dt$, has to match the average annihilation $2wp_+p_-Ldt$. As a necessary condition for stationarity the density of up- and down-steps has to be preserved, which implies $p_+p_- = \xi/(2w)$.

To simplify notation we set $w = 1$ and $\xi = 2$ in the sequel, reinstating w and ξ only in some formulas where it seems appropriate. This convention is obtained for any values of w and ξ by measuring x in units of $\sqrt{w/\xi}$ and t in units of $1/\sqrt{w\xi}$.

The fact that the full distribution of up- and down-steps remains independent Poisson is not obvious but not very hard to show. One way is to explicitly solve for the steady state of the master equation for the step positions in finite volume with periodic boundary conditions and then to take the infinite volume limit [19]. On the other hand it is an immediate consequence of the following Poisson property of the stationary PNG process extended to arbitrary negative times, which is proven in Section 4.4 by taking the continuum limit of a discretized version of the PNG model.

Proposition 3.1 *For the stationary height process $h(x,t)$ with mean slope 0 the crossing positions of up- and down-step trajectories along a space-like direction $\{t = bx\}$ with $|b| \le 1$ are distributed like two independent Poisson point processes with line densities $p_+^b = (1+b)/\sqrt{1+b^2}$ and $p_-^b = (1-b)/\sqrt{1+b^2}$, respectively.*

Thus for a space-like separation $|x| \ge t$ the height difference $h(x,t) - h(0,0)$, is distributed as the position of a drifting random walk with mean $2t$ and variance $2x$. Furthermore, the stationary process with mean slope u can be constructed from the stationary process with mean slope 0 by means of the Lorentz transformation

$$x' = (1-c^2)^{-1/2}(x - ct), \quad t' = (1-c^2)^{-1/2}(t - cx), \tag{3.1}$$

where the speed of "light" is 1 and the velocity parameter $c = -u/\sqrt{4+u^2}$. The mapping preserves the deterministic dynamics, leaves invariant the space-time density of nucleation events and maps the Poisson rates $p_\pm$ for $t = 0$ correctly.

For the slope dependent growth velocity $v(u) = \partial_t \langle h(x,t)\rangle$ we thus obtain the relation

$$v(u) = w(p_+ + p_-) = w\sqrt{\frac{2\xi}{w} + u^2}, \tag{3.2}$$

Obviously it is a convex function of u with non-vanishing curvature. Together with the locality of the stochastic growth rule it tells us already that the model lies in the KPZ universality class.

Since $x \mapsto h(x,t)$ is a random walk the static roughness exponent is $1/2$, consistent with the KPZ prediction in one dimension. The roughness amplitude $A = x^{-1}\langle (h(x,t) - h(0,t) - ux)^2$, by the Poisson property, is given by

$$A(u) = p_+ + p_- = \sqrt{\frac{2\xi}{w} + u^2}. \tag{3.3}$$

Indeed, (3.2) and (3.3) fix already all the model dependent parameters (again with $w = 1$, $\xi = 2$), $\lambda(u) = v''(u) = 4(4+u^2)^{-3/2}$ and $A(u) = \sqrt{4+u^2}$, which allows to extract universal quantities from the quantitative scaling properties of the PNG height process.

The directed polymer. There is an equivalent formulation of the PNG model as a zero temperature directed polymer in a random environment. We fix the initial conditions $x \mapsto h(x,0)$ and take a realization of nucleation events in the half plane $\{t \geq 0\}$. In Figure 3.2 the trajectories of up- and down-steps are drawn. They

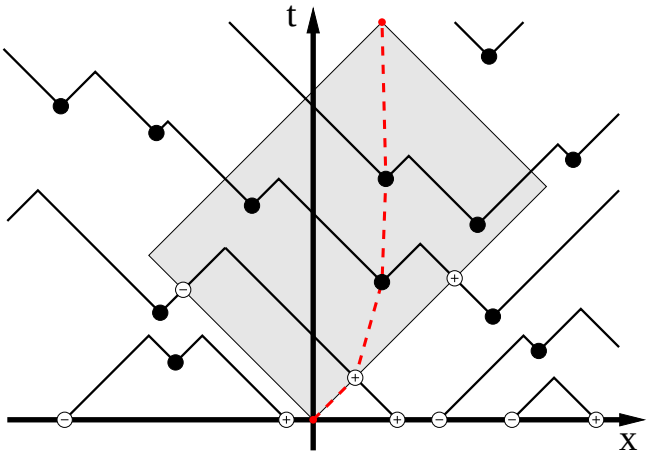

Figure 3.2: *A space-time picture of the PNG model and a corresponding longest polymer.*

form the height lines of $h(x,t)$ in space-time. The height difference $h(y,t) - h(x,s)$, where (y,t) lies in the forward light cone of (x,s), i.e. $|y-x| \leq t-s$, is given by the number of height lines crossed by a time-like path $\gamma : [s,t] \to \mathbb{R}$ from (x,s) to (y,t), where time-like means that $|\gamma(s') - \gamma(s'')| \leq |s' - s''|$ for $s', s'' \in [s,t]$. A directed path is a piecewise linear time-like path γ where jumps in the gradient of γ are only allowed at nucleation events inside the rectangle $R = \{(x',s');\ |x'-x| \leq s'-s,\ |x'-y| \leq t-s'\}$ or at incoming height lines at the lower edges of R, $\{(x',s');\ x-x' = s-s'\} \cap R$ and $\{(x',s');\ x'-x = s-s'\} \cap R$ which we address as nucleation events for R as well.

We define the length of such a directed path γ as the number of nucleation events met by γ and claim that $h(y,t) - h(x,s)$ equals the length of the longest directed path from (x,s) to (y,t). To see this, note that two points on such a path always belong to nucleation events in different levels, thus the number of points on a path is always smaller or equal to $h(y,t) - h(x,s)$. But a maximal path with $h(y,t) - h(x,s)$ points is easily constructed by starting from (y,t) and working one's way back to (x,s), since each nucleation event in R which belongs to level l has at least one nucleation event belonging to level $l-1$ in its backward light cone. Note that the directed path can pick up nucleation events along either of the lower edges of R only until it eventually enters the bulk of R.

A directed polymer is a directed path γ whose energy is given by the negative length of γ. Since the mapping from PNG to the directed polymer is realization-wise we conclude that the distribution of $h(x,s) - h(y,t)$ equals the ground state energy of a directed polymer from (x,s) to (y,t).

The PNG cluster. A nice geometric interpretation of the PNG model is in terms of the set $D = \{(x,t,h);\, h \le h(x,t)\}$, the space-time image of the PNG cluster. $D \subset \mathbb{R}^3$ is a random set made up of level sets $D_l \subset \mathbb{R}^2$, $l \in \mathbb{Z}$, such that $D = \bigcup_{l\in\mathbb{Z}} D_l \times [l-1, l]$. Now fix an arbitrary subset $A \subset [c, \infty[^2$, $c \in \mathbb{R}$ some constant, as initial condition and set $D_l = A + [0,\infty[^2$ for $l \le 0$. Randomness is introduced by taking for each level $l > 0$ independent Poisson point processes P_l on $\mathbb{R}^2$ with density 2, $P_l \subset \mathbb{R}^2$ being the set of Poisson points. The level sets are than defined recursively as

$$D_l = (P_l \cap D_{l-1}) + [0,\infty[^2, \quad l > 0. \tag{3.4}$$

In Figure 3.3 a part of a PNG cluster with initial condition $A = \{(0,0)\}$ is shown, it corresponds to the "droplet" initial condition $h(0,0) = 0$ and $h(x,0) = -\infty$ for $x \neq 0$. The PNG cluster is just a static description of the PNG dynamics of the height function $h(x,t) = \max\{l;\, (x,t) \in D_l\}$. In order to recover arbitrary initial conditions $x \mapsto h(x,0)$ one has to allow for initializing sets $A_l = \{x;\, h(x,0) \ge l\}$ in level l respectively. The recursion (3.4) is modified to $D_l = \big((A_l \cup P_l) \cap D_{l-1}\big) + [0,\infty[^2$ with $l \in \mathbb{Z}$. In the case that $h(x,0)$ is unbounded from below one has to construct D as the limit $k \to \infty$ of clusters with initial condition $x \mapsto \max\{h(x,0), -k\}$.

The Aldous-Diaconis-Hammersley process. Yet another equivalent formulation of the PNG model is the Aldous-Diaconis-Hammersley (ADH) process [60, 5, 76] whose hydrodynamics and diffusive properties have been studied by Seppäläinen [111, 112, 113]. We have a countable collection of point particles on $\mathbb{R} \cup \{\infty\}$ whose positions at time s are labeled by $r_i(s)$, $i \in \mathbb{Z}$. Particles are

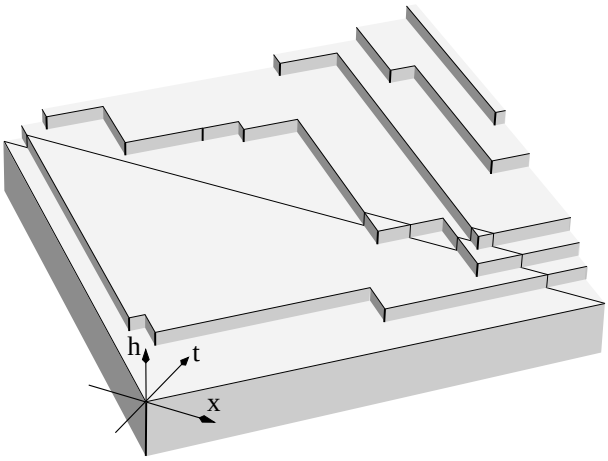

Figure 3.3: *A small PNG cluster with initial condition* $A = \{(0,0)\}$.

ordered, $r_{i-1}(s) \leq r_i(s)$, which is preserved under the dynamics. They can only jump to the left and are otherwise at rest. At time s the i'th particle jumps with rate $r_i(s) - r_{i-1}(s)$ independently of all other particles and lands anywhere in the interval $[r_{i-1}(s), r_i(s)]$ with uniform probability. The process is well defined if the distance between adjacent particles with large negative index does not get to large, more precisely if $r_i = o(i^2)$ for $i \to -\infty$ [113]. Note that the end points of particle jumps, irrespectively of particle positions, form a Poisson point process in the whole (r,s)-plane with density 1. If $\lim_{i\to-\infty} r_i = r > -\infty$ the Poisson points are restricted to $[r,\infty[\times\mathbb{R}$.

To establish the connection to the PNG model, we define the height function $H(r,s) = \int_0^r \sum_i \delta\big(r - r_i(s)\big)dr$. Now it is fairly obvious that the transformed height function

$$h(x,t) = H(t+x, t-x) \tag{3.5}$$

is a PNG height process with initial/boundary condition $x \mapsto h(x,-x) = H(x,0)$ and only defined in $\{(x',t');\, x \geq -t\}$. Under the rotation by $45°$ up-step trajectories of PNG correspond to particles at rest in ADH and down-step trajectories correspond to jumps of particles. The overall scaling by a factor $\sqrt{2}$ accounts for the nucleation rate 2 in PNG.

3.1 The PNG droplet

Droplet growth for the PNG model is obtained by the proper choice of initial conditions. We choose $h(0,0) = 0$ and $h(x,0) = -\infty$ for $x \neq 0$. The ground layer at level zero starts at $t = 0$ and extends laterally with velocity one in both

directions. Thus only nucleation events above the ground layer, i.e. at space-time points (x,t) with $|x| \le t$, are relevant. Obviously $h(\pm t,t) = 0$ with probability 1, growth occurs only in the interval $[-t,t]$. These initial condition correspond to an initial set $A = \{(0,0)\}$ for the PNG cluster.

From the macroscopic theory, Section 2.1, at large times we expect the PNG cluster to form a droplet whose shape is given by the Wulff construction. Thus from (3.2) (with $w = 1$, $\xi = 2$) we have $h(x,t) \simeq 2\sqrt{t^2 - x^2}$. The initial conditions for the PNG droplet correspond to an initial set $A = \{(0,0)\}$ for the three-dimensional PNG cluster, which macroscopically has the shape of a cone. Figure 3.4 shows a piece of such a PNG cone.

From the KPZ theory for curved growth, Section 2.1.1, we estimate the height fluctuations of the PNG cone as

$$h(x,t) \simeq 2\sqrt{t^2 - x^2} + C(x/t)t^{1/3}\chi_1^{\text{droplet}}, \quad \text{as } t \to \infty,\ x = ct, \tag{3.6}$$

in distribution. The dynamical exponent $\beta = \frac{1}{3}$ follows from the scaling relation (2.30). The distribution of χ_1^{droplet} is the universal distribution for one-dimensional curved KPZ growth. The function $C(c)$ depends only on the direction of the ray $x = ct$ along which one observes the distribution of $h(x,t)$. It determines the absolute scale on which χ^{droplet} is observed. By the scaling form (2.41) it is given by $C(c) = (\frac{1}{2}\lambda(u)A(u)^2)^{1/3}$ with u such that $v'(u) = c$, thus we can predict $C(c) = (1-c^2)^{1/6}$.

In the directed polymer picture the rectangle $R_{(x,t)} = \{(x',t');\ |x'| \le t', |x - x'| \le t - t'\}$ has no incoming lines at all. Its length is determined exclusively by the Poisson points of density 2 inside the rectangle. Since the Lorentz transformation (3.1) leaves invariant the PNG dynamics we can map $R_{(x,t)}$ to the square $R_{(0,v)}$ with $v = \sqrt{t^2 - x^2}$. We conclude that the distribution of $h(x,t)$ for the PNG droplet depends only on v. Therefore, provided the dynamical exponent $\beta = \frac{1}{3}$ is correct, one has

$$h(x,t) \simeq 2v + C\, v^{1/3}\chi_1^{\text{droplet}} \tag{3.7}$$

confirming (3.6), where the constant C is set to one by convention and thereby defines the absolute scale of χ_1^{droplet}.

3.1.1 Ulam's problem.

Take a random permutation of length N, i.e. each permutation $p \in S_N$ has the same probability $1/N!$. An increasing subsequence of length n of the permutation $p = \big(p(1), \dots, p(n)\big)$, is specified by the indices $i_1 < \cdots < i_k$, such that $p(i_1) < \cdots < p(i_k)$. In 1961 Ulam [124] presented the problem to determine the asymptotics of the length l_N of the longest increasing subsequence in such a

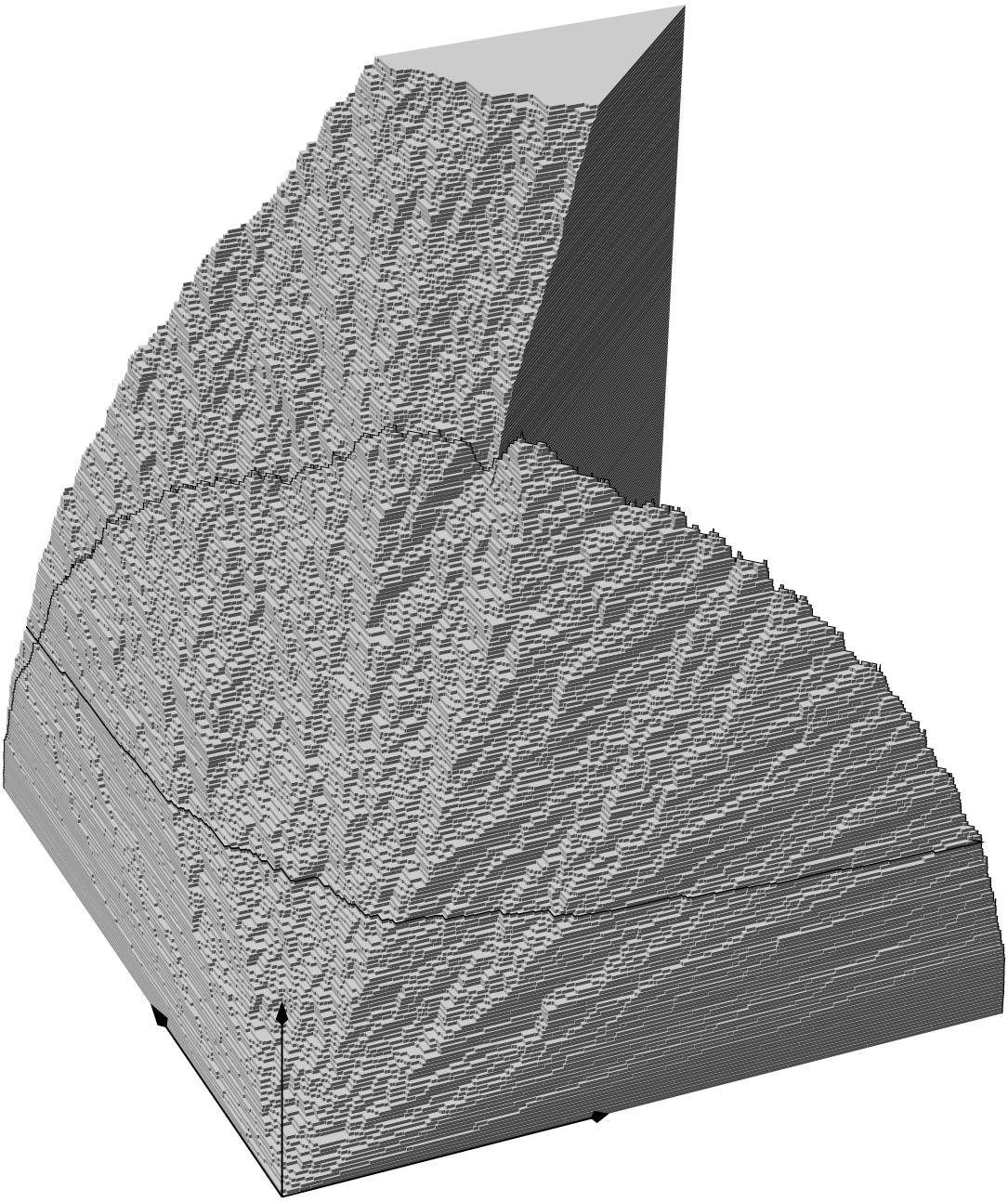

Figure 3.4: *A large piece of a PNG cone in light coordinates. It has been cut in a way to improve the 3d impression. The black vertical line represents a PNG line* $x \mapsto h(x,t)$*. The horizontal line marks a level set* D_l*.*

random permutation. As example take the permutation $p = (4, 7, 5, 2, 8, 1, 3, 6)$. Then (5), $(4, 7)$, $(2, 3, 6)$, $(4, 5, 8)$ are increasing subsequences of p, but only the last two of them are maximal.

A survey of the history of Ulam's problem is given in [6]. Ulam already conjectured that $l_N/\sqrt{N} \to c$ for large N, Hammersley's treatment of the question [60] strongly suggested $c = 2$. Logan and Shepp [84] and Vershik and Kerov [125] independently showed, in essence, convergence to $c = 2$ in probability. Then, 1999, Baik, Deift, and Johansson in their by now already famous work [10] settled the problem by determining not only the rate of convergence but also identifying the limiting distribution. They show that

$$\lim_{N\to\infty} \text{Prob}\{l_N - 2N^{1/2} \le N^{1/6}s\} = F_{\text{GUE}}(s), \tag{3.8}$$

which means that l_N is distributed asymptotically for large N as $2N^{1/2}+N^{1/6}\chi_{\text{GUE}}$ were χ_{GUE} is a random variable with distribution function $F_{\text{GUE}}(s) = \text{Prob}\{\chi_{\text{GUE}} \le s\}$. It is called the Tracy-Widom GUE distribution [121] and arises as the distribution of the properly rescaled largest eigenvalue of a random matrix drawn from the general unitary ensemble (GUE), see Mehta [90] for an introduction.

The definition of $F_{\text{GUE}}(s)$ is slightly involved. We have to introduce the Hastings-McLeod solution $u(s)$ to the Painlevé II equation

$$u''(s) = 2u(s)^3 + s\,u(s). \tag{3.9}$$

which is specified uniquely by requiring $u(s) < 0$ for $s \in \mathbb{R}$ [61]. It has asymptotics

$$u(s) \sim -\text{Ai}(s) \quad \text{for } s \to \infty \tag{3.10}$$

and

$$u(s) \sim -\sqrt{\frac{-s}{2}} \quad \text{for } s \to -\infty. \tag{3.11}$$

$u(s)$ interpolates smoothly between its left and right asymptotics with $u'(s) > 0$ for $s \in \mathbb{R}$. We define the auxiliary functions

$$U(s) = -\int_s^\infty u(x)dx, \tag{3.12}$$

$$v(s) = (u(s)^2 + s)u(s)^2 - u'(s)^2, \tag{3.13}$$

$$V(s) = -\int_s^\infty v(x)dx. \tag{3.14}$$

Note that $U' = u$, $V' = v$, and $v' = u^2$ by (3.9). Finally the Tracy-Widom GUE distribution function is defined as

$$F_{\text{GUE}}(s) = e^{-V(s)}. \tag{3.15}$$

Before we further explain the result let us get the connection to the PNG droplet. We fix a realization of nucleation events in the square $R_{(0,v)}$. The alignment of an enumeration of the nucleation events (x_i, t_i), $i = 1, \dots, N$, with respect to the light-like coordinates $r_i = t_i + x_i$ and $s_i = t_i - x_i$ uniquely defines a permutation p of length N with probability one. To see this assume that the points are ordered such that $r_1 < r_2 < \cdots < r_n$. Now there is a unique permutation $\big(p(1), p(2), \dots, p(N)\big)$ such that $s_{p(1)} < s_{p(2)} < \cdots < s_{p(N)}$, cf. Fig. 3.5. The

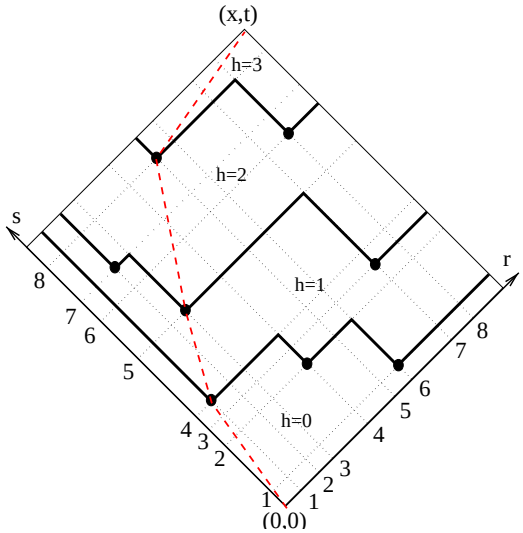

Figure 3.5: *Space-time picture for the height of a small PNG droplet at* (x, t) *with light-like coordinates* r, s*. The dashed line is a maximal directed path. The nucleation events correspond to the permutation* $(4, 7, 5, 2, 8, 1, 3, 6)$.

nucleation events met by a directed path define an increasing subsequence of p, which yields a one-to-one correspondence between directed paths and increasing subsequences.

Conditioned on a fixed number N of points in $R_{(0,v)}$ the Poisson point process induces equal weight $1/N!$ for all permutations $p \in S_N$. Therefore we conclude that $h(x, t)$ is distributed as the length l_v of the longest increasing subsequence of a random permutation having random length N, where N has Poisson distribution with mean v^2, $v = \sqrt{t^2 - x^2}$.

This is almost the statement (3.8). It turns out that the Poissonized version of l_N, l_v with $\langle N \rangle = v^2$ is much easier to study than l_N directly. In [10] actually (3.8)

is proven for l_v and the result for l_N follows from "depoissonization" lemmas. In summary let us state the result obtained for the height distribution of the PNG droplet [98]:

Theorem 3.2 *Let $h(x,t)$ be the height process corresponding to the PNG droplet, $|c| \leq 1$, then*

$$\lim_{t\to\infty} \text{Prob}\Big\{ \frac{h(ct,t) - 2t\sqrt{1-c^2}}{(1-c^2)^{1/6} t^{1/3}} \leq s \Big\} = F_{\text{GUE}}(s). \tag{3.16}$$

Let us describe the derivation of (3.8). The starting point is an explicit expression for $F_n^{\text{GUE}} = \text{Prob}\{h(0,v) \leq n\}$. We suppress writing down the explicit dependence on v in the following. In short F_n^{GUE} is expressed as an expectation with respect to the Haar measure over the unitary group $U(n)$, which can be written as a Toeplitz determinant,

$$\begin{aligned} F_n^{\text{GUE}} &= e^{-v^2} \mathbb{E}_{U\in U(n)} \big(e^{v\,\text{tr}(U+U^{-1})} \big) \\ &= e^{-v^2} \det T_n \big(e^{2v\cos\theta} \big). \end{aligned} \tag{3.17}$$

$T_n\big(f(\theta)\big) = (\mu_{k-l})_{0\leq k,l<n}$ is a $n \times n$ Toeplitz matrix with weight function $f(\theta)$. Its entries are the Fourier coefficients of $f(\theta)$, $\mu_k = (2\pi)^{-1} \int_0^{2\pi} e^{ik\theta} f(\theta) d\theta$. The first identity in (3.17) follows from work of Gessel [51]. It is a very remarkable relation which is based on the Robinson-Schensted-Knuth correspondence between permutations and pairs of standard Young tableaus. Concise derivations can be found in [6] or in the Appendix of [10]. The second identity is a very general correspondence between determinantal expectations of the unitary group and Toeplitz determinants. One has for arbitrary functions f and g integrable on the unit circle ([12], Thm. 2.1)

$$\mathbb{E}_{U\in U(n)} \det \big(f(U) g(U^{-1}) \big) = \det T_n \big(f(e^{i\theta}) g(e^{-i\theta}) \big). \tag{3.18}$$

As a side remark let us mention that there is a similar formula as (3.17) for random permutations with fixed length N [104, 6],

$$\text{Prob}\{l_N \leq n\} = (N!)^{-1} \mathbb{E}_{U\in U(n)} \big(|\text{tr}(U)^N|^2 \big). \tag{3.19}$$

One recovers (3.17) by noting that

$$F_n^{\text{GUE}} = \sum_{N\geq 0} \frac{v^{2N}}{N!} \text{Prob}\{l_N \leq n\} \tag{3.20}$$

and that $\mathbb{E}_{U\in U(n)} \big([\text{tr}(U) + \text{tr}(U^{-1})]^{2N} \big) = \binom{2N}{N} \mathbb{E}_{U\in U(n)} \big([\text{tr}(U)^N + \text{tr}(U^{-1})^N]^2 \big)$. The latter holds because $\mathbb{E}_{U\in U(n)} \big(\text{tr}(U)^k \text{tr}(U^{-1})^l \big) = 0$ for $k \neq l$ by the invariance of the Haar measure under the transformation $U \mapsto e^{i\varphi} U$.

3.1.2 Orthogonal polynomials.

We need to deal with the Toeplitz determinant $D_n = \det T_n\big(f(\theta)\big)$. A standard tool to do so are orthogonal polynomials on the unit circle [118]. We introduce the polynomials $\pi_n(z)$ which arise from the Gram-Schmidt orthogonalization procedure of the functions z^n, $n \geq 0$, with respect to the measure concentrated on the unit circle $d\mu(z) = e^{-v(z+z^{-1})}dz(2\pi iz)^{-1}$. Thus the polynomials are orthogonal with respect to the inner product

$$\langle p, q\rangle = \oint p(z)\overline{q}(z^{-1})d\mu(z) = (2\pi)^{-1}\int_0^{2\pi} p(e^{i\theta})\overline{q(e^{i\theta})}e^{2v\,\cos\theta}d\theta, \tag{3.21}$$

where $\overline{\cdot}$ denotes complex conjugation, and $\overline{q}$ means conjugating the coefficients of q. The polynomials are defined to be monic, $\pi_n(z) = z^n + \mathcal{O}(z^{n-1})$. Their squared norm is denoted by N_n, thus

$$\langle \pi_m, \pi_n\rangle = \delta_{m,n}N_n. \tag{3.22}$$

The Toeplitz determinant $D_n = T_n\big(e^{-2v\,\cos\theta}\big)$ in this notation reads

$$D_n = \det(\langle z^k, z^l\rangle)_{0\leq k,l<n} \in \mathbb{R}. \tag{3.23}$$

We define the reciprocal polynomials

$$\pi^*(z) = z^n\overline{\pi_n}(z^{-1}) \tag{3.24}$$

and abbreviate $p_n = \pi_n(0)$. Let us mention that since all the coefficients of π_n are real one has $\overline{\pi_n}(z) = \pi_n(z)$.

Classical results from the theory of orthogonal polynomials on the circle [118] relate the Toeplitz determinants to the norms of π_n.

$$D_n = \prod_{k=0}^{n-1} N_k \tag{3.25}$$

and for the squared norm one has

$$N_n = N_0\prod_{k=1}^{n}(1-p_k^2). \tag{3.26}$$

With the special weight function $f(\theta) = e^{-2v\,\cos(\theta)}$ one obtains a nonlinear recursion relation for the p_n, the discrete Painlevé II equation. It has been derived in the context of orthogonal polynomials for the first time in [94], and later on more or less independently in [62, 123, 9, 24]. One has

$$p_{n+1} = -\frac{\frac{n}{v}p_n}{1-p_n^2} - p_{n-1} \quad \text{for } n > 0, \tag{3.27}$$

with initial values $p_0 = 1$, $p_1 = -\frac{I_1(2v)}{I_0(2v)}$. For the convenience of the reader we prove equations (3.25), (3.26), and (3.27) in Appendix A.

Setting

$$R_n = -(-1)^n p_n, \tag{3.28}$$

we rewrite (3.27) as

$$R_{n+1} - 2R_n + R_{n-1} = \frac{(\frac{n}{v} - 2)R_n + 2R_n^3}{1 - R_n^2}. \tag{3.29}$$

In order to obtain a non trivial continuum limit of this second order difference equation we introduce the scaling variable s in the limit $v \to \infty$ and set

$$n = [2v + v^{1/3}s] \tag{3.30}$$

Approximating R_n by the the smooth function $u(s)$ as

$$R_n = v^{-1/3}u\big(v^{-1/3}(n - 2v)\big) + \mathcal{O}(v^{-1}) \tag{3.31}$$

and taking the limit $v \to \infty$ implies that $u(s)$ satisfies the Painlevé II equation (3.9). The starting value $R_0 = -1$ is consistent with the left asymptotics of $u(s)$ only if

$$u(s) \sim -\sqrt{-s/2} \quad \text{as } s \to -\infty, \tag{3.32}$$

which singles out the Hastings-McLeod solution $u(s) < 0$. We conclude that

$$u(s) = \lim_{v\to\infty} v^{1/3} R_{[2v+v^{1/3}s]}, \tag{3.33}$$

provided the limit exists. We do not know of a direct proof of this convergence. In [10] it is shown by means of the Deift-Zhou steepest decent method for associated Riemann-Hilbert problems [37]. The convergence $F_n^{\text{GUE}} \to F_{\text{GUE}}(s)$ under the scaling (3.30) follows from (3.33) by noting that the second log-derivative of the latter is

$$\frac{d^2}{ds^2} \ln(F_{\text{GUE}}(s)) = -u(s)^2 \tag{3.34}$$

and

$$\frac{D_{n+1}D_{n-1}}{D_n^2} = 1 - R_n^2, \tag{3.35}$$

since $F_n^{\text{GUE}} = e^{-v^2} D_n$.

3.2 Flat initial conditions and other symmetry restrictions

In the physical literature it is very common to study flat initial conditions for surface growth. For Monte-Carlo simulations this is a preferred situation since the flat initial profile is easily prepared and the growth process is spatially translation invariant. This property is preserved when the infinitely extended substrate is approximated by a finite substrate with periodic boundary conditions. Thus the ensemble averaging of the local height statistics can be replaced or supplemented by spatial averaging.

For the PNG model flat initial conditions are defined by $h(x,0) = 0$ for $x \in \mathbb{R}$ with nucleation events possible everywhere on the real line. The KPZ scaling theory predicts for the distribution of the height above $x = 0$

$$h(0,t) \simeq 2t + t^{1/3}\chi_1^{\text{flat}}, \quad \text{as } t \to \infty. \tag{3.36}$$

The absolute scale for the random variable χ_1^{flat} is the same as for the droplet at zero slope, i.e. $c = 0$ in (3.6). Analogously to the droplet case a mapping to longest increasing subsequences of random permutations [99] leads to a proof of (3.36) [14] and the identification of χ_1^{flat} as the Tracy-Widom GOE distribution [122].

Let us describe the directed polymer picture for flat initial conditions. For a given space-time realization of nucleation events $h(0,t)$ depends only on Poisson points inside the triangle $T_t = \{(x',t');\ |x'| \le t - t',\ t' \ge 0\}$. The height $h(0,t)$ equals the length of a longest directed path in the square $R_t = \{(x',t');\ |x'| \le |t| - |t'|\}$ from $(0,-t)$ to $(0,t)$, where all the points lie in the upper half T_t. Equivalently we can define a line-to-point directed polymer in the triangle T_t. It ends in $(0,t)$ but is allowed to start anywhere in $[-t,t] \times \{0\}$. Since the distribution of the length of a longest directed path is invariant under the transformation $t' \mapsto t - t'$ the distribution of $h(0,t)$ equals the realizationwise maximum of directed polymers starting from $(0,0)$ and ending somewhere in $\{(x',t);\ |x'| \le t\}$. This simple observation of the connection between point-to-line and point-to-point directed polymers (first mentioned, to our knowledge, in the context of growth in a footnote in [77]) allows us to express $h(0,t)$ in terms of the PNG droplet process from the previous section, denoted here $h^{\text{droplet}}(x,t)$, as

$$h(0,t) = \max_{x \in [-t,t]} h^{\text{droplet}}(x,t) \qquad \text{in distribution.} \tag{3.37}$$

To access the asymptotic distribution of $h(0,t)$ let us mirror the Poisson points in T_t into $\left(\begin{smallmatrix} 1 & 0 \\ 0 & -1 \end{smallmatrix}\right) T_t$. Obviously $2h(0,t)$ is now distributed as a point-to-point directed polymer from $(0,-t)$ to $(0,t)$, where the random environment, the set of

Poisson points, P, is symmetric, $P = \left(\begin{smallmatrix} 1 & 0 \\ 0 & -1 \end{smallmatrix}\right) P$. As in the droplet case each realization of $2N$ Poisson points inside R_t corresponds to a random permutation p of length $2N$ which has the symmetry restriction $p\big(2N+1-p(k)\big) = 2N+1-k$, and we need the length l_t of the longest increasing subsequence in such a random permutation of length $2N$, where N is Poisson distributed with mean $2t^2$. Equivalently, by defining the permutation $q(k) = p(2N+1-k)$ one can think of the longest *decreasing* subsequence in a random involution, $q^2 = id$. Baik and Rains study exactly this case in [14]. They start with

$$\text{Prob}\{l_t \le 2n\} = e^{-t^2/2}\mathbb{E}_{U\in Sp(2n)}\big(e^{t\,\text{tr}\,U}\big), \tag{3.38}$$

where the expectation is over the Haar measure of the symplectic group $Sp(2n)$ [104, 12]. Similarly to the case of the unitary group, such an expectation can be expressed by the determinant of a combination of Toeplitz and Hankel matrices (a Hankel matrix has entries constant along anti-diagonals). It is dealt with the same orthogonal polynomials (3.22) as in the pure Toeplitz case. Baik and Rains obtain [12]

$$\mathbb{E}_{U\in Sp(2n)}\big(e^{t\,\text{tr}\,U}\big) = \prod_{k=0}^{n-1} N_{2k+2}(1-p_{2j+2})^{-1}. \tag{3.39}$$

We scale as in the droplet case, $n = [2t + t^{1/3}s]$. Given the limit (3.33) one arrives at the limiting distribution

$$\lim_{t\to\infty} \text{Prob}\{l_t - 4t \le (2t)^{1/3}s\} = F_{\text{GOE}}(s), \tag{3.40}$$

where

$$F_{\text{GOE}}(s) = e^{-\frac{1}{2}(U(s)+V(s))} \tag{3.41}$$

is the Tracy-Widom GOE distribution which appears in the theory of random matrices as the properly scaled distribution of the largest eigenvalue of a random matrix from the general orthogonal ensemble (GOE) [122]. Since $h(t,0) = \frac{1}{2}l_t$ we can state the final result for $h(0,t)$.

Theorem 3.3 *Let $h(x,t)$ be the height process corresponding to the PNG model with flat initial conditions, then*

$$\lim_{t\to\infty} \text{Prob}\Big\{\frac{h(0,t)-2t}{t^{1/3}} \le 2^{-2/3}s\Big\} = F_{\text{GOE}}(s). \tag{3.42}$$

Note that because of the relation $l_t = 2h(0,t)$, the universal random variable $\chi_1^{\text{flat}} = 2^{2/3}\chi^{\text{GOE}}$.

In the beautiful work of Baik and Rains ([14] for a survey, [12, 13] for the details) longest increasing subsequences of random permutations restricted to other symmetry classes are analyzed. We translate their results to identify further asymptotic distributions arising when the growth process is confined by a rigid wall.

We restrict the PNG model to the half line, $x \geq 0$, up-steps reaching $x = 0$ just disappear. With the initial condition $h(0,0) = 0$ and $h(x,0) = -\infty$ for $x > 0$ a half droplet is growing with macroscopic shape $\sqrt{t^2 - x^2}$, $x \geq 0$. $h(0,t)$ is determined by the Poisson points in $\{(x',t');\, 0 \leq x' \leq t', x' \leq t - t'\}$. Alternatively one can think of the original PNG model on the whole line $x \in \mathbb{R}$ growing symmetrically around $x = 0$. Thus a nucleation event occurring at (x,t), $x \geq 0$ is mirrored and implies a similar nucleation event at $(-x,t)$. The permutations corresponding to Poisson point realizations inside the square $\{(x',t');\, |x'| \leq t', |x'| \leq t - t'\}$ are involutions. In this case a similar expression is obtained as in (3.38) with the symplectic group replaced by the orthogonal group $O(n)$. The analysis of the corresponding Hankel/Toeplitz determinants in terms of the orthogonal polynomials (3.22) in the scaling limit leads to the Tracy-Widom GSE distribution

$$F_{\mathrm{GSE}}(s) = \tfrac{1}{2}\big(e^{-\frac{1}{2}U(s)} + e^{\frac{1}{2}U(s)}\big)e^{-V(s)}, \tag{3.43}$$

the properly rescaled distribution of the largest eigenvalue of a random matrix from the general symplectic ensemble (GSE) [122].

Theorem 3.4 *Let $h(x,t)$ be the height process corresponding to the PNG half droplet, then*

$$\lim_{t\to\infty} \mathrm{Prob}\Big\{\frac{h(0,t) - 2t}{t^{1/3}} \leq s\Big\} = F_{\mathrm{GSE}}(s). \tag{3.44}$$

Here the height $h(ct,t)$ is obtained only for $c = 0$ where $x = ct$. For other values of c no analytic results are available. From KPZ theory we expect that for any $0 < c \leq 1$ the droplet case (3.16) should be recovered, since the correlation length for height fluctuations increases only with $t^{2/3}$. In the polymer picture the symmetry of the Poisson points is seen by the polymer only in the very beginning up to a time t' of order $t^{1/3}$. This does not affect the scaling limit.

Let us mention that Baik and Rains can also deal with a source of Poisson points of arbitrary line density $\alpha \geq 0$ above the origin $x = 0$. The result is as expected. When $\alpha < 2$ the limiting distribution (3.44) is unchanged. It does not pay for the polymer to go along the line of Poisson points for a macroscopic fraction of time. For $\alpha > 2$ the polymer stays at $x = 0$ for most of the time

because, on the average, it there collects more Poisson points than in the bulk. By the central limit theorem the asymptotic height distribution is given by a Gaussian on the scale $t^{1/2}$. Only if $\alpha = 2 + t^{-1/3}y$, y fixed, the number of Poisson points from the line is such that their fluctuations are on the same order as the bulk fluctuations. One obtains a smooth transition from GSE for $y \ll 0$ to a Gaussian with variance proportional to y for $y \gg 0$. For $\alpha = 2$, the critical value, F_{GOE} is recovered as limiting distribution, exactly.

Finally flat initial conditions for the PNG model on the half line, $h(x, 0) = 0$ for $x \geq 0$ can be treated in a similar way. The Poisson points in the region $\{(x', t');\, x', t' \geq 0, x' + t' \leq t\}$ are mirrored at $t = 0$ and $x = 0$, to fill the square R_t with points of fourfold symmetry. The limiting distribution for the height turns out to be again GUE, but is narrower by a factor of $2^{2/3}$, since the length of the polymer corresponds to $2h(0, t)$

Theorem 3.5 *Let $h(x, t)$ be the height process corresponding to the PNG model with flat initial conditions on the half line, then*

$$\lim_{t\to\infty} \text{Prob}\Big\{\frac{h(0,t) - 2t}{t^{1/3}} \leq 2^{-2/3}s\Big\} = F_{\text{GUE}}(s). \tag{3.45}$$

A source at the origin results in the same qualitative behavior as for the half droplet. For the critical value $\alpha = 2$ the limiting distribution is $F_{\text{GOE}}(2^{2/3}s)^2$, which can be thought of as the maximum of two independent GOE random variables.

3.3 Stationary initial conditions, the stationary two-point function

When the initial conditions for the PNG model at $t = 0$ are drawn from the stationary distribution, say at slope zero, the resulting growth process is spatially and temporarily translation invariant. The variance of the height difference $h(x, t) - h(0, 0)$ defines the stationary two-point function of the PNG model,

$$C(x, t) = \big\langle (h(x, t) - h(0, 0) - 2t)^2 \big\rangle, \tag{3.46}$$

where $\langle\cdot\rangle$ means expectation with respect to initial conditions and nucleation events. By the KPZ scaling and universality hypothesis the properly rescaled two-point function converges to the universal scaling function, $g_1^{\text{dyn}}(y)$, for one-dimensional KPZ growth,

$$\frac{C(t^{2/3}y, t)}{t^{2/3}} \to g_1^{\text{dyn}}(y) \quad \text{for } t \to \infty, \tag{3.47}$$

which has been defined in (2.33). It will be denoted by $g(y)$ throughout this section. There have been numerous approaches to study $g(\cdot)$ [18, 63, 119, 49, 44]. For historical reasons the equivalent scaling function, $F(\cdot)$, is analyzed in some of these works. As a reference we indicate here their relation,

$$F(\xi) = (\xi/2)^{2/3}\, g\left((2\xi^2)^{-1/3}\right), \quad \text{resp.} \quad g(y) = 2y\, F\big(1/(2^{1/2}y^{3/2})\big). \tag{3.48}$$

The large y behavior of g is fixed by definition as $g(y) \sim 2|y|$. The special value $g(0) = 1.150394478259470972996 1$ is the Baik-Rains constant [11, 99]. In the literature the universal amplitude ratio $R_G = 2^{-2/3}g(0) = 0.7247031092$ and the universal coupling constant $g^* = g(0)^{-3/2} = 0.81045670$ have been investigated. Approximate values have been determined by means of Monte-Carlo simulations for the single step model [119], numerically within a mode-coupling approximation [63, 49, 35], and even experimentally for slowly combusting paper [91] yielding estimates for $g(0)$ within reasonable ranges around the (numerically) exact value indicated.

3.3.1 Convexity of the scaling function.

By the asymptotics of $g(y)$ the function

$$f(y) = \tfrac{1}{2}g''(y) \tag{3.49}$$

has integral 1. It turns out to be positive, which implies that $g(y)$ is a convex function and thus $f(y)$ can be interpreted as a probability density.

To prove that $f(y) \geq 0$ we introduce the structure function for the step density,

$$S(x,t) = \langle \rho(x,t)\rho(0,0)\rangle, \tag{3.50}$$

where $\rho(x,t) = \partial_x h(x,t)$ is the signed step density, which has delta peaks at the up-step positions and negative delta peaks at the down-step positions. By stationarity $S(x,t)$ is closely related to the correlation function $C(x,t)$. An easy calculation yields

$$\begin{aligned}
\tfrac{1}{2}\partial_x^2 C(x,t) &= \tfrac{1}{2}\partial_x^2 \big\langle \big(h(x,t) - h(0,0) - 2t\big)^2 \big\rangle \\
&= \partial_x \big\langle \rho(x,t)\big(h(x,t) - h(0,0) - 2t\big)\big\rangle \\
&= \partial_x \big\langle \rho(0,t)\big(h(0,t) - h(-x,0) - 2t\big)\big\rangle \\
&= \big\langle \rho(0,t)\rho(-x,0)\big\rangle \\
&= S(x,t).
\end{aligned} \tag{3.51}$$

$f(y)$ is the scaling function for $S(x,t)$, by (3.47) one has

$$\tfrac{1}{2}t^{2/3}S(t^{2/3}y,t) \to f(y) \quad \text{for } t \to \infty. \tag{3.52}$$

To show that $S(x,t) \geq 0$ we interpret $\frac{1}{2}S(x,t)$ as the transition probability for a second class particle starting at the origin. Its initial velocity is ± 1 with probability $\frac{1}{2}$, as for the "first-class" up/down-steps. In contrast to an ordinary step the second class particle is never destroyed upon colliding with another step. Rather it eats up the step encountered and, by reversing its own direction of motion, continues along the trajectory of the absorbed step, cf. Figure 3.6. Let $\rho(x,t)$ be a

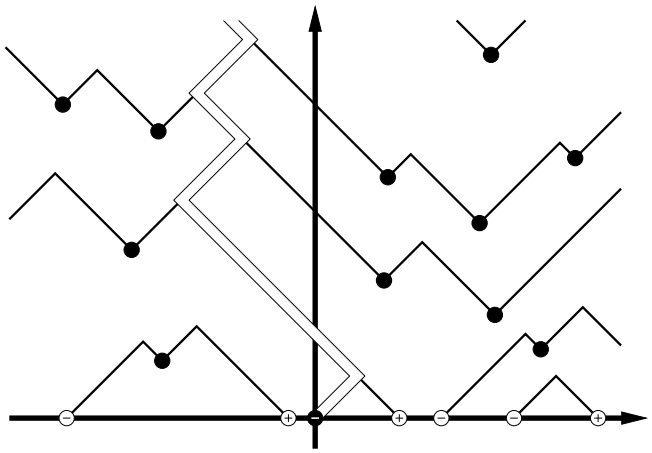

Figure 3.6: *The trajectory of a second-class particle.*

given realization of the PNG process. The second class particle is added as

$$\rho^{(\sigma)}(x,0) = \rho(x,0) + \sigma\delta(x), \quad \sigma = \pm 1. \tag{3.53}$$

$\rho^{(\sigma)}(x,0)$ evolves to $\rho^{(\sigma)}(x,t)$ with nucleation events identical to the one for $\rho(x,t)$. By construction, if X_t denotes the position of the second class particle at time t,

$$\rho^{(\sigma)}(x,t) - \rho(x,t) = \sigma\delta(x - X_t). \tag{3.54}$$

Noting that by the Poisson property $\rho^{(\sigma)}(x,0)$ is given by $\rho(x,0)$ conditioned on the presence of either an up-step ($\sigma = +1$) or down-step ($\sigma = -1$) at the origin,

we obtain

$$\begin{aligned} 0 \;\le\; p_t(x) &= \frac{1}{2}\sum_{\sigma=\pm1}\big\langle \sigma\big(\rho^{(\sigma)}(x,t)-\rho(x,t)\big)\big\rangle = \frac{1}{2}\sum_{\sigma=\pm1}\big\langle \sigma\rho^{(\sigma)}(x,t)\big\rangle \\ &= \lim_{\delta\searrow 0}\frac{1}{2}\sum_{\sigma=\pm1}\sigma\Big\langle \rho(x,t)\,\theta\big(\big\{\textstyle\int_{-\delta}^{\delta}\rho(y,0)\,dy=\sigma\big\}\big)\Big\rangle \\ &= \lim_{\delta\searrow 0}\frac{1}{2}\sum_{\sigma,\sigma'=\pm1}\sigma\sigma'\,\frac{\big\langle\theta\big(\big\{\int_{-\delta}^{\delta}\rho(x+y,t)\,dy=\sigma',\int_{-\delta}^{\delta}\rho(y,0)\,dy=\sigma\big\}\big)\big\rangle}{2\,\delta\,\big\langle\theta\big(\big\{\int_{-\delta}^{\delta}\rho(y,0)\,dy=\sigma\big\}\big)\big\rangle} \\ &= \tfrac{1}{2}\big\langle\rho(x,t)\rho(0,0)\big\rangle = \tfrac{1}{2}S(x,t), \end{aligned} \tag{3.55}$$

where $\theta(\{\cdot\})$ is the characteristic function of a subset $\{\cdot\}$ of configurations $(x,t)\mapsto h(x,t)$. For arbitrary slope u, employing the Lorentz invariance of the stationary height process (3.1) the normalization of $S_u(x,t)$ is given by $v(u)=\sqrt{4+u^2}$ and the mean of $p_t(x)$ evolves along the characteristics of the macroscopic evolution equation $\partial_t u=-\partial_x v(u)$. Thus

$$\int S_u(x,t)dx=\sqrt{4+u^2},\quad \text{and}\quad \int x\,S_u(x,t)dx=-t\,u. \tag{3.56}$$

3.3.2 The distribution of height differences.

In order to find $g(y)$, resp. $f(y)$, we study the distribution of height differences $h(x,t)-h(0,0)=h(x,t)$, since we fix $h(0,0)=0$. It can be determined explicitly for all values of (x,t). For a space-like separation, $|x|\ge|t|$, by the Poisson property of Prop. 3.1, $h(x,t)$ is the difference of two independent Poisson distributed integer valued random variables with mean $|x|+|t|$ and $|x|-|t|$, respectively. Other signs for x and t follow by symmetry. Thus, explicitly, the height distribution function $F_{|x|,|t|}(n)=\text{Prob}\{h(x,t)=n\}$ is given as

$$\begin{aligned} F_{x,t}(n) &= \sum_{k,l\ge0}\delta_{l-k,n}\frac{(x+t)^k(x-t)^l}{k!\,l!}e^{-2x} \\ &= \big(\tfrac{x+t}{x-t}\big)^{n/2}I_n\big(2\sqrt{x^2-t^2}\big)e^{-2x},\quad 0\le t\le x \end{aligned} \tag{3.57}$$

where $I_n(z)=\sum_{k\ge0}\frac{z^{2k+n}}{k!(k+n)!}$ is the modified Bessel function. Obviously, by the central limit theorem $h(x,t)$ is close to a Gaussian distribution, for large x with exact mean $2t$ and variance $2x$. Nevertheless it has non-vanishing fully truncated third and fourth moments. They can be calculated as $2t$ and $2x$, respectively. Let us mention that for space-like separations arbitrary n-point correlation functions are trivial in the sense that the corresponding joint distributions are expressed as joint distributions of points along a corresponding simple random walk.

For time-like separations, $|x| < t$, the distribution of $h(x,t)$ is non-trivial. From the mapping to directed polymers we know that $h(x,t)$ equals in distribution the length of the longest polymer from $(0,0)$ to (x,t) inside the rectangle $R_{(x,t)} = \{(x',t');\, |x'| \le t, |x-x'| \le t-t'\}$. The incoming up- and down-steps at the lower edges of $R_{(x,t)}$, according to Proposition 3.1, are Poisson distributed with line densities $\sqrt{2}$. With the Lorentz transformation (3.1) we map $R_{(x,t)}$ into a square. An additional overall scaling by $\sqrt{2}/v$, $v = \sqrt{t^2-x^2}$, leads to a unit square, with bulk density v^2 and line densities αv for the lower left, and βv for the lower right side, where $\alpha = \sqrt{(t-x)/(t+x)}$ and $\beta = 1/\alpha$. We thereby have recovered precisely the setting in [11, 9] with t replaced by v. Let us explain their result.

Take a directed polymer with boundary parameters α and β, $\alpha\beta < 1$ and add an additional source of points at the origin. The number of points, n_0, at the origin is geometrically distributed with strength $\alpha\beta$, i.e. $\text{Prob}\{n_0 = n\} = (1-\alpha\beta)(\alpha\beta)^n$. The distribution of the length $l_{v,\alpha,\beta}$ of the longest directed polymer in this case is given by

$$\begin{aligned} P_n &= \text{Prob}\{l_{v,\alpha,\beta} \le n\} \\ &= e^{-v^2-(\alpha+\beta)v}\mathbb{E}_{U\in U(n)} \det\left((1+\alpha U)(1+\beta U^{-1})e^{v(U+U^{-1})}\right) \end{aligned} \tag{3.58}$$

Using standard results for orthogonal polynomials with a weight function multiplied by a polynomial it is shown in [12] that the corresponding Toeplitz determinant factorizes by means of the orthogonal polynomials (3.22) and (3.24) into

$$\begin{aligned} P_n &= e^{-(\alpha+\beta)v}\,\frac{\pi_n^*(-\alpha)\pi_n^*(-\beta) - \alpha\beta\pi_n(-\alpha)\pi_n(-\beta)}{1-\alpha\beta} F_n^{\text{GUE}} \\ &= e^{-(\alpha+\beta)v}\, N_n \sum_{k=0}^{n} \frac{\pi_k(-\alpha)\pi_k(-\beta)}{N_k} F_n^{\text{GUE}}. \end{aligned} \tag{3.59}$$

The second equality follows by a simple application of the Christoffel-Darboux formula

$$N_n \sum_{k=0}^{n-1} \frac{\pi_k(a)\pi_k(b)}{N_k} = \frac{\pi_n^*(a)\pi_n^*(b) - \pi_n(a)\pi_n(b)}{1-ab}, \tag{3.60}$$

cf. Appendix A.

Conditioning on $n_0 = 0$ yields

$$\text{Prob}\{l_{v,\alpha,\beta} \le n,\, n_0 = 0\} = P_n - \alpha\beta P_{n-1}. \tag{3.61}$$

If α is fixed, P_n seems to have a simple pole at $\beta = 1/\alpha$. But by the second equality in (3.59) it is obvious that P_n is entire as a function of β. Altogether we

arrive at

$$F_{x,t}(n) = g_n(\alpha) F_n^{\mathrm{GUE}} - g_{n-1}(\alpha) F_{n-1}^{\mathrm{GUE}}, \qquad |x| < t, \tag{3.62}$$

with

$$g_n(\alpha) = e^{-v(\alpha+\alpha^{-1})} N_n \sum_{k=0}^{n} N_k^{-1} \pi_k(-\alpha)\pi_k(-\alpha^{-1}). \tag{3.63}$$

An alternative form is obtained by applying l'Hospital's rule to the first expression for P_n in (3.59) when β tends to $1/\alpha$.

$$\begin{aligned} g_n(\alpha) &= e^{-v(\alpha+\alpha^{-1})}\big(\pi_n(-\alpha)\pi_n(-\alpha^{-1}) \\ &\quad +\alpha^{-1}\pi_n^*(-\alpha)\pi_n^{*\prime}(-\alpha^{-1}) - \alpha^{-1}\pi_n(-\alpha)\pi_n'(-\alpha^{-1})\big) \\ &= e^{-v(\alpha+\alpha^{-1})}\big((1-n)\pi_n(-\alpha)\pi_n(-\alpha^{-1}) \\ &\quad -\alpha\pi_n'(-\alpha)\pi_n(-\alpha^{-1}) - \alpha^{-1}\pi_n(-\alpha)\pi_n'(-\alpha^{-1})\big) \end{aligned} \tag{3.64}$$

where the second, more symmetric form follows from the simple identity

$$\pi_n^*(z) z^{-1} \pi_n^{*\prime}(z^{-1}) + z\,\pi_n'(z)\pi_n(z^{-1}) = n\,\pi_n(z)\pi_n(z^{-1}) = n\,\pi_n^*(z)\pi_n^*(z^{-1}). \tag{3.65}$$

By stationarity the mean of $h(x,t)$ is $2t$. Therefore the PNG two-point-function (3.46) is given by

$$C(x,t) = \sum_{n\geq 0} \big(2(n-2t)-1\big)\mathrm{Prob}\{h(x,t) \leq n\}. \tag{3.66}$$

As a remark let us note that the value of the mean of $h(x,t)$ is far from being obvious by looking at (3.62). Remember that $\alpha = \sqrt{(t-x)/(t+x)}$, $v = \sqrt{t^2-x^2}$, and that the orthogonal polynomials are implicitely depending on v. In a more general context [105] this mean identity has been shown to hold directly from the explicit expression for the distribution function.

3.3.3 The scaling limit of the height distribution.

In order to determine the scaling function $g(y)$ (3.47) we need to study the scaling properties of $\mathrm{Prob}\{h(x,t) \leq n\}$. Since (3.62) depends explicitly on $v = \sqrt{t^2-x^2}$ it is favorable to introduce the scaling variables y and s as

$$\begin{aligned} x &= v^{2/3} y, \\ t &= v + \tfrac{1}{2} v^{1/3} y^2, \\ n &= [2v + v^{1/3} s], \end{aligned} \tag{3.67}$$

and determine the limit

$$\text{Prob}\{h(x,t) \le n\} \to F_y(s) \quad \text{for } v \to \infty. \tag{3.68}$$

The finite height distribution is expressed in terms of the orthogonal polynomials $\pi_n(z)$. They satisfy the classical recursion relations

$$\begin{aligned} \pi_{n+1}(z) &= z\,\pi_n(z) + p_{n+1}\pi_n^*(z), \\ \pi_{n+1}^*(z) &= z\,p_{n+1}\pi_n(z) + \pi_n^*(z), \end{aligned} \tag{3.69}$$

which hold for an arbitrary weight function, and the differential equations

$$\begin{aligned} \pi_n{}'(z) &= (n/z + v/z^2 - p_{n+1}p_n v/z)\pi_n(z) + (p_{n+1}v/z - p_n v/z^2)\pi_n^*(z) \\ \pi_n^{*\prime}(z) &= (-p_{n+1}v/z + p_n v)\pi_n(z) + (-v + p_{n+1}p_n v/n)\pi_n^*(z), \end{aligned} \tag{3.70}$$

which heavily rely on (3.27), compare Appendix A for a proof. They are implicitly derived in [9] and in this form written down explicitly for the first time. Ismail and Witte [65] have derived a differential-difference equation for orthogonal polynomials with a general weight function. Specializing to the weight $e^{v(z+z^{-1})}$ also yields (3.70).

The scaling (3.67) implies $\alpha = 1 - v^{-1/3}y + \mathcal{O}(v^{-2/3})$. In order to obtain a nontrivial limit as $v \to \infty$ of the above equations we approximate $\pi_n^*(z)$ and $\pi_n(z)$ in the vicinity of $z = -1$ by two smooth functions $a(s,y)$ and $b(s,y)$ as

$$\pi_n^*(-\alpha) \simeq e^{v\alpha} a\big(v^{-1/3}(n-2v), v^{1/3}(1-\alpha)\big), \tag{3.71}$$

$$\pi_n(-\alpha) \simeq -e^{v\alpha}(-1)^n b\big(v^{-1/3}(n-2v), v^{1/3}(1-\alpha)\big). \tag{3.72}$$

$$\tag{3.73}$$

Using that the asymptotical behavior (3.31) of R_n is given by the Hastings-McLeod solution to Painlevé II, $u(s)$, one obtains from (3.69) the differential equations with respect to s

$$\begin{aligned} \partial_s a &= u\,b, \\ \partial_s b &= u\,a - y\,b, \end{aligned} \tag{3.74}$$

and from (3.70) after some calculation the differential equations with respect to y

$$\begin{aligned} \partial_y a &= u^2 a - (u' + y\,u)b, \\ \partial_y b &= (u' - y\,u)a + (y^2 - s - u^2)b. \end{aligned} \tag{3.75}$$

From (3.69) one immediately obtains $\pi_n^*(-1) = (-1)^n\pi_n(-1) = \prod_{k=1}^n (1-R_k)$. One has the limit $\prod_{k=1}^\infty (1-R_k) = e^v$ since $e^{-v^2+v}N_0\prod_{k=1}^n N_k(1-R_k)^{-1}$ has

an interpretation as a probability distribution function [12]. Therefore the initial conditions to (3.75) are

$$a(s,0) = -b(s,0) = e^{-U(s)}. \tag{3.76}$$

The scaling limit of $g(n,\alpha)$ as defined in Eq. (3.63) is the function

$$\begin{aligned} g(s,y) &= \int_{-\infty}^{s} a(x,y)a(x,-y)dx \\ &= a(s,-y)\partial_y a(s,y) - b(s,-y)\partial_y b(s,y), \end{aligned} \tag{3.77}$$

where the second equality can be verified by differentiation with respect to s and using the identity

$$a(s,y) = -b(s,-y)e^{\frac{1}{3}y^3 - sy}, \tag{3.78}$$

itself being a direct consequence of (3.75) and (3.76). Putting these pieces together we obtain as scaling limit for the distribution functions $F_{x,t}(n)$,

$$F_y(s) = \frac{d}{ds}\big(g(s+y^2,y)F_{\mathrm{GUE}}(s+y^2)\big). \tag{3.79}$$

The shift in (3.79) by y^2 comes from the fact that $F_y(s)$ is evaluated for constant $t = v + \frac{1}{2}v^{1/3}y + \mathcal{O}(v^{-1/3})$.

Finally we can write down the scaling function $g(y)$ of (3.47), which by the scaling (3.67) is given as

$$g(y) = \int s^2 dF_y(s). \tag{3.80}$$

As in the droplet case we do not provide a proof for the existence of limits. This has been accomplished by Baik and Rains in a series of works [12, 13, 11, 9]. We gave a heuristic derivation of the limiting distributions which avoids introducing the machinery of Riemann-Hilbert techniques. All the above relations, apart from (3.70) appeared already elsewhere. Nevertheless we find it instructive to present the above derivation, stressing the origin of the differential equations (3.74) and (3.75) as the continuum limit of their discrete counterparts (3.69) and (3.70). For completeness let us collect some more properties of $a(s,y)$ shown in [11]:

$$\begin{aligned} a(s,y) &\to 1, \quad \text{as } s \to +\infty, \\ a(s,y) &\to 0, \quad \text{as } s \to -\infty, \\ a\big((2y)^{1/2}x + y^2, y\big) &\to 1, \quad \text{as } y \to +\infty, \\ a\big((-2y)^{1/2}x + y^2, y\big) &\to \frac{1}{(2\pi)^{1/2}} \int_{-\infty}^{x} e^{-\frac{1}{2}\xi^2} d\xi, \quad \text{as } y \to -\infty. \end{aligned} \tag{3.81}$$

Therefore $F_y(s)$ is asymptotically Gaussian and we recover $g(y) \simeq 2|y|$ for large y.

In Appendix B we describe the method to determine the scaling function numerically. One first needs to find the Hastings-McLeod solution to Painlevé II and then integrate (3.75) starting from $y = 0$. Then one has to integrate (3.74) for different values of y to obtain the variance of $F_y(S)$. And finally $g(y)$ has to be differentiated twice numerically to get the scaling function $f(y)$. The high precision we wanted to achieve rules out any conventional numerical integration methods for ordinary differential equations. As explained in the Appendix we used a Taylor expansion method with multiprecision arithmetic, to estimate the fast decaying tails of $f(y)$ with an absolute accuracy of about 10^{-100}, and to be able to determine reliable Fourier transforms of the scaling function.

3.3.4 Discussion of the scaling function.

In Figure 3.7 the scaling function $f(y) = \frac{1}{4}g''(y)$ is shown as determined by the

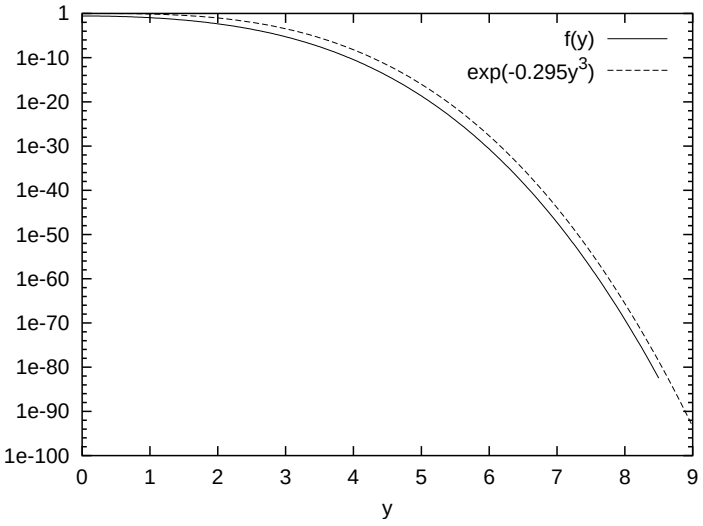

Figure 3.7: *The scaling function $f(y)$ versus y in a semilogarithmic plot. The dotted line $\exp(-0.295|y|^3)$ is drawn as a guide to the eye for the large y asymptotics of f.*

multiprecision expansion method explained in Appendix B. We estimate its large y asymptotics as

$$\log f(y) \approx -c|y|^3 + o(|y|) \text{ for } y \to \infty. \tag{3.82}$$

The cubic behavior is very robust and numerical fits yield about 2.996–2.998 quite independently of the assumed nature of the finite size corrections. The prefactor

$c = 0.295(5)$ has a relatively high uncertainty because of the unknown subleading corrections. Even though inaccessible systematically we estimate the error term, as indicated in (3.82), to be sublinear or even only logarithmic from the numerical data. Possibly, the exact asymptotic behavior could be extracted from a refined asymptotic analysis of the Riemann-Hilbert problem.

Colaiori and Moore [35, 33] tackled the same scaling function by completely different means. Starting from the continuum version of the KPZ equation they numerically solved the corresponding mode-coupling equation [18, 49], which contains an uncontrolled approximation, since diagrams which would renormalize the three-point vertex coupling are neglected. Nevertheless a qualitative comparison of their result with the exact scaling function $f(y)$ shows reasonable similarity, cf. Figure 3.8. Both functions are normalized to integral 1 by definition. The mode coupling solution oscillates around 0 for $|y| > 3$, whereas $f(y) > 0$

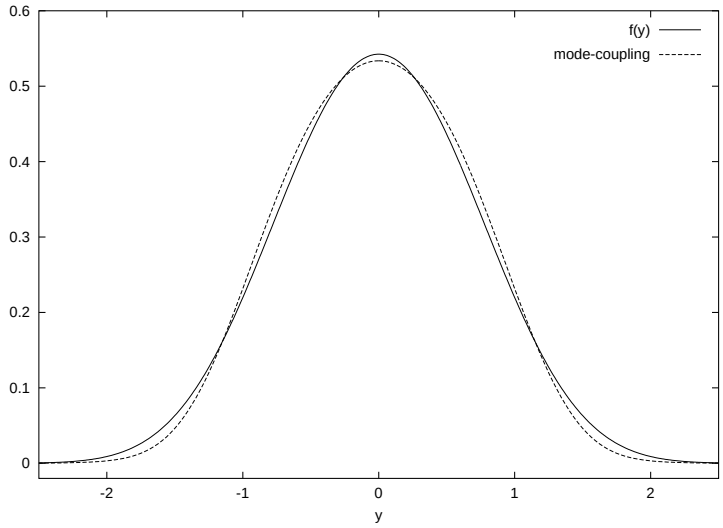

Figure 3.8: *The exact scaling function $f(y)$ compared to the mode coupling result of Colaiori and Moore [35](dotted line). Both functions are even.*

for the exact solution. We do not know whether this is a numerical artifact or an inherent property of the mode-coupling approximation. On the other hand, the second moments are reasonably close together, 0.510523 for $f(y)$, and 0.4638 for the mode-coupling approximation. So is the value of the Baik-Rains constant $g(0) = 2\int |y| f(y) dy$ for which mode-coupling predicts the value 1.1137.

From the solution to the mode-coupling equations one does not directly obtain $f(y)$, but rather its Fourier transform. The function $G(\tau)$ from [35] is defined

through

$$G(k^{3/2}/2^{7/2}) = \widehat{f}(k) = 2\int_0^\infty \cos(ky)f(y)dy. \tag{3.83}$$

Colaiori and Moore predict a stretched exponential decay of the function $G(\tau)$ as $\propto \exp(-c|\tau|^{2/3})$ [33] and numerically find a superimposed oscillatory behavior on the scale $|\tau|^{2/3}$ [35]. In Figure 3.9 $\widehat{f}(k)$ is plotted as obtained by a numerical

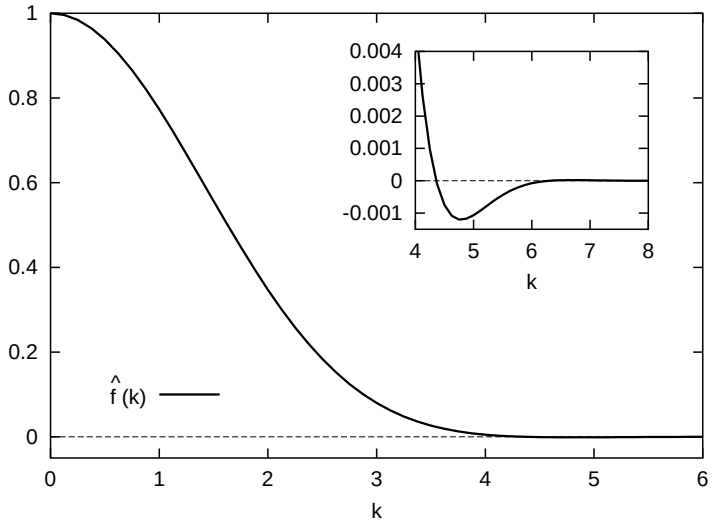

Figure 3.9: *The Fourier transform $\widehat{f}(k)$ of the scaling function $f(y)$.*

Fourier transform of $f(y)$. Indeed it exhibits an oscillatory behavior as can be seen in Figure 3.10 where the modulus of $\widehat{f}(k)$ is shown on a semilogarithmic scale. The dotted line in the plot is the modulus of the function

$$10.9k^{-9/4}\sin(\tfrac{1}{2}k^{3/2} - 1.937)e^{-\frac{1}{2}k^{3/2}}, \tag{3.84}$$

shifted by a factor of 1000 for visibility, which fits $\widehat{f}(k)$ very well in phase and amplitude for $k \gtrapprox 15$. This behavior is not in accordance with the results of Colaiori and Moore, since the oscillations and the exponential decay of $G(\tau)$ for the exact solution are apparently on the scale τ and not $\tau^{2/3}$.

Note that $\widehat{f}(k)$ is the scaling function for the intermediate structure function

$$S(k,t) = \int dx e^{ikx} S(x,t) \simeq 2\widehat{f}(t^{2/3}k). \tag{3.85}$$

By Fourier transforming with respect to t we determine the dynamical structure function,

$$S(k,\omega) = \int dx\, dt e^{i(kx+\omega t)} S(x,t) \simeq 2k^{-3/2}\, \mathring{f}\,(\omega/k^{3/2}), \tag{3.86}$$

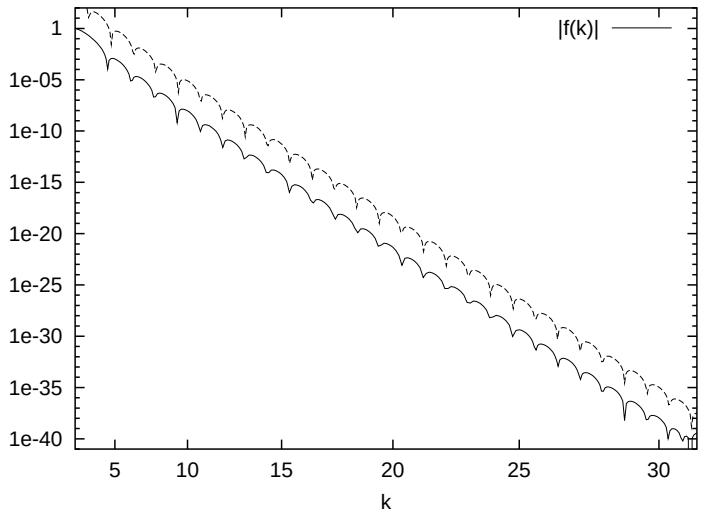

Figure 3.10: *The modulus of $\widehat{f}(k)$ on a semilogarithmic scale. The dotted line is a heuristic fit, shifted by a factor* 1000 *for visibility.*

where

$$\overset{\circ}{f}(\tau) = \int ds\, e^{i\tau s} \widehat{f}(s^{2/3}) = 2\int_0^\infty dy\, \tau^{-1} L'(y/\tau^{2/3}) f(y) \tag{3.87}$$

and L has the representation

$$L(\kappa) = 2 \cdot 3^{2/3} \mathrm{Ai}(-3^{-4/3}\kappa^2) \sin(2\kappa^3/27). \tag{3.88}$$

The correlation function (3.46) in Fourier space is given by

$$C(k,\omega) = 2k^{-2} S(k,\omega) \sim C^{\mathrm{KPZ}}(k,\omega) \overset{\mathrm{def}}{=} 4k^{-7/2}\, \overset{\circ}{f}(\omega/k^{3/2}), \tag{3.89}$$

describing the asymptotic behavior at $k, \omega = 0$. Note that $C(k,\omega) > 0$ by definition, since $\langle h_{k,\omega} h_{k',\omega'} \rangle = \delta_{k,-k'} \delta_{\omega,-\omega'} C(k,\omega)$ for $(k,\omega) \neq (0,0)$. The anomalous scaling behavior in real space is reflected by the exponents for the divergence of $C^{\mathrm{KPZ}}(k,\omega)$ at $k = \omega = 0$. In the linear case, the Edwards-Wilkinson equation $\lambda = 0$ in (2.45), one easily obtains

$$C^{\mathrm{EW}}(k,\omega) = \frac{D}{\omega^2 + \nu^2 k^4}. \tag{3.90}$$

A 3d-plot of $C^{\mathrm{KPZ}}(k,\omega)$ is shown in Figure 3.11. Its striking features are the smooth behavior away from $k, \omega = 0$, especially on the lines where $k = 0$ and

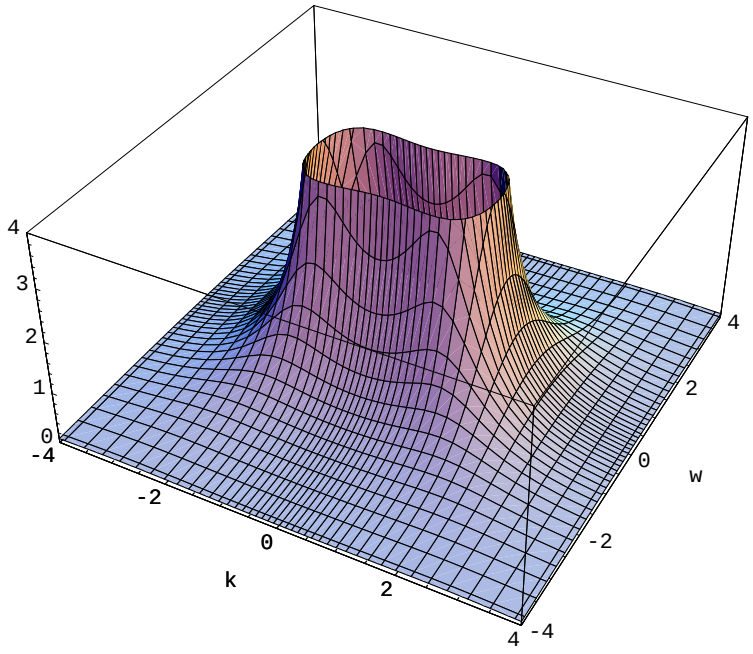

Figure 3.11: *The correlation function $C(k,\omega)$ in Fourier space.*

$\omega = 0$ and the two symmetric maxima of $k \mapsto C^{\mathrm{KPZ}}(k,\omega)$ for constant ω. Our numerical data yield for the singular behavior at $k = 0$, $\omega = 0$,

$$\begin{aligned} C^{\mathrm{KPZ}}(k,\omega) &= \omega^{-7/3}\big(2.10565(1) + 0.85(1)\, k^2 w^{-4/3} + \mathcal{O}(k^4\omega^{-8/3})\big), \\ &= k^{-7/2}\big(19.4443(1) - 52.5281(1)\, \omega^2 k^{-3} + \mathcal{O}(\omega^4 k^{-6})\big). \end{aligned} \tag{3.91}$$

CHAPTER 4

The Bernoulli cone

The Bernoulli cone is a random subset of $\mathbb{R}^3$ with parameter $p \in [0,1]$. It is defined as the wetted cluster of a layered directed bond percolation model [106]. Active bonds can be passed only in the direction of increasing coordinates. The Bernoulli cone is made up of those sites which can be reached from the origin through a chain of active bonds. Horizontal bonds are always active, and vertical bonds are active with probability p. The statistics of the Bernoulli cone has various interpretations in the form of well-known statistical mechanics models, such as last passage percolation, directed polymers in random media, random growth, and driven diffusive systems. The Bernoulli cone always maps to the simplest discrete versions of these type of models. The two limiting cases, $p \to 0, 1$ also map to various well-known problems. The PNG limit, $p \to 0$ is equivalent to Ulam's problem of the length of the longest increasing subsequences in random permutations, compare the previous chapter, and the TASEP limit, $p \to 1$, maps to the continuous–time totally asymmetric simple exclusion process with special initial conditions, first considered by Rost [108].

4.1 The directed bond percolation cluster

We define the Bernoulli cone D as a random subset of $\mathbb{R}^3$, made up of unit cubes $(n_1, n_2, n_3) +]\text{–}1, 0]^3$. There are three types of nearest neighbor bonds pointing in the direction of the three coordinate axes 1, 2, and 3. Some of the bonds are active, the others are not. The directed percolation cluster $D \cap \mathbb{Z}^3$ consists of all those lattice sites which can be reached from site $(1, 1, 0)$ by a sequence of sites, which is non decreasing in the coordinates, such that adjacent sites in the sequence are always connected by an active bond. The bonds are active independently with probabilities p_1, p_2, and p_3, corresponding to the direction, 1, 2, and 3, they are pointing to. Thus if one thinks of the active bonds as diodes and the sites as grounded light bulbs, D contains all the glowing bulbs, when a voltage is applied at site $(1, 1, 0)$.

If the probabilities are small enough, D will be finite almost surely, but for any direction $r \in \mathbb{R}_0^{+3}$, $|r| = 1$, D extends to infinity above certain critical values for p_1, p_2, and p_3. When approaching these critical values from below, not only the

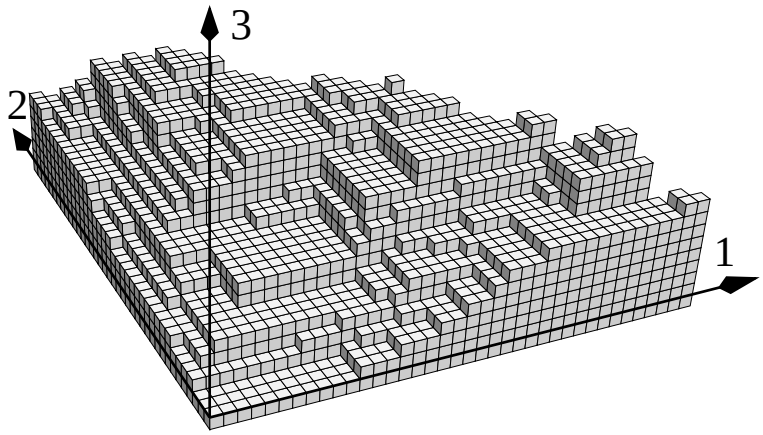

Figure 4.1: *Part of a Bernoulli cone with* $p = 0.1$.

mean of the radius $R(r) = \max\{\lambda;\ \lambda r \in D\}$ tends to infinity, but also its variance diverges with characteristic exponents (see [106] for a more detailed description).

Here we are exclusively interested in the special case of layered percolation, i.e. the maximally anisotropic case $p_1 = p_2 = 1$, $p_3 = p \in]0, 1[$. Since horizontal bonds are always active, for each site $(n_1, n_2, n_3) \in D$ all sites $(m_1, m_2, n_3) \in D$ for $m_1 \geq n_1$, $m_2 \geq n_2$. Since there is a chain of active bonds from $(1, 1, 0)$ to (n_1, n_2, n_3) also the sites (m_1, m_2, m_3), $m_1 \geq n_1$, $m_2 \geq n_2$, $0 \leq m_3 \leq n_3$ lie in D. Therefore D is uniquely specified by the height function

$$h(x_1, x_2) = \max\{x_3 \in \mathbb{R};\ (x_1, x_2, x_3) \in D\}. \tag{4.1}$$

(compare with Figure 4.1). The definition of the Bernoulli cone D can be formalized by the following recursive rules:

(i) $D \subset \mathbb{R}^+ \times \mathbb{R}^+ \times]{-}1, \infty[, \quad D = (D \cap \mathbb{Z}^3) +]{-}1, 0]^3$,
(ii) $(1, 1, 0) \in D$,
(ii) if $\{(x_1 - 1, x_2, x_3), (x_1, x_2 - 1, x_3), (x_1, x_2, x_3 - 1)\} \subset D$, and the vertical bond ending in (x_1, x_2, x_3) is active, then $(x_1, x_2, x_3) \in D$.

(4.2)

Thus for the height function one has the relation

$$h(i, j) = \max\{h(i - 1, j), h(i, j - 1)\} + w(i, j), \tag{4.3}$$

for $(i, j) \in \mathbb{N}^2 \setminus \{(1, 1)\}$ and $h(1, 1) = w(1, 1)$. The $w(i, j)$ count the number of consecutive active vertical bounds right above $(1, 1, 0)$ for $i = j = 1$, and right above $(i, j, \max\{h(i - 1, j), h(i, j - 1)\})$, for $(i, j) \in \mathbb{N}^2 \setminus \{(1, 1)\}$. Therefore

they are geometrically i.i.d. with strength p, i.e. Prob$\{w(i,j) = k\} = (1-p)p^k$, $k \in \mathbb{N}_0$.

We are going to study the asymptotic shape of D upon rescaling, $\lim_{\lambda\to\infty} \frac{1}{\lambda} D$ which almost surely is a convex cone of a certain shape. As we will see D can be interpreted as the space-time image of a self–similarly growing droplet. Therefore the scaling theory of Chapter 2 is applicable. However, first we will explain the various interpretations of the Bernoulli cone mentioned above. All the following processes can be constructed realizationwise from the Bernoulli distributed active vertical bonds. Thus the equivalences are in distribution with an explicit identification of the underlying probability spaces.

Last passage percolation

Let $w(i,j)$, $i,j \in \mathbb{N}$ be geometrically i.i.d. random variables of strength p. A directed path, γ, from $(1,1)$ to (M,N) is a sequence of lattice points (i,j), which is non–decreasing in its components and contains both endpoints. The cost of such a path γ is the sum of the $w(i,j)$ with (i,j) belonging to γ. We set

$$t(M,N) = \max_{\gamma} \sum_{(i,j)\in\gamma} w(i,j). \tag{4.4}$$

If we regard the $w(i,j)$ as waiting times, $t(M,N)$ has the interpretation of the last passage time of an ensemble of walkers getting from $(1,1)$ to (M,N) along the directed bonds of $\mathbb{N}^2$ [68]. In queuing theory one asks for the processing time of M customers, passing one after another through N queues, where customer i needs $w(i,j)$ units of time to be served in queue j. Thus $t(M,N)$ is the total time needed for the last customer to exit the last queue. In more physical terms one can think of $-w(i,j)$ as a random potential. The energy of a directed polymer configuration γ from $(1,1)$ to (M,N) is then given by $-\sum_{(i,j)\in\gamma} w(i,j)$. Thus $-t(M,N)$ is the ground state energy of the point–to–point directed polymer.

To see that $t(x_1,x_2)$ equals the height function (4.1) at integer arguments in distribution, we set $t(i,j) = -\infty$ for $i \le 0$ or $j \le 0$, $t(1,1) = w(1,1)$. Then for $i,j \in \mathbb{N}^2 \setminus \{1,1\}$ one has the recursive relation

$$t(i,j) = \max\{t(i-1,j), t(i,j-1)\} + w(i,j), \tag{4.5}$$

which is identical to (4.3).

The corner growth model

Let $A_t \subset \mathbb{R}^2$, $t \in \mathbb{N}_0$ be a set valued process as follows. For each $t \in \mathbb{N}_0$ the random set A_t is made up of unit squares of the form $(i,j) +]$–$1,0]^2$. Initially

$A_0 = \mathbb{R}^2 \setminus (\mathbb{R}^+)^2$, a perfect corner. A_{t+1} arises from A_t by adding squares to its boundary at random. The square $(i,j) +]\text{–}1,0]^2$ is added with probability $1-p$, only if $(i-1,j)$ and $(i,j-1)$ belong already to A_t [68]. Thus A_t always stays connected without overhangs. We define the time, $T(i,j)$, when the square at (i,j) is added to A_t,

$$T(i,j) = \min\{t \in \mathbb{N}_0;\ (i,j) \in A_t\}. \tag{4.6}$$

Then it is easy to see that $T(i,j) = 0$ for $(i,j) \in \mathbb{Z}^2 \setminus \mathbb{N}^2$ and

$$T(i,j) = \max\{T(i-1,j), T(i,j-1)\} + w(i,j) + 1, \tag{4.7}$$

for $i,j \in \mathbb{N}$, where the $w(i,j)$ just count the number of rejected attempts to add the square $(i,j) +]\text{–}1,0]^2$, and thus again are geometrically i.i.d. with strength p. Comparing (4.5) with (4.7) one has $T(i,j) = t(i,j) + i + j - 1$, in distribution.

Emphasizing the geometric picture, we can obtain the sets A_t directly from the Bernoulli cone by slicing D perpendicularly to the body diagonal and fixing the intersection with the 3–axis as origin,

$$A_t = \{(i,j) \in \mathbb{Z}^2;\ (i,j,t-i-j) \notin D \cup \mathbb{R}^+ \times \mathbb{R}^+ \times \mathbb{R}_0^-\} +]\text{–}1,0]^2. \tag{4.8}$$

Conversely the graph of A_t, $A = \bigcup_{t\in\mathbb{N}_0} (t+]\text{–}1,0] \times A_t$ becomes the Bernoulli cone, by shifting all the unit cubes $(i,j,k)+]\text{–}1,0]^3$, $i,j,k \in \mathbb{Z}$ vertically by $-(i+j)$ units.

In the literature the corner growth model is also known as the single–step model, the $(1+1)$–dimensional version of the hypercube–stacking model [120]. For given t one parameterizes A_t by the height function, $h_t : \mathbb{R} \to \mathbb{R}$,

$$h_t(x) = \max\{i+j;\ (i,j) \in A_t \text{ with } i-j = x\}. \tag{4.9}$$

The values at integer x are enough to specify the function, since h_t interpolates linearly between those points. Clearly for $x \in \mathbb{Z}$ one has that $t + x + h_t(x)$ is even and $|h_t(x+1) - h_t(x)| = 1$, hence the name of the model. The update rule is $h_{t+1}(x) = h_t(x) + 2$ with probability $1-p$ if the single–step constraint is not violated, $h_{t+1}(x) = h_t(x)$ otherwise.

The discrete–time parallel–update TASEP

Let $\eta_t(x)$, $x \in \mathbb{Z}$, $t \in \mathbb{N}_0$ be $\{0,1\}$ random variables with $\eta_0(x) = 1$ for $x \le 0$, $\eta_0(x) = 0$ for $x > 0$. $\eta_t(x) = 1$ is interpreted as a particle on site x at time t, if $\eta_t(x) = 0$ the site is empty. The update rule for the TASEP (totally asymmetric simple exclusion) is very simple. At each time step particles jump to their immediate right independently with probability $1-p$, given the target site is

empty (simple exclusion). Jumps to the left are prohibited (totally asymmetric). Thus the waiting time for a particle to jump to an empty site is again geometrically distributed with strength p. The connection to the single–step model is immediate, one just sets

$$\eta_t(x) = \frac{h_t(x) - h_t(x+1) + 1}{2}. \tag{4.10}$$

Conversely $h_t(x)$ has the interpretation as integrated current from $(0,0)$ up to (x,t), which equals for the given initial condition the number of particles to the right of x, at time t. This discrete–time version of the TASEP has been studied, for example, in the context of traffic flow models by Schreckenberg et al. [110].

The asymmetric zero range process

Let $n_t(i) \in \mathbb{N}_0$, $i \in \mathbb{N}$, $t \in \mathbb{N}_0$, be integer valued random variables with $n_0(i) = 0$ for $i \in \mathbb{N}$ initially. $n_t(0) = \infty$ takes the role of an infinite reservoir of particles, $n_t(x) \geq 0$ is regarded as the number of particles in x at time t. At each time step at most one particle from each nonempty site (including the reservoir) jumps to the right nearest neighbor site independently with probability t. This process arises from the corner growth model by parameterizing A_t by the height function

$$h_t(i) = \max\{j \in \mathbb{N}_0;\, (i,j) \in A_t\} \tag{4.11}$$

The zero range process now can be defined as

$$n_t(i) = h_t(i) - h_t(i+1). \tag{4.12}$$

Discrete polynuclear growth

There are two versions of the discrete polynuclear growth (PNG) model, the first has no restrictions on the step heights [69], the second, restricted one, allows only step heights $-1, 0, +1$[102]. The height function of the former, $h_t(x)$, $t \geq 0$, $x \in \mathbb{R}$ is defined as

$$H_t(x) = h(\tfrac{t+x}{2}, \tfrac{t-x}{2}) \in \mathbb{N}_0 \cup \{-\infty\}, \tag{4.13}$$

where $h(\cdot,\cdot)$ is the height function of the Bernoulli cone. For $t \in \mathbb{R} \setminus \mathbb{N}_0$, H_t evolves deterministically, up–steps of integer height move to the left with velocity -1 and down–steps move to the right with velocity 1. If an up–step and a down–step meet (which happens only at integer times t with $x + t \in 2\mathbb{N}$), they coalesce, and either they disappear, if they are of the same height, or the larger step swallows the smaller one, and proceeds with its size reduced, accordingly. At the same time

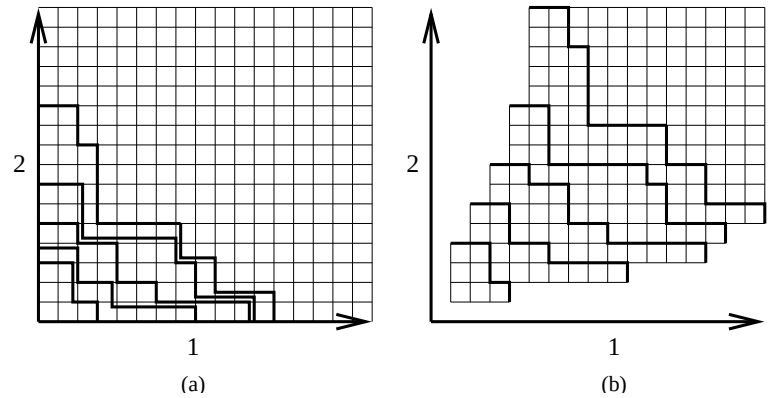

Figure 4.2: *(a) The height lines of the Bernoulli cone D from Fig. 4.1, and (b) the shifted height lines for the stretched Bernoulli cone D^{r} (Courtesy of D. Dhar and R. Rajesh).*

new islands of geometrically distributed integer height are produced randomly on top of existing ones, again only at integer times t and at integer values of x, with $x + t \in 2\mathbb{N}_0$, and start to extend laterally according to the deterministic rule. Formally, since H_t is by definition lower semi–continuous, i.e. $H_t(x_0) = \liminf_{x \to x_0} H_t(x)$, at times $t \in \mathbb{N}_0$ there might be isolated local minima at integer values of x with $x + t \in 2\mathbb{N}$. $H_t(x)$ is modified at these integer values to

$$\tilde{H}_t(x) = \lim_{\epsilon \to 0} \max\{H_t(x - \epsilon), H_t(x + \epsilon)\} + w(\tfrac{t+x}{2}, \tfrac{t-x}{2}), \tag{4.14}$$

where the $w(i, j)$, $i, j \in \mathbb{N}$ are the geometrically i.i.d. random variables from the last passage percolation. Afterwards in the time interval $]t, t + 1]$, $h_{t'}(x)$ evolves deterministically with initial condition $H_t(x) = \tilde{H}_t(x)$. The overall initial condition is $\tilde{H}_0(x) = -\infty$ for $x \neq 0$, and $H_0(0) = 0$.

To define the restricted discrete PNG model we modify the Bernoulli cone be shifting its layers along the horizontal diagonal in order to allow only steps of size one, compare with Figure 4.2,

$$D^{\mathrm{r}} = \{(x_1, x_2, x_3);\ (x_1 - \lceil x_3 \rceil, x_2 - \lceil x_3 \rceil, x_3) \in D \cup \mathbb{R}^+ \times \mathbb{R}^+ \times \mathbb{R}_0^-\}. \tag{4.15}$$

The corresponding height function

$$h^{\mathrm{r}}(x_1, x_2) = \max\{x_3 \in \mathbb{R};\ (x_1, x_2, x_3) \in D^{\mathrm{r}}\}. \tag{4.16}$$

now has only jumps of at most 1. The PNG height function $H_t^{\mathrm{r}}(x)$, $t \geq 0$, $x \in \mathbb{R}$ is defined analogously as

$$H_t^{\mathrm{r}}(x) = h^{\mathrm{r}}(\tfrac{t+x}{2}, \tfrac{t-x}{2}) \in \mathbb{N}_0 \cup \{-\infty\}. \tag{4.17}$$

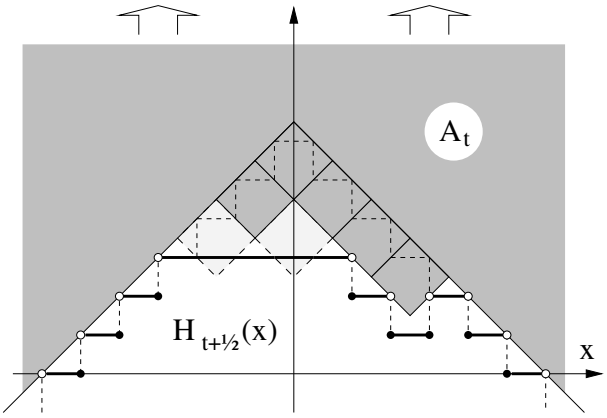

Figure 4.3: *The mapping from the restricted discrete PNG height function $H_t^{\mathrm{r}}(x)$ to the corner growth model. A_t moves upward during the evolution. The light shaded squares are added in going from A_t to A_{t+1}. Therefore no step pair is created there at time t.*

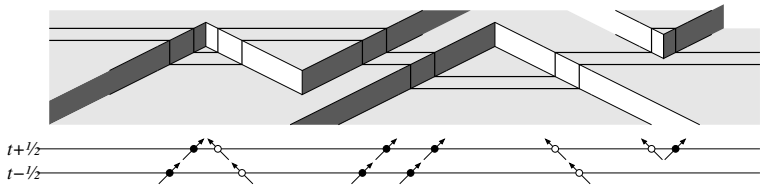

Figure 4.4: *The kink–antikink gas at two half-integer time steps.*

Its deterministic evolution is exactly the same as in the unrestricted case. The relative height of new islands now is not any more geometrically distributed, but is one with probability p and zero with probability $1-p$. Furthermore islands can nucleate, only at integer times t at points x with $x + t + H_t^{\mathrm{r}}(x) \in 2\mathbb{N}$.

The restricted discrete PNG model, having a somewhat tricky definition, arises naturally as the borderline between the bulk and the north polar region of the Aztec diamond [67]. Actually it is a version of the single–step model (4.9) via the mapping sketched in Fig. 4.3.

The discrete kink–antikink gas

The height differences in the unrestricted discrete PNG model have integer values, and thus can be identified with an occupation number of particles, called kinks for up–steps and antikinks for down–steps. Let $m_t(x) \in \mathbb{Z}$ be the signed occupation

number at $x \in \mathbb{R}$ and time $t \geq 0$, i.e. if $m_t(x) > 0$ there are $m_t(x)$ kinks, if $m_t(x) < 0$ there are $-m_t(x)$ antikinks, and $m_t(x) = 0$ means no particles at x. kinks move leftward with velocity -1, antikinks rightward with velocity 1. Kinks and antikinks can not cross each other, upon collision they immediately annihilate in pairs until only one kind remains. If there are survivors they proceed in their direction. In addition to that, kink–antikink pairs are created infinitesimally after integer times $t + \epsilon$, $t \in \mathbb{N}_0$, and at positions $x \pm \epsilon$, $x + t \in \{0, 2, \ldots, 2t\}$, for some small $\epsilon > 0$. The number of created pairs is geometrically distributed with strength p. Initially there are no particles at all and the restriction on the space–time location of possible nucleation events ensures that

For the restricted case there is a simple exclusion constraint. At most one particle, kink or antikink, is allowed to be at a place, $m_t^{\mathrm{r}}(x) \in \{-1, 0, 1\}$. Nucleations are allowed only one pair at a time with probability p at integer times t but with the nonlocal constraint that inter-particle distances have to be always even integers at the time of creation. With these definitions the correspondence to the discrete–time TASEP can be seen as follows. The mapping is exact for all values of the jump rate p but becomes especially easy to see if we think of p being close to 1.

We think of a TASEP configuration $\eta_t(j)$ with alternating 0's and 1's, say $\cdots 101010101010 \cdots$. This corresponds to the configuration with no (anti)kinks at all. If at the next time step every 1 in the TASEP jumps to its right one has $\cdots 010101010101 \cdots$ and no kink/antikink pairs are produced. If in the following time step a 1 decides not to jump there is a 1100 subsequence, one has $\cdots 101011001010 \cdots$, corresponding to the production of a kink antikink pair. Subsequently, assuming that all TASEP particles which can jump to there right do so, one has $\cdots 010110100101 \cdots$. The 11 pair has moved to the left, and thus corresponds to the kink and the 00 pair has moved to the right corresponding to an antikink. Annihilation of kink/antikink pairs takes place in much the same way. To conclude we obtain the occupation numbers for the kink/antikink gas at half integer times as $m_{t-\frac{1}{2}}(j + \frac{1}{2}) = \eta_t(j) + \eta_t(j + 1)$, $t \in \mathbb{Z}$. Positions inbetween these discrete time steps can be linearly interpolated.

Oriented digital boiling

Gravner et al [53] study the so called oriented digital boiling (ODB) model, see also [55, 54] for a nonhomogeneous generalization. It is specified by the height function $h_t^{\mathrm{ODB}} : \mathbb{N}_0 \to \{-\infty\} \cup \mathbb{Z}$, $t \in \mathbb{N}_0$. Initially $h_0^{\mathrm{ODB}}(j) = -\infty$ for $j > 0$ and $h_0^{\mathrm{ODB}}(0) = 0$. The dynamics is given by

$$h_j^{\mathrm{ODB}}(t + 1) = \max\{h_{j-1}^{\mathrm{ODB}}(t), h_j^{\mathrm{ODB}}(t) + p(j, t)\}, \tag{4.18}$$

where $p(j,t) \in \{0,1\}$ are Bernoulli random variables with Prob$\{p(j,t)=1\} = p$. In [55] an inhomogeneous version of this model is studied where the probability for $p(t,j)=1$ is allowed to depend on j. The ODB is just another interpretation of the Bernoulli cone. We distort D by the following (lattice-)affine transformation,

$$D^{\text{ODB}} = \{(x_1,x_2,x_3) \in \mathbb{Z}^3;\, (x_1 - x_2 + 1, x_2 + 1, x_3 - x_2) \in D\} +]\text{–}1,0]^3. \tag{4.19}$$

If we now set

$$h_j^{\text{ODB}}(t) = \max\{x_3;\, (j,t,x_3) \in D^{\text{ODB}}\}, \quad j,t \in \mathbb{N}_0, \tag{4.20}$$

the rule for D, (4.2), implies the law for $h_j^{\text{ODB}}(t)$ as given by (4.18), where the value of each $p(j,t)$ correspond to the activeness of exactly one vertical bond determining D.

Finally let us mention that as for the last passage percolation interpretation of the Bernoulli cone itself, $h_j^{\text{ODB}}(t)$ can be expressed analogously to $t(M,N)$ in (4.4), as the maximum over all paths γ, running from $(0,0)$ to (j,t), The set of paths is restricted to those sequences, which are strictly increasing in the j–direction, i.e. if $(j,t) \in \gamma$, $t > 0$, then necessarily either $(j-1,t-1) \in \gamma$ or $(j,t-1) \in \gamma$. with these settings

$$h_j^{\text{ODB}}(t) = \max_{\gamma} \sum_{(0,0)\neq(j,t)\in\gamma} p(j,t), \tag{4.21}$$

with the Bernoulli random variables $p(j,t)$ as "random potential".

Translations between the models

There are further distortions of the Bernoulli cone which upon time slicing lead to new or already described discrete height processes. We enumerated the most important of them which have been studied in the literature. Our main point here is to illustrate that any statement for one of the above mentioned models gives some insight in properties of any of the other models. The way to obtain these translations most conveniently is to translate first from one model into the language of the Bernoulli cone, and then back to any other model of interest.

Especially we would have the most detailed information of the statistics of the Bernoulli cone if we knew all the correlation functions, i.e, for subsets $A \subset \mathbb{Z}^3$, the probability

$$p_A(D) = \text{Prob}\{A \subset D\}. \tag{4.22}$$

Although we do not explore it any further, let us note that for $|A| = 1$ one has explicit expressions for p_A, which has been found by Baik and Rains [12]. It holds

even for spatially dependent activation rates for vertical bonds. Let α_j, β_j be two arbitrary sequences in $[0,1[$. Let the vertical bonds, which start at $(l,m,n) \in \mathbb{N}_0^3$, be active with probability $\alpha_l \beta_m$, i.e. all vertically aligned bonds have the same probability, then

$$\begin{aligned} &\text{Prob}\big\{(l,m,n) \notin D\big\} \\ &= \mathbb{E}_{U\in\mathcal{U}(n)}\Big(\det \prod_{i=1}^{l}\prod_{j=1}^{m}(1-\alpha_i\beta_j)(1+\alpha_i U)(1+\beta_j U^\dagger)\Big). \end{aligned} \tag{4.23}$$

Note that the distribution depends only on the values but not on the order of the constants α_i and β_j. It would be of considerable interest to have similar expressions for the probability of a subset of the lattice with two or more elements having empty intersection with D.

4.2 The PNG limit

In order to obtain a nontrivial limit $p \to 0$ of the Bernoulli cone, we have to rescale horizontally, such that the density of active vertical bonds stays fixed. We define

$$D^{\text{PNG}} = \lim_{p\to 0} \begin{pmatrix} \sqrt{p/2} & 0 & 0 \\ 0 & \sqrt{p/2} & 0 \\ 0 & 0 & 1 \end{pmatrix} D_p \tag{4.24}$$

The number of active vertical bonds rarefies when p gets small. The limit is chosen in such a way, that there density remains finite. In the limit $p \to 0$ the vertical bonds in each layer are distributed according to a homogeneous Poisson point process of density 2 in $[0,\infty[^2$. Since the probability that two vertical bonds right above each other are active is zero, the corresponding height function

$$h^{\text{PNG}}(x_1,x_2) = \max\{x_3 \in \mathbb{Z};\ (x_1,x_2,x_3) \in D^{\text{PNG}}\} \tag{4.25}$$

has maximum step size 1 with probability one. We have recovered the height function of the PNG model of Chapter 3 with droplet initial conditions. Without giving details we mention that obviously one can obtain PNG clusters with arbitrary initial conditions by properly choosing a sequence of initial conditions for the Bernoulli cluster.

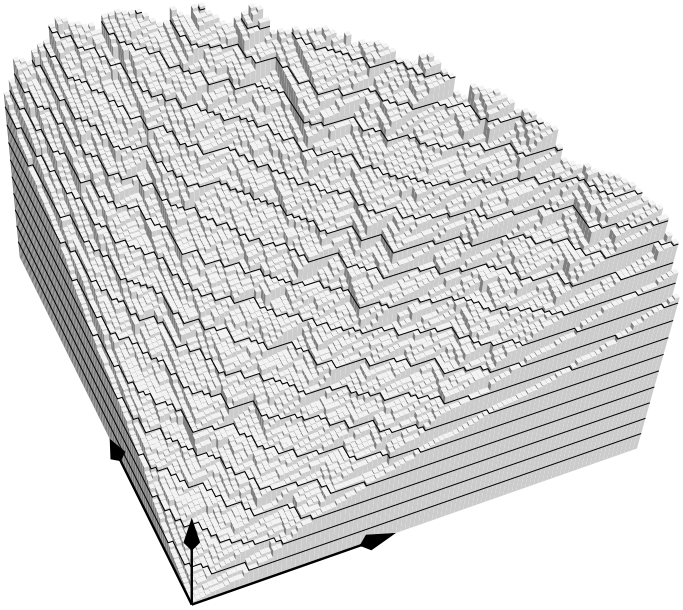

Figure 4.5: *A piece of a TASEP cone. The height lines are corner growth configurations at different times.*

4.3 The TASEP limit

The opposite limit $p \to 1$ of the droplet process requires a rescaling of the 3–axis by the factor $1-p$, in order to obtain a well defined process. We set

$$D^{\text{TASEP}} = \lim_{p\to 1} \begin{pmatrix} 1 & 0 & 0 \\ 0 & 1 & 0 \\ 0 & 0 & 1-p \end{pmatrix} D_p. \tag{4.26}$$

The lateral lattice structure is retained. Look at the recursive law for the height of the Bernoulli cone (4.3)

$$h_p(i,j) = \max\{h_p(i-1,j), h_p(i,j-1)\} + w_p(i,j), \tag{4.27}$$

with i.i.d. random variables $w_p(i,j)$ having geometrical distribution of strength p. Under the scaling (4.26) one obtains the law for the height of the TASEP cone $h(i,j) = \lim_{p\to 1}(1-p)h_p(i,j)$ as

$$h(i,j) = \max\{h(i-1,j), h(i,j-1)\} + w(i,j), \tag{4.28}$$

where $w(i,j)$ are now real valued positive i.i.d. random variables with exponential distribution $\text{Prob}\{w(i,j) > s\} = e^{-s}$. All of the models equivalent to

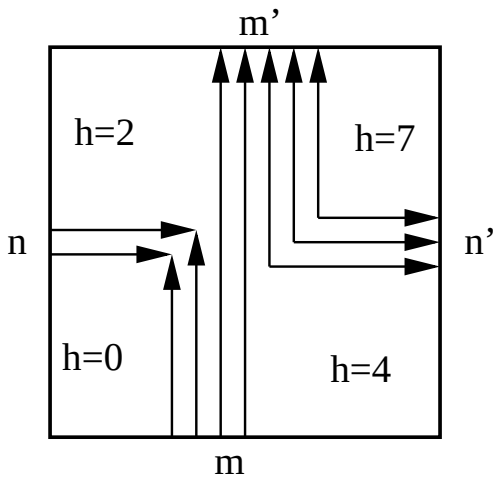

Figure 4.6: *One square of the model with height lines. Three new height lines are produced corresponding to three consecutive active vertical bonds being wetted.*

the Bernoulli cone enumerated in Section 4.1 have their analogue in the TASEP limit. Notably the corner growth, resp. single-step model, become continuous time growth processes with exponentially distributed waiting times for adding a square, cf. Figure 4.5. Also the corresponding particle models, the discrete-time TASEP and zero range processes converge to their well-known continuous-time counterparts, the standard totally asymmetric simple exclusion process and zero range process [82, 83].

4.4 Stationarity

Coming back to the percolation model, we introduce boundary sources, i.e. the vertical bonds at the borders $n_1 = 0$ and $n_2 = 0$ now have a probability α and β, respectively, to become active. The vertical bonds in the bulk still have probability p. The bond at the origin is chosen to be inactive by convention. In the Johansson picture this corresponds to a geometric distribution of the first row and the first line of the integer valued random matrix with strength α and β, respectively, the entry in the corner being fixed as zero. By properly choosing α and β one can arrange the height function $h(n_1, n_2)$ to have stationary increments in the direction of increasing coordinates. We are not aware of any publications which investigate this property. Although the stationary state has been determined for the various mappings to vertex and lattice gas models [106, 110], the height lines of $h(n_1, n_2)$ provide the simplest way to investigate stationarity, since one does not have to impose periodic boundary conditions in order that the steady state has a simple

product form.

The key observation is that it is enough to look at one single square of the shifted lattice $(\mathbb{N}_0 - 1/2)^2$ and study the statistics of incoming and outgoing height lines, projected vertically. If there are m lines entering from the bottom and n lines from the left, $m \wedge n = \min\{m, n\}$ of them annihilate. Let k denote the number of created line pairs in the square, then the number of outgoing lines at the top is $m' = m-(m\wedge n)+k$, and $n' = n-(m\wedge n)+k$ at the right side, see Fig. 4.6. Now let k, m, and n be independent and geometrically distributed with parameters p, α, and β, respectively. The joint probability, $P_{m',n'}$, for m' and n' outgoing lines is

$$\begin{aligned} P_{m',n'} &= (1-p)(1-\alpha)(1-\beta) \sum_{m,n\geq 0} p^{m'\wedge n'} \alpha^m \beta^n \delta_{m-m',n-n'} \\ &= \tfrac{(1-p)(1-\alpha)(1-\beta)}{1-\alpha\beta} p^{m'\wedge n'} \alpha^{(m'-n')\vee 0} \beta^{(n'-m')\vee 0} \\ &= \frac{1-p}{1-\alpha\beta} \left(\frac{p}{\alpha\beta}\right)^{m'\wedge n'} (1-\alpha)(1-\beta)\alpha^{m'}\beta^{n'}, \end{aligned} \tag{4.29}$$

where $m \vee n = \max\{m, n\}$. Thus if $\alpha\beta = p$ the outgoing lines are again distributed independently and geometrically with the same strength as the incoming lines,

$$P_{m',n'} = (1-\alpha)\alpha^{m'}(1-\beta)\beta^{n'}. \tag{4.30}$$

For a given p we arrive at a one-parameter family $\alpha \in]p, 1[$ of stationary solutions, which extend to product measures on space-like paths, i.e. chains of sites connected by bonds and being mutually non-time-like, $(m_1 - n_1)(m_2 - n_2) \leq 0$, for each two sites (m_1, m_2) and (n_1, n_2) in the path. More precisely, we take two space-like paths γ_1 and γ_2, having a time-like separation, i.e. for each site (n_1, n_2) in γ_2 there is at least one site (m_1, m_2) in γ_1 with $m_1 \leq n_1$ and $m_2 \leq n_2$. The (possibly infinite) region enclosed by the two paths is bounded by bonds with incoming lines belonging to γ_1, and bonds with outgoing lines belonging to γ_2. If the numbers of incoming lines for each bond are distributed independently geometrically with strength α for horizontal bonds and p/α for vertical bonds, eq. (4.30) immediately tells us by induction that the numbers of outgoing lines for each bond are still independent with the same distribution for horizontal and vertical bonds as for the incoming lines.

For a space-like path approximating the straight line $n_2 = -\frac{1-b}{1+b} n_1$, $b \in [-1, 1]$, one obtains a proof for Proposition 3.1 of Chapter 3 in the PNG limit. We choose $\alpha = \beta = \sqrt{p}$. The geometric distribution of incoming lines at vertical, resp. horizontal bonds becomes independent Poisson point processes along the straight line in the limit $p \to 0$ upon rescaling the lattice by $\sqrt{p}$. The line densities

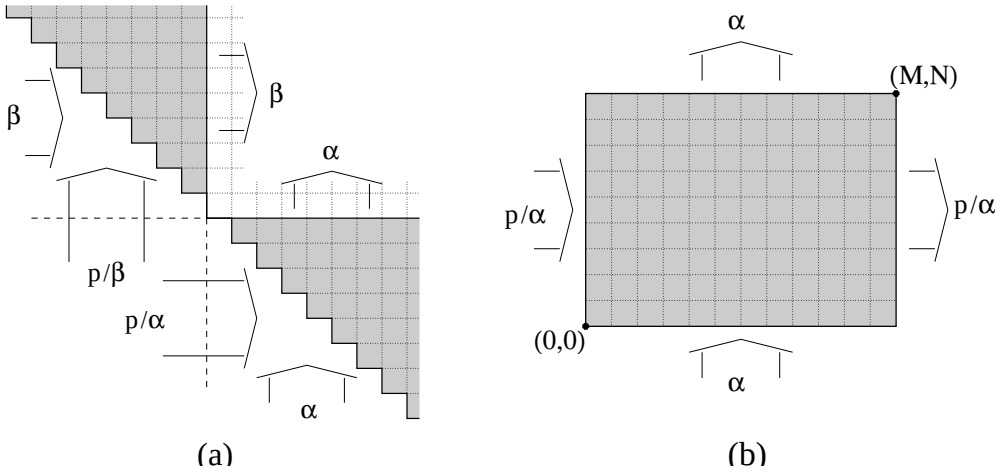

Figure 4.7: *Two examples of propagating the product measure: (a) from a staircase to the border of a quadrant (the parameters $\alpha, \beta \in]p, 1[$ can be chosen independently), and (b) from the lower-left sides of a rectangle to the upper-right sides.*

for entering horizontal lines can be easily calculated as $(1+b)/\sqrt{1+b^2}$, likewise the density for vertical lines is $(1-b)/\sqrt{1+b^2}$.

Two special cases of interest are sketched in Fig. 4.7. Viewed as the discrete PNG model, the anti-diagonal defines initial conditions in form of a fixed macroscopic slope, being different for $x > 0$ and $x < 0$. The macroscopic shapes arising from these initial conditions cover all self-similar macroscopic shapes, possible for this model.

The $M \times N$ rectangle in (Fig. 4.7(b)) can be regarded as a piece of a truely stationary height process defined on the whole plane. This is the discrete analogue of the setting in Section 3.3 and one expects that one could recover the same scaling result. Explicit expressions for the distribution of $h(M, N)$ are available [11]. Unfortunately, the Riemann-Hilbert techniques used for the proof in the PNG case work only for the square case of $H(M, M)$ which allows to prove convergence to the scaling function $g_1^{\text{dyn}}(y)$ only at $y = 0$, so far. In the next section we illustrate how the stationarity property allows to determine the generator of asymptotics by application of the KPZ scaling theory.

4.5 The generator of asymptotics for the Bernoulli cone

For an arbitrary large rectangular piece of the stationary height process as in Fig. 4.7(b) the mean slope of $h(m,n)$ and its roughness amplitude along its sides are immediately obtained from (4.30) as

$$\begin{aligned} u_\alpha &= \mathbb{E}\big(h(m+1,n)-h(m,n)\big) = \frac{\alpha}{1-\alpha}, \\ v_\alpha &= \mathbb{E}\big(h(m,n+1)-h(m,n)\big) = \frac{p}{\alpha-p}, \end{aligned} \tag{4.31}$$

and the roughness amplitude

$$A_\alpha = \mathbb{E}\big((h(m+1,n)-h(m,n)-u_\alpha)^2\big) = \frac{\alpha}{(1-\alpha)^2}. \tag{4.32}$$

If we interpret m as the spatial direction and n as the time direction we obtain for the slope dependent growth velocity

$$v(u) = \frac{p(1+u)}{(1-p)u-p}, \tag{4.33}$$

and the roughness amplitude reads

$$A(u) = u(1+u), \tag{4.34}$$

where $u > 0$.

This information is indeed enough to determine the scaling form of the height process (4.1) for the Bernoulli cone completely. Solving $c = -v'(u)$ for u with $c > 0$, we have $u = \sqrt{p/c}(\sqrt{pc}+1)/(1-p)$. We are looking at a macroscopic reference point (M,N). By setting $c = M/N$ the Legendre transform of (4.33) yields the macroscopic part of the scaling form for a growing droplet

$$h^{\text{det}}(M,N) = Nv(u) + Mu = \frac{p(M+N)+2\sqrt{pMN}}{1-p}. \tag{4.35}$$

The scale of fluctuations, $C(M,N) = (\frac{1}{2}v''(u)A(u)^2N)^{1/3}$ becomes

$$C(M,N) = \frac{1}{1-p}\left(\frac{p}{MN}\right)^{1/6}\left(\sqrt{pM}+\sqrt{N}\right)^{2/3}\left(\sqrt{M}+\sqrt{pN}\right)^{2/3}. \tag{4.36}$$

For the lateral scale of fluctuations, $c(M,N) = (2\lambda^2 AN^2)^{1/3}$, in the scaling form (2.43) we obtain

$$c(M,N) = 2\left(\frac{M^2}{\sqrt{p}N}\right)^{1/3}\big(\sqrt{pM}+\sqrt{N}\big)^{1/3}\big(\sqrt{M}+\sqrt{pN}\big)^{1/3}. \tag{4.37}$$

Putting the pieces together, KPZ scaling theory predicts the scaling limit for the Bernoulli cone

$$\frac{h(M + c(M,N)m, N) - (h^{\text{det}}(M,N) - \partial_1 h^{\text{det}}(M,N)c(M,N)m)}{C(M,N)} \longrightarrow H_1^{\text{curved}}(m) - m^2 \tag{4.38}$$

for $M, N \to \infty$, $M/N = const.$

Let us determine the generator of asymptotics for the Bernoulli cone. We make the ansatz

$$G(m,n,h) = \left([(1-p)h - p(m+n)]^2 - 4pmn\right) f(m,n,h), \tag{4.39}$$

where $f(m,n,h)$ has to be chosen such that

$$\partial_h G(m,n,h) = C(m,n)^{-1}, \tag{4.40}$$

whenever $G(m,n,h) = 0$. Thus we can set

$$G(m,n,h) = \frac{[(1-p)h - p(m+n)]^2 - 4pmn}{4p^{2/3}(mn)^{1/3}\left(\sqrt{pm} + \sqrt{n}\right)^{2/3}\left(\sqrt{m} + \sqrt{pn}\right)^{2/3}}. \tag{4.41}$$

This generator of asymptotics can be used to determine the scaling form in any of the coordinates introduced for the different models described in Section 4.1. Also the limiting cases $p = 0$, $p = 1$ can be easily obtained from (4.41). Performing the PNG limit $p \to 0$, whith new coordinates $r = (p/2)^{1/2}\, m$, $s = (p/2)^{1/2}\, n$ one arrives at

$$G^{\text{PNG}}(x,t,h) = \frac{h^2 - 8\,rs}{4(2\,rs)^{2/3}} = \frac{h^2 - 4(t^2 - x^2)}{4(t^2 - x^2)^{2/3}} \tag{4.42}$$

expressed in the variables for space and time taken as in the original PNG model, $t = (r+s)/2^{1/2}$, $x = (r-s)/2^{1/2}$.

In the TASEP limit $p \to \infty$, the height h has to be rescaled by $1 - p$ and we obtain

$$G^{\text{TASEP}}(m,n,h) = \frac{(h - m - n)^2 - 4mn}{4(mn)^{1/3}(\sqrt{m} + \sqrt{n})^{4/3}} \tag{4.43}$$

In the following chapter the scaling form (2.43) for the PNG model will be shown to be correct, at the same time identifying the limiting process. This strongly confirms the validity of (4.42). Furthermore in a recent preprint [69] Johansson proves the same scaling form for the Bernoulli cone in the language of the unrestricted discrete polynuclear growth model of Section 4.1. As expected, the scaling parameters are given in terms of (4.41). In [100] the consequences of the KPZ scaling theory for the continuous-time TASEP are discussed. All prefactors in scaling relations are in fact contained in (4.43).

CHAPTER 5

The multi-layer PNG model

Up to now we studied one-point distribution functions for given initial conditions. Since they can be interpreted as distributions of height differences, in the stationary case of Section 3.3 we were able to derive two-point correlation functions for arbitrary relative positions in space-time. To go beyond a single height (difference) distribution we need a better understanding of the law for the whole process $(x,t) \mapsto h(x,t)$. To this end we extend the PNG model to a multi-layer version with several interacting copies of PNG lines below the original one. The dynamics we introduce for the lower lying lines resembles very much Viennot's geometric construction to prove the Robinson-Schensted-Knuth correspondence [127]. Therefore we call it RSK dynamics. The dynamics does not affect the statistics of the first line. Surprisingly, the whole line ensemble has a simple distribution with Boltzmann weights. The energy associated with a configuration is very simple. One the one hand the difficulty lies in the structure of the configuration space, which is restricted to non-overlapping PNG lines. On the other hand we need to recover the statistics of the first line as the marginal distribution of the line ensemble.

The equilibrium statistics of the non-intersecting line ensemble is rephrased as a theory of non-interacting lattice fermions on the line in Euclidean space-time. Height fluctuations can be written as expectations of fermionic densities and currents, which have determinantal form.

The scaling limit of the PNG line translates to the continuum limit of the lattice fermions. One obtains non-interacting fermions on the line governed by a Hamiltonian with linear potential. The position of the first fermion at Euclidean time y defines the Airy process $A(y)$. It is stationary in y, the distribution of $A(0)$ is the Tracy-Widom GUE distribution. Very roughly the Airy process looks like one-dimensional Brownian inside a confining potential with long-range correlations.

For the first line of the multilayer PNG model, the original PNG droplet $h(x,t)$, one obtains the limit

$$\frac{h(t^{2/3}y,t)-2t}{t^{1/3}} \to A(y)-y^2 \quad \text{for } t\to\infty, \tag{5.1}$$

identifying $H_1^{\text{curved}}(y)$ as the Airy process $A(y)$. Thus the limiting distribution for curved growth, F_{GUE}, is recovered. But (5.1) contains much more information. It predicts the scaling limit for arbitrary static n-point correlation functions. In [102] the Airy process was introduced and (5.1) proved in the sense of joint distributions. In a recent preprint [69] Johansson proves for the discrete PNG model of Section 4.1 convergence of the probability measures themselves, confirming the universality claim.

5.1 The Airy process

The Airy process can be obtained as the position of the first particle in Dyson's Brownian motion [41]. The first line of N non-intersecting Brownian paths confined to a quadratic potential converges in the limit $N \to \infty$ to the Airy process. Dyson's particle trajectories correspond to the eigenvalues of a GUE random matrix valued process. Let $a_{jk}(s)$, $1 \le j, k \le N$ be real-valued mutually independent stationary Ornstein-Uhlenbeck processes of variance $\frac{1}{4}$. Then the hermitian matrix $H(s)$ with entries $H_{jk} = a_{jk} + ia_{kj} = \overline{H_{kj}}$ for $j < k$ and $H_{jj} = \sqrt{2}\, a_{jj}$ is, for fixed s, distributed according to the standard Gaussian unitary ensemble (GUE) of hermitian $N \times N$ matrices. The eigenvalues of $H(s)$, $\lambda_1(s) < \cdots < \lambda_N(s)$ have the stationary distribution $Z_N^{-1} \prod_{i<j} (\lambda_i - \lambda_j)^2 \prod_i e^{-\lambda_i^2}$. They are the trajectories of Dyson's particles. The largest eigenvalue converges to the Airy process,

$$\sqrt{2}\, N^{1/6} (\lambda_N(N^{-1/3} y) - \sqrt{2N}) \to A(y) \tag{5.2}$$

in the sense of joint distributions.

Explicitly $A(y)$ is defined by means of the extended Airy kernel [102, 69]

$$K(u, y;\, u', y') = \begin{cases} \int_{-\infty}^{0} e^{\lambda(y'-y)} \mathrm{Ai}(u-\lambda)\mathrm{Ai}(u'-\lambda) d\lambda & \text{for } y \le y' \\ -\int_{0}^{\infty} e^{\lambda(y'-y)} \mathrm{Ai}(u-\lambda)\mathrm{Ai}(u'-\lambda) d\lambda & \text{for } y > y'. \end{cases} \tag{5.3}$$

Note that the exponents in the integrand are always decaying. For $y = y'$ it reduces to the ordinary Airy kernel [121], which has integral form

$$\begin{aligned} K(u, u') &= \int_{-\infty}^{0} \mathrm{Ai}(u-\lambda)\mathrm{Ai}(u'-\lambda) d\lambda \\ &= \frac{\mathrm{Ai}(u)\mathrm{Ai}'(u') - \mathrm{Ai}'(u)\mathrm{Ai}(u')}{u - u'}. \end{aligned} \tag{5.4}$$

The Airy process $A(y)$ is defined through its finite-dimensional distributions at $y_1, \ldots, y_m \in \mathbb{R}$. For $y_1 < \cdots < y_m$ we define the projector P on $\Omega = \mathbb{R} \times \{y_1, \ldots, y_m\} \subset \mathbb{R}^2$ as multiplication by the characteristic function of the set

$\bigcup_{1\le j\le m}]u_j,\infty[\times\{y_j\}\subset\Omega$. PKP, with K given by the kernel (5.3) is a trace class operator on $L^2(\Omega,\mu)$ with counting measure on $\{y_1,\dots,y_m\}$ and Lebesgue measure on $\mathbb{R}$ ([69], Prop. 2.4) and one sets

$$\text{Prob}\{A(y_1)\le u_1,\dots,A(y_m)\le u_m\}=\det(1-PK)_{L^2(\Omega,\mu)}. \tag{5.5}$$

The determinant is defined by the Fredholm expansion

$$\det(1-K)=\sum_{m=0}^{\infty}\frac{(-1)^m}{m!}\int_\Omega \det\big(K(x_k;x_l)\big)_{1\le k,l\le m}d^m\mu(x) \tag{5.6}$$

for any trace class operator K on $L_2(\Omega,\mu)$ with integral kernel $K(x;y)$. One has $\det(1-KK')=\det(1-K'K)$. For a finite counting measure (5.6) is just the ordinary determinant.

In the Appendix of [102] it is shown that $A(y)$ has a version with continuous sample paths. The distribution at y is given by

$$\text{Prob}\{A(y)\le s\}=\det(1-K)_{L_2(]s,\infty[)}=F_{\text{GUE}}(s), \tag{5.7}$$

independently of y, where K reduces to the ordinary Airy kernel (5.4). The variance increases linearly for short distances,

$$\mathbb{E}\big([A(y)-A(0)]^2\big)=2|y|+\mathcal{O}(y^2), \tag{5.8}$$

and correlations are slowly decaying,

$$\mathbb{E}\big(A(y)A(0)\big)-\mathbb{E}\big(A(y)\big)\mathbb{E}\big(A(0)\big)=c\,y^{-2}+\mathcal{O}(y^{-4}) \tag{5.9}$$

with a positive constant c, whose value $\approx 1.5\pm 0.3$ is estimated from a Monte-Carlo simulation.

5.2 The multi-layer PNG droplet

Let us define the multi-layer PNG model with the RSK dynamics. In addition to the original PNG line $h(x,t)=h_0(x,t)$ we have an infinite hierarchy of height lines $h_\ell(x,t)\in\mathbb{Z}$, $\ell\le 0$, subject to the constraint of no overlap, $h_{\ell-1}(x,t)<h_\ell(x,t)$, as a static and dynamical restriction. The deterministic dynamics for each of the height lines is the same as for the PNG model, up/down-step motion with constant velocity and annihilation upon collision. Nucleations of up/down-step pairs for the lower lying lines are not independently random but occur whenever an annihilation event takes place in the adjacent line above. Thus at time t if in the ℓ-th height line a collision of an up-step and a down-step occurs at position x, they

disappear in this line only to reappear as nucleation at (x,t) in line $\ell-1$. Only in the first line nucleations happen randomly with space-time density 2. Clearly this dynamics respects the ordering $h_\ell < h_{\ell+1}$.

As initial conditions we take $h_\ell(x,0) = \ell$ with nucleations on the first line only allowed in the region $\{|x| \le t\}$. Inside the interval $[-t,t]$ the first line $h_0(x,t)$ has the law of the PNG droplet, Section 3.1. Note that the total number of up-steps, which equals the total number of down-steps, can not decrease in the course of time. At time t it is Poisson distributed with mean $2t^2$, two times the space-time volume up to time t. In Figure 5.1 a typical realization at time t is shown.

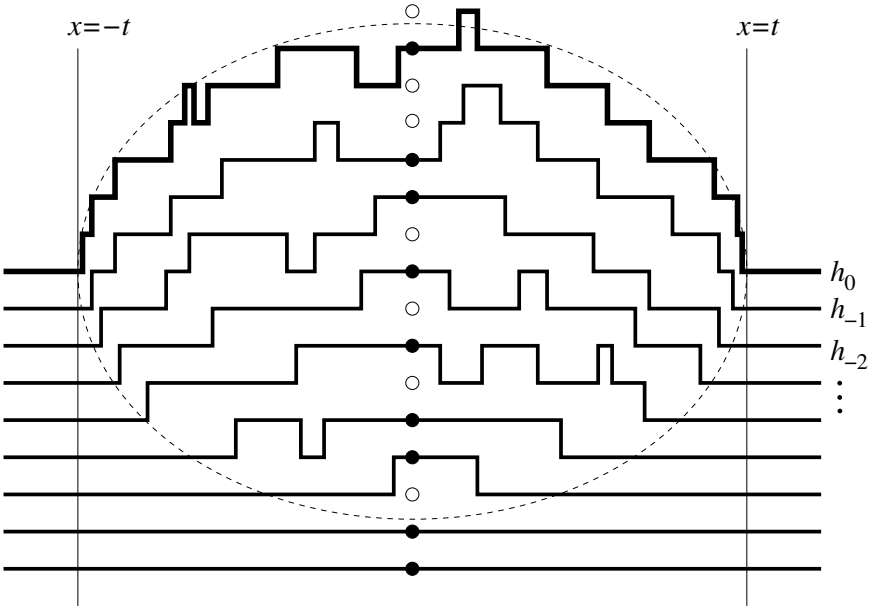

Figure 5.1: *A multi-layer PNG droplet at time t. The asymptotic droplet shape is indicated by the dotted line. For $x = 0$ a corresponding fermionic configuration is drawn.*

Let us define a measure on the space Γ_t of all non-intersecting height line configurations $h_\ell(x,t)$ at time t, with finitely many steps, by parameterizing with respect to the step positions. For definiteness we require $h_\ell(x,t)$ to be upper semi-continuous, i.e. $\{x;\, h_\ell(x,t) \ge c\}$ is closed for all $c \in \mathbb{R}$. One has $h_\ell(x,t) = \ell$ for $|x| > t$ and $h_\ell(x,t) < h_{\ell-1}(x,t)$ for $\ell \le 0$. Let n_ℓ be the number of up-steps in height line ℓ which always equals the number of down-steps. If $n_\ell = 0$, $h_\ell(x,t) = \ell$ for all $x \in \mathbb{R}$. If $n_\ell > 0$, the position of the j-th up-step in height line ℓ is denoted by $y_j^{\ell,+}$, $-t < y_1^{\ell,+} < \cdots < y_{n_\ell}^{\ell,+} < t$ and the position of the j-th down-step in the same height line is denoted by $y_j^{\ell,-}$, $-t < y_1^{\ell,-} < \cdots < y_{n_\ell}^{\ell,-} < t$. We set $\mathbf{n} = (n_0, n_{-1}, \dots)$, and $|\mathbf{n}| = \sum_{\ell \le 0} n_\ell$. We denote by $\Gamma_t(\mathbf{n})$ the set of

all step configurations $\big((y_j^{\ell,+}, y_j^{\ell,-})_{1\le j\le n_\ell}\big)_{\ell\le 0}$ such that the corresponding height lines do not intersect. $\Gamma_t(0)$ is a single point and $\Gamma_t(\mathbf{n})$ is naturally embedded in $[-t,t]^{2|\mathbf{n}|}$. By the upper semi-continuity if an up-step and a down-step in the same height line are at the same location, they represent a nucleation and not a collision. We set $\Gamma_t(n) = \bigcup_{|\mathbf{n}|=n} \Gamma_t(\mathbf{n})$ as a disjoint union, and finally $\Gamma_t = \bigcup_{n\ge 0} \Gamma_t(n)$.

Let w_t be the uniform measure on Γ_t, which means that $w_t\big(\Gamma_t(0)\big) = 1$ and $w_t \restriction \Gamma_t(\mathbf{n})$ is the $2|\mathbf{n}|$-dimensional Lebesgue measure on $\Gamma_t(\mathbf{n})$. For arbitrary nucleation rate ξ we define the probability measure μ_t on Γ_t as

$$\mu_t = Z_t^{-1}\big(\tfrac{\xi}{2}\big)^{|\mathbf{n}|} w_t. \tag{5.10}$$

Thus μ_t is proportional to the Lebesgue measure in each sector.

Theorem 5.1 *The probability measure induced by the multilayer droplet process $h_\ell(x,t)$ at time t on Γ_t is μ_t. Furthermore $Z_t = e^{\xi t^2}$ and*

$$w_t\big(\Gamma_t(n)\big) = \frac{(2t^2)^n}{n!}. \tag{5.11}$$

Proof: The mapping defined by the RSK dynamics from Poisson point configurations inside the triangle $T_t = \{(x',t');\, |x'| \le t' \le t\}$ into Γ_t is clearly locally linear in an open dense set. More precisely, for Poisson points $(x_i,t_i) \in T_t$, $1 \le i \le n$, such that all $r_i = t_i + x_i$ are pairwise distinct and all $s_i = t_i - x_i$ are pairwise distinct, up-step positions at time t are at $t - s_i$ and down-step positions are at $t + r_i$. Therefore the determinant of this mapping is 2^n. The probability to have n points in T_t is $(\xi\, t^2)^n/n!$. The theorem follows provided the RSK mapping is onto.

This can be easily seen by running the RSK dynamics backwards in time. Take any element $\big((y_j^{\ell,+}, y_j^{\ell,-})_{1\le j\le n_\ell}\big)_{\ell\le 0}$ of Γ_t. The corresponding height lines are defined as

$$h_\ell(x,t) = \ell + \sum_{j=1}^{n_\ell} \theta(x - y_j^{\ell,+}) + \big(\theta(y_j^{\ell,+} - x) - 1\big) \tag{5.12}$$

with the Heaviside function $\theta(x) = 1$ for $x \ge 0$, $\theta(x) = 0$ for $x < 0$. The evolution backward in time is completely deterministic. When an up-step and a down-step collide inside the same height line ℓ they are bumped into line $\ell + 1$. Collisions in the first line $\ell = 0$ mark the space-time coordinates of nucleation events. At $t = 0$ one has recovered all nucleation events, which obviously lie in T_t. $\square$

We introduce the occupation variables $\eta_j(x)$ with values in $\{0,1\}$ by setting

$$\eta_j(x) = \begin{cases} 1, & \text{if } h_\ell(x,t) = j \text{ for some } \ell, \\ 0, & \text{otherwise.} \end{cases} \tag{5.13}$$

Their expectations with respect to μ_t can be written in the form of a path integral,

$$\mathbb{E}\big(\eta_{j_1}(x_1)\cdots\eta_{j_m}(x_m)\big) = Z_t^{-1}\int \big(\tfrac{\xi}{2}\big)^{\sum_\ell \int_{-t}^t |\partial_x h_\ell(x)|dx}\eta_{j_1}(x_1)\cdots\eta_{j_m}(x_m)dw_t. \tag{5.14}$$

To proceed we introduce a cut-off $M > 0$. Height lines with index $\ell < M$ are neglected. The remaining height lines are restricted vertically to the interval $\{-M,\dots,M\}$. We will suppress the index M in the following formulas, eventually we send $M \to \infty$. Let us compute the general partition sum $Z_{[x,y]}(\eta,\vartheta)$, with arbitrary left and right boundary conditions $\eta,\vartheta \in \{0,1\}^{\{-M,\dots,M\}}$, $\sum_j \eta_j = \sum_j \vartheta_j = N$,

$$Z_{[x,y]}(\eta,\vartheta) = \int_{\eta(x)=\eta,\eta(y)=\vartheta} \big(\tfrac{\xi}{2}\big)^{\sum_\ell \int_x^y |\partial_x h_\ell(x')|dx'} dw_{[x,y]}. \tag{5.15}$$

$w_{[x,y]}$, $y > x$, denotes the Lebesgue measure with respect to step positions restricted to the interval $[x,y]$ of non-intersecting line configurations. $Z_{[x,y]}(\eta,\vartheta)$ is the weighted phase space volume for configurations of N height lines in the interval $[x,y]$ with fixed left and right boundary and confined to values in $\{-M,\dots,M\}$. Clearly $Z_t = Z_{[-t,t]}(\omega,\omega)$, $\omega_j = 1$ for $j \le 0$ and $\omega_j = 0$ for $j > 0$, in the limit $M \to \infty$. $Z_{[x,y]}$ is a square matrix of dimension $\binom{2M+1}{N}$ with the semi group property $Z_{[x,y]}Z_{[y,z]} = Z_{[x,z]}$. Assume that in (5.14) the x_k are ordered, $-t \le x_1 \le \cdots \le x_m \le t$. Then the path integral can be written as

$$\begin{aligned}\mathbb{E}\big(\eta_{j_1}(x_1)\cdots\eta_{j_m}(x_m)\big) \;&=\; \lim_{M\to\infty}\big(Z_{[-t,t]}(\omega,\omega)\big)^{-1}\\ &\times\big(Z_{[-t,x_1]}\delta_{j_1}Z_{[x_1,x_2]}\delta_{j_2}\cdots Z_{[x_{m-1},x_m]}\delta_{j_m}Z_{[x_m,t]}\big)(\omega,\omega),\end{aligned} \tag{5.16}$$

where $\delta_j(\eta,\vartheta)$ is the diagonal matrix with entries 1 if $\eta_j = 1$ and 0 otherwise.

At this point we switch to the fermionic language which facilitates the task to calculate these expectation values explicitly. The CAR algebra over $\mathbb{Z}$ is generated by the fermionic creation and annihilation operators $a^*(j)$, $a(j)$, $j \in \mathbb{Z}$, respectively. They satisfy the canonical anticommutation relations

$$\{a(i),a^*(j)\} = \delta_{ij}, \quad \{a(i),a(j)\} = 0, \quad \{a^*(i),a^*(j)\} = 0. \tag{5.17}$$

The Hamiltonian for the free fermions is

$$H = -\sum_{j\in\mathbb{Z}} \sqrt{\tfrac{\xi}{2}}\big(a^*_{j+1}a_j + a^*_j a_{j+1}\big) \tag{5.18}$$

with $a^*_j, a_j = 0$ for $j \in \mathbb{Z}\setminus\{-M,\dots,M\}$. From now on we specify to $\xi = 2$, without loss of generality. The state with fermionic occupation $\eta \in \{0,1\}^{\{-M,\dots,M\}}$

is denoted as

$$|\eta\rangle = \prod_{j=-M}^{M} (a_j^*)^{\eta_j}|0\rangle, \tag{5.19}$$

where $|0\rangle$ is the vacuum vector with no fermions at all. With this notation at hand it is easy to see that the partition function (5.15) can be written as

$$Z_{[x,y]}(\eta,\vartheta) = \langle\eta|e^{-(y-x)H}|\vartheta\rangle, \tag{5.20}$$

compare with [102], where the construction of the fermionic Fock space is explained in detail. General expectations now read (with proper time order in force)

$$\begin{aligned}\mathbb{E}\big(\eta_{j_1}(x_1)\cdots\eta_{j_m}(x_m)\big) &= \lim_{M\to\infty}\langle\omega|e^{-2tH}|\omega\rangle^{-1}\langle\omega|e^{-(x_1+t)H}a_{j_1}^*a_{j_1}\\ &\times e^{-(x_2-x_1)H}a_{j_2}^*a_{j_2}\cdots e^{-(x_m-x_{m-1})H}a_{j_m}^*a_{j_m}e^{-(t-x_m)H}|\omega\rangle.\end{aligned} \tag{5.21}$$

Exponentials of operators quadratic in a, a^* are easily handled. For $H = \sum_{ij} a_i^* h_{ij} a_j$ one has

$$e^{-xH}a_i e^{xH} = \sum_j (e^{xh})_{ij}a_j, \quad e^{-xH}a_j^* e^{xH} = \sum_i a_i^*(e^{-xh})_{ij}, \tag{5.22}$$

easily verified by differentiation with respect to x. Therefore we first focus on expectations at $x = 0$.

We define the density matrix

$$\rho_t = \langle\omega|e^{-2tH}|\omega\rangle^{-1}e^{-tH}|\omega\rangle\langle\omega|e^{-tH}. \tag{5.23}$$

Its trace is 1 and arbitrary expectations can be reduced to quadratic ones by

$$\mathrm{tr}(\rho_t a_j^*) = 0 = \mathrm{tr}(\rho_t a_j), \tag{5.24}$$

$$B_{M,t}(i,j) \stackrel{\mathrm{def}}{=} \mathrm{tr}(\rho_t a_i^* a_j) = \big(e^{-th}P_\omega(P_\omega e^{-2th}P_\omega)^{-1}P_\omega e^{-th}\big)_{ij}, \tag{5.25}$$

$$\mathrm{tr}(\rho_t a_{i_1}^*\cdots a_{i_m}^* a_{j_m}\cdots a_{j_1}) = \det\big(B_{M,t}(i_k,j_l)\big)_{1\le k,l\le m}, \tag{5.26}$$

where $(P_\omega)_{ij} = \delta_{ij}\omega_j$ is the projection onto sites occupied in the ground state. The inverse in (5.25) is taken within the image of P_ω. It can be simplified for a Cholesky decomposition of e^{2th}. Let U and L be invertible operators and P a projection such that $UP = PUP$ and $PL = PLP$. One has $PU^{-1} = PU^{-1}P$ and $L^{-1}P = PL^{-1}P$. Therefore

$$P\big((1-P)+PLUP\big)^{-1}P = U^{-1}PL^{-1}. \tag{5.27}$$

In finite dimensions one can think of U as an upper triangle matrix and of L as a lower triangle matrix, and P a diagonal projector, for example $P_{ij} = \delta_{i,j}$ for $i < k \in \mathbb{N}$ and zero otherwise.

From (5.18) we have that $h = -d - d^*$, where d is the left shift $d_{ij} = \delta_{i,(j-1)}$, an upper triangle matrix, and d^*, its transpose, lower triangle. If d and d^* were commuting we could apply (5.27). For finite M this is not the case. The situation simplifies when $M \to \infty$.

In the limit $M \to \infty$ we have to give up the Fock space, for we have infinitely many fermions. In [102] it is shown that $\mathrm{tr}(\rho_t \cdot)$ converges to a quasifree state $\omega_t(\cdot)$, i.e. a bounded linear functional on the CAR algebra over $\mathbb{Z}$ [26]. It is defined by

$$\begin{aligned} \omega_t(1) &= 1, && (5.28)\\ \omega_t(a_j^*) &= 0 = \omega_t(a_j), && (5.29)\\ \omega_t(a_i^* a_j) &= B_t(i,j) \stackrel{\text{def}}{=} \lim_{M\to\infty} B_{M,t}(i,j), && (5.30)\\ \omega_t(a_{i_1}^* \cdots a_{i_m}^* a_{j_m} \cdots a_{j_1}) &= \det\big(B_t(i_k, j_l)\big)_{1\le k,l\le m}. && (5.31) \end{aligned}$$

Since d and d^* commute on $\mathbb{Z}$, by (5.27) we can identify B_t as

$$B_t = e^{-th} P_\omega (P_\omega e^{2td^*} e^{2td} P_\omega)^{-1} P_\omega e^{-th} = e^{t(d^*-d)} P_\omega e^{-t(d^*-d)}. \tag{5.32}$$

By Fourier transforming one has

$$\big(e^{t(d^*-d)}\big)_{mn} = \tfrac{1}{2\pi} \textstyle\int_{-\pi}^{\pi} e^{ik(n-m)} e^{-2it\sin k} dk = J_{n-m}(2t), \tag{5.33}$$

the modified Bessel function of order $n-m$. Thus B_t is the well-known discrete Bessel kernel

$$B_t(i,j) = \sum_{\ell \le 0} J_{i-l}(2t) J_{j-l}(2t) \tag{5.34}$$

It has integral representation

$$B_t(i,j) = t \frac{J_{i-1}(2t) J_j(2t) - J_i(2t) J_{j-1}(2t)}{i-j} \quad \text{for } i \neq j, \tag{5.35}$$

which holds also on the diagonal, employing l'Hospital's rule for $i \to j$. To verify one has to convert (5.34) into a telescoping sum using the identity $\frac{n}{t} J_n(2t) = J_{n-1}(2t) + J_{n+1}(2t)$. The shifted Bessel functions $n \mapsto J_{n-l}(2t)$ form a complete system of eigenfunctions with eigenvalues $\frac{l}{t}$ for the Hamiltonian h_t,

$$h_t \psi(n) = -\psi(n-1) - \psi(n+1) + \frac{n}{t} \psi(n) \tag{5.36}$$

regarded as an operator on $\ell_2(\mathbb{Z})$. Note that this is the free one-particle Hamiltonian (5.18) together with a linear potential. Thus B_t is the spectral projection onto $\{h_t \leq 0\}$.

Using the anticommutation relations (5.17) we can already compute expectations at $x = 0$. For pairwise distinct $j_1, \ldots, j_m$ one has

$$\begin{aligned} \mathbb{E}\big(\eta_{j_1}(0) \cdots \eta_{j_m}(0)\big) &= \omega_t(a^*_{j_1} a_{j_1} \cdots a^*_{j_m} a_{j_m}) \\ &= \det\big(B_t(j_k, j_l)\big)_{1 \leq k,l \leq m}. \end{aligned} \tag{5.37}$$

The second equality holds for there is always an even number of transpositions needed to propagate the a_j to the right as in (5.31). Thus the probability measure for $\eta_j(0)$ has determinantal correlations. In the probabilistic literature point processes of this structure are known as determinantal [114]. We need (5.37) for arbitrary j_k. One has to take care of the anticommutation relations (5.17) when normal ordering. $B_t(i,j)$ has to be replaced by $B_t(i,j) - \delta_{i,j}$ when a_j is left of a^*_i. This yields

$$\mathbb{E}\big(\eta_{j_1}(0) \cdots \eta_{j_m}(0)\big) = \det\big(B_t(j_k, j_l) - \theta(k-l)\delta_{j_k, j_l}\big)_{1 \leq k,l \leq m}. \tag{5.38}$$

For arbitrary x we have to employ (5.22). In order to allow for coinciding sites one has to respect the time order. We define the extended discrete Bessel kernel [102]

$$B_t(i,x;j,y) = \begin{cases} \omega_t(e^{-xH} a^*_i e^{xH} e^{-yH} a_j e^{yH}) = (e^{-xh} B_t e^{yh})_{ij} & \text{for } x \leq y \\ -\omega_t(e^{-yH} a_j e^{yH} e^{-xH} a^*_i e^{xH}) = (e^{-xh}(B_t - \mathbb{1}) e^{yh})_{ij} & \text{for } x > y, \end{cases} \tag{5.39}$$

where $\mathbb{1}$ is the identity matrix.

Let us write the extended Bessel kernel in the eigenbasis of h_t. The integer order Bessel function has the representation

$$J_n(2t) = \frac{1}{2\pi i} \oint \frac{dz}{z} e^{t(z^{-1} - z)} z^n \tag{5.40}$$

where the contour integration is a circle around $z = 0$. Therefore

$$\big(e^{-xh} J_\cdot(2t)\big)_n = \frac{1}{2\pi i} \oint \frac{dz}{z} e^{t(z^{-1} - z)} e^{x(z^{-1} + z)} z^n \,. \tag{5.41}$$

Substituting z by $(t+x)^{1/2}(t-x)^{1/2} z$ yields

$$\big(e^{-xh} J_\cdot(2t)\big)_n = J_n\big(2\sqrt{t^2 - x^2}\big) \Big(\frac{t+x}{t-x}\Big)^{n/2}. \tag{5.42}$$

We substitute into (5.39) and obtain

$$B_t(j,x;j',x') = \begin{cases} \sum_{l\le 0} \alpha^{j-l} J_{j-l}(2v) J_{j'-l}(2v) \alpha^{-(j'-l)} & \text{for } x \le x' \\ -\sum_{l>0} \alpha^{j-l} J_{j-l}(2v) J_{j'-l}(2v) \alpha^{-(j'-l)} & \text{for } x > x' \end{cases} \tag{5.43}$$

with $\alpha = \left(\frac{t+x}{t-x}\right)^{1/2}$ and $v = \sqrt{t^2-x^2}$.

The expectation (5.21) with arbitrary j_k and time ordered $x_1 < \cdots < x_m$ is

$$\begin{aligned} \mathbb{E}\big(\eta_{j_1}(x_1)\cdots\eta_{j_m}(x_m)\big) &= \omega_t\big((e^{-x_1 H} a_{j_1}^* e^{x_1 H})(e^{-x_1 H} a_{j_1} e^{x_1 H}) \times \cdots \\ &\quad \cdots \times (e^{-x_m H} a_{j_m}^* e^{x_m H})(e^{-x_m H} a_{j_m} e^{x_m H})\big) \\ &= \det\big(B_t(j_k,x_k;\, j_l,x_l)\big)_{1\le k,l\le m}. \end{aligned} \tag{5.44}$$

Expectation with equal times $x_k = x_{k+1}$ are recovered in the limit $x_k \nearrow x_{k+1}$. Here is a subtlety which merits to be stressed. $\mathbb{E}\big(\eta_{j_1}(x_1)\cdots\eta_{j_m}(x_m)\big)$ is a continuous function of $x_1,\ldots,x_m$ even if some of the j_k are coinciding. Obviously it is symmetric with respect to permutations of the (j_k,x_k). The same is true for $\det\big(B_t(j_k,x_k;\, j_l,x_l)\big)_{1\le k,l\le m}$. But the determinant is always zero if there are k,l with $j_k = j_l$ and one sets $x_k = x_l$. Nevertheless the limits $x_k \nearrow x_l$ and $x_k \searrow x_l$ exist, are equal, and in general nonzero. In conclusion Expectations for arbitrary pairwise distinct points $(j_k,x_k)_{1\le k\le m}$ are given by the determinantal formula in (5.44).

We mention that the extended kernel $B_t(j,x;\,j',x')$ can be replaced by the kernel $g(j,x)B_t(j,x;\,j',x')g(j',x')^{-1}$ with arbitrary $g(j,x) \neq 0$. The additional factors for such a similarity transformation cancel always upon evaluating the determinant in (5.44).

We promised to learn something about joint distributions of the first PNG line $h_0(x,t) = h(x,t)$. We look at the m-point distribution at $(j_k,x_k)_{1\le k\le m}$, $j_k \in \mathbb{Z}$ arbitrary and $x_1 < \cdots < x_m$ in $[-t,t]$. Define the set

$$Q_M = \bigcup_{k=1}^{m} (\{x_k\} \times \{j_k+1,\ldots,M\}) \subset \Omega, \tag{5.45}$$

$\Omega = \{x_1, \ldots, x_m\} \times \mathbb{Z}$. The joint distribution function is given by

$$\begin{aligned}
&\text{Prob}\{h(x_1,t) \le j_1, \ldots, h(x_m,t) \le j_m\} \quad = \\
&= \lim_{M\to\infty} \mathbb{E}\Big(\prod_{(x,j)\in Q_M} \big(1-\eta_j(x)\big)\Big) \\
&= \lim_{M\to\infty} \sum_{n=0}^{|Q_M|} (-1)^n \sum_{A\subset Q_M,\,|A|=n} \mathbb{E}\Big(\prod_{(x,j)\in A} \eta_j(x)\Big) \\
&= \lim_{M\to\infty} \sum_{n=0}^{|Q_M|} (-1)^n \sum_{A\subset Q_M,\,|A|=n} \det\big(B_t(j,x;\,j',x')\big)_{(x,j),(x',j')\in A} \\
&= \lim_{M\to\infty} \sum_{n=0}^{|Q_M|} \frac{(-1)^n}{n!} \sum_{((\xi_1,i_1),\ldots(\xi_n,i_n))\in(Q_M)^n} \det\big(B_t(i_k,\xi_k;\,i_l,\xi_l)\big)_{1\le k,l\le n} \\
&= \det(1-P_Q B_t)_{\ell^2(\Omega)}, \qquad (5.46)
\end{aligned}$$

where the projector P_Q is multiplication by the characteristic function of the set $Q = \lim_{M\to\infty} Q_M$ and B_t is regarded as an operator on $\ell^2(\Omega)$. To prove the existence of the limit $M \to \infty$ we need to show that

$$\text{Prob}\{h(x_1,t) > M, \ldots, h(x_m,t) > M\} \to 0 \qquad \text{for } M \to \infty. \qquad (5.47)$$

Since the maximum of $h(x,t)$ is smaller than the number of nucleation events up to time t, we have for $M > 2t^2$, the average number of nucleation events, an exponential bound on the left expression in (5.47).

5.3 The scaling limit

The statement (5.1) is shown in the sense of joint distributions. For the single point distribution this reduces to the limit

$$F_n^{\text{GUE}} = \det(1-B_t)_{\ell^2(\{n+1,\infty\})} \to F_{\text{GUE}}(s) \qquad (5.48)$$

with $n = [2t + t^{1/3}s]$ as $t \to \infty$. Here B_t is the ordinary discrete Bessel kernel (5.35). Comparing (5.48) with (3.17) we encounter a special instance of the Borodin-Okounkov identity [25] which constructively relates any Toeplitz determinant to a corresponding Fredholm determinant. The proof of the convergence of the m-point distribution function (5.46) to (5.5) in the proper scaling limit is shown essentially by the convergence of the extended Bessel kernel to the Airy kernel.

Before going into details, let us first note that the Airy kernel can be regarded as the spectral projection $P_{\{H_{\rm Ai}\leq 0\}}$ onto the negative spectrum of the selfadjoint operator $H_{\rm Ai}$ on $L_2(\mathbb{R})$,

$$H_{\rm Ai} = -\frac{d^2}{du^2} + u. \tag{5.49}$$

H is the Hamiltonian of a particle in a linear potential with generalized eigenfunctions $u \mapsto {\rm Ai}(u-\lambda)$, for we have ${\rm Ai}''(s) = s{\rm Ai}(s)$. The extended Airy kernel (5.3) can be written as

$$K(u,y;\,u',y') = \big(e^{-yH_{\rm Ai}}\big(P_{\{H_{\rm Ai}\leq 0\}} - \theta(y'-y)\mathbb{1}\big)e^{y'H_{\rm Ai}}\big)(u,u'). \tag{5.50}$$

$H_{\rm Ai}$ determines not only the ground state of non-interacting fermions at chemical potential zero corresponding to the line ensemble, but also their dynamical correlations in Euclidean time. This is in contrast to the fermions on the lattice for the multi-layer PNG, whose ground state is determined by h_t but their dynamics is governed by the free Hamiltonian h. Note that we have to rescale in (5.36) n by $t^{-1/3}$ and fermionic time x by $t^{-2/3}$ in order to obtain $H_{\rm Ai}$ from h_t in the continuum limit $t\to\infty$. Focusing on the asymptotic mean $2t$ of $h_0(0,t)$ and removing the curvature, $h_0(x,t) \simeq 2t - x^2/t$ for small x, we arrive at the scaling

$$\begin{aligned} n &= [2t + t^{1/3}(u-y^2)], \\ x &= t^{2/3}y, \end{aligned} \tag{5.51}$$

where we expect a nontrivial limit. Indeed one has

$$\lim_{t\to\infty} t^{1/3} J_{[2t+t^{1/3}(u-y^2)]}\big(2t\sqrt{1-t^{2/3}y^2}\big) = {\rm Ai}(u) \tag{5.52}$$

uniformly for u varying over a compact set [1].

Let us define the rescaled Bessel kernel

$$K_t(u,y;u',y') \;=\; t^{1/3}e^{-t^{-1/3}ny}B_t(n,x;\,n',x')e^{t^{1/3}n'y'} \tag{5.53}$$

with (5.51) also for the primed variables. The multiplication by $e^{t^{1/3}(n'-n)y}$ does not affect determinants, for it is a similarity transformation. It is needed to tame the diverging factors $\big(\frac{t+x}{t-x}\big)^{n/2}$, $\big(\frac{t+x'}{t-x'}\big)^{-n'/2}$ in the extended Bessel kernel. Indeed one has

$$\Big(\frac{1+t^{-1/3}y}{1-t^{-1/3}y}\Big)^{(2t+t^{1/3}u)/2} \to e^{2t^{2/3}y+(u-y^2)y}, \tag{5.54}$$

uniformly on compact u, y sets, as $t \to \infty$. These ingredients are enough to show [102]

$$\lim_{t\to\infty} K_t(u, y;\, u', y') = K(u, y;\, u', y') \tag{5.55}$$

uniformly for u, u' varying over a compact set.

From the convergence of kernels the convergence of join distributions

$$\det(1 - P_Q B_t)_{\ell^2(\{x_1,\dots,x_m\}\times\mathbb{Z})} \to \det(1 - PK)_{L_2(\{y_1,\dots,y_m\}\times\mathbb{R})} \tag{5.56}$$

follows in the same way as the $M \to \infty$ limit in (5.46). We replace Q by Q_M, defined in (5.45), with $M = 2t + t^{1/3}a$, a large. By (5.55) we have convergence in (5.56) with P replaced by P_a, the projector on $\bigcup_{k=1}^m (\{y_k\}\times]u_k, a + y_k^2[)$. The remainder converges to zero when $a \to \infty$ since both kernels decay exponentially for large arguments, compare with [102].

CHAPTER 6

Anisotropic Growth in $2+1$ Dimensions – The Gates-Westcott Model

Crystal growth usually takes place in three dimensions. Many of the microscopic growth models in one substrate dimension are easily generalized to higher dimensions. The simplicity of the steady state allows there to exploit the anomalous fluctuations and even to extract dynamical information of the growth process. In 2+1 or higher dimensions in the isotropic KPZ regime already the static fluctuations show anomalous roughness [70]. The steady state is completely inaccessible by any currently known analytical methods. A vicinal surface driven by step-flow growth is expected to lie in the anisotropic KPZ or Wolf regime [130]. If the growth velocity depends saddlelike on the surface slope, the steady state has the same large scale statistics as a thermally roughened surface, which is governed by a Gaussian free field fixed point. In particular the roughness is only logarithmic. Jeong, Kahng, and Kim verified this behavior for a Toom interface in three dimensions numerically [66]. We present here the Gates-Westcott model [50] where the steady state is known explicitly and which can be analyzed in the limit of infinite substrate size to determine an analytic expression for the macroscopic growth velocity and the roughness.

A vicinal surface is formed by miscutting a crystal by a small angle with respect to one of its high symmetry planes, e.g. (100) for a simple cubic lattice. Thus the surface is made up of terraces separated by step lines of height one in units of the lattice constant, see Fig. 6.1. Exposed to its supersaturated vapor phase the crystal grows by continuous deposition of material. Bulk cohesion causes particles to attach predominantly at a step line thereby enlarging the upper terrace at the expense of the lower one. If the mean step line spacing is not to large, island formation on the terraces can be neglected. Similarly overhangs are energetically very unfavorable and suppressed completely in an SOS (solid on solid) model description, where the surface is characterized by a single valued height function above the high symmetry reference plane. Thus the projected step lines do not cross.

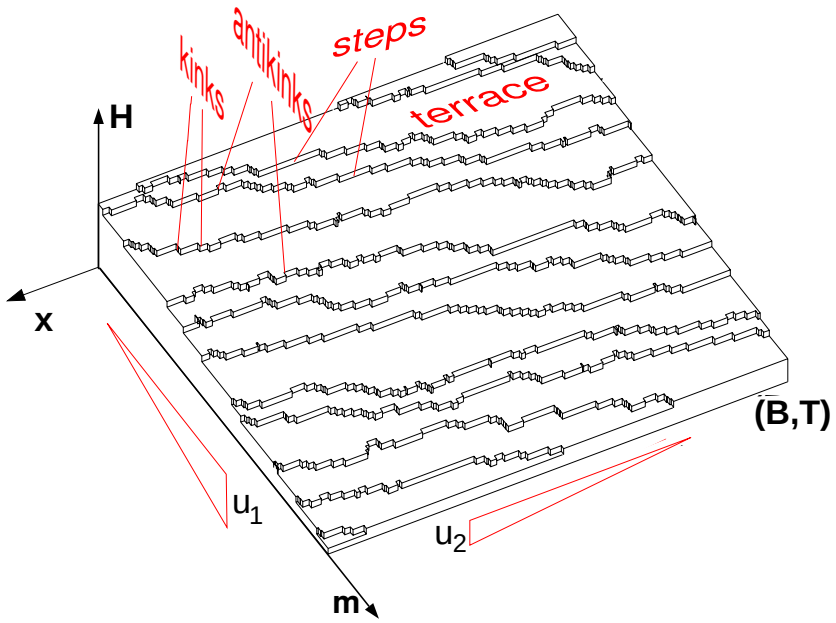

Figure 6.1: *A terrace-step-kink model of a vicinal surface. The slope* (u_1, u_2) *determines the density and the inclination of lines.*

If island formation is completely suppressed, the surface dynamics is described in terms of the dynamics of the individual step lines, governed by $(1+1)$–dimensional growth dynamics, modified by interactions between the lines. The no-crossing condition is incorporated by a hard core repulsion of lines, but there might be also long ranged elastic forces due to lattice distortion along the steps. A perfectly flat surface with no step lines does not change in time, its growth velocity is zero. For a very small tilt u the step lines evolve independently and the vertical growth velocity $v(u)$ is proportional to the step density, thus to lowest order one expects $v(u) \propto |u|$. Increasing the tilt the overall mobility of the step lines will be reduced because of the no-crossing condition. Thus roughly $v(u) \propto |u| - \gamma|u|^3$ with $\gamma > 0$. We see that besides the cusp at $u = 0$ the curvature of the slope dependent growth velocity is saddlelike, i.e. $\partial_u^2 v(u)$ is indefinite. Thus the surface is in the Wolf regime of anisotropic surface growth [130] predicting logarithmic roughness for the height fluctuations. Note, that if one admits island formation at some small rate, the growth velocity at $u = 0$ is nonzero. Effectively the cusp smoothens and the growth velocity depends on the slope in a convex form for small enough $|u|$.

6.1 The Gates-Westcott model

A very simple realization of the Wolf scenario is to choose for the stochastic evolution of an individual step line the dynamics of the one-dimensional PNG model without any interactions between lines besides the no-crossing condition. It has been introduced by Gates and Westcott [50]. We represent a vicinal surface at time t by a collection of non-crossing PNG lines $\phi_\ell(x,t)$, $\ell \in \mathbb{Z}$, $x \in \mathbb{R}$, with $\phi_\ell(x,t) \le \phi_{\ell+1}(x,t)$ for all ℓ, x, and t. The graph of ϕ_ℓ, $\{(x,\phi_\ell(x,t)),\, x \in \mathbb{R}\}$ marks the position of the step line separating the terrace at level $l+1$ from the terrace at level l. In this chapter we call up- and down-steps of the individual PNG lines antikinks and kinks, respectively, to avoid confusion with the notion of step lines for the ϕ_ℓ. Antikinks move in the direction of negative x, having velocity -1, and kinks move in the opposite direction with velocity 1. A kink and an antikink belonging to the same step line disappear upon collision. New kink/antikink pairs are created randomly for each step line with space-time density ξ, provided the non-crossing constraint is not violated. This means that whenever one has $\phi_\ell(x,t) = \phi_{\ell+1}(x,t)$ nucleations on ϕ_ℓ are suppressed at position x.

This model is very similar to the multilayer PNG model introduced in chapter 5. In fact if we define $h_\ell(x,t) = \phi_\ell(x,t) + \ell$, the non-crossing condition for the ϕ_ℓ, $\phi_\ell \le \phi_{\ell+1}$, translates to the non-intersection condition for the h_ℓ, $h_\ell < h_{\ell+1}$. Via this mapping the configuration space for the Gates-Westcott (GW) model and the multi-layer PNG model are identified, provided initial and boundary conditions are adapted accordingly. But note that the GW dynamics is quite different from the RSK dynamics. In the GW dynamics nucleations take place independently on each line, only subject to the non-intersection constraint. In the RSK dynamics, except for the first line, nucleations are completely deterministic. It is very remarkable that nevertheless for some special types of initial/boundary conditions the distribution induced by the GW dynamics is as simple as for the RSK dynamics.

The formulation with a non-crossing condition has to advantages. Firstly it is physically more realistic, since it allows for arbitrary inclinations of the crystal surface, corresponding to unrestricted step line densities (the inverse mean step line spacing $\phi_{\ell+1} - \phi_\ell$). Whereas for non-intersecting lines the line density can not exceed 1. Secondly it exhibits a symmetry in exchanging the ℓ- and ϕ-direction. More precisely, let $C_t = \{(x,y,z);\, \phi_{[y]}(x,t) \ge z\}$ represent the crystal. Then

$$H_m(x,t) = \min\{y;\, (x,y,m) \in C_t\} \in \mathbb{Z}, \tag{6.1}$$

regarded as the step lines indexed by m, also follow the GW dynamics.

6.2 The steady state

We restrict to periodic surface configurations obeying $\phi_{\ell+L}(x) = \phi_\ell(x) + B$ and $\phi_\ell(x+T) = \phi_\ell(x) - M$, where $T \in \mathbb{R}^+$, $B, L, M \in \mathbb{N}$. If we regard ℓ as the vertical direction, the height function of the surface is $H_m(x,t)$, compare with Figure 6.2. It has mean slope $\mathbf{u} = (u_1, u_2)$ with $u_1 = -L/B$ and $u_2 = u_1 M/T$.

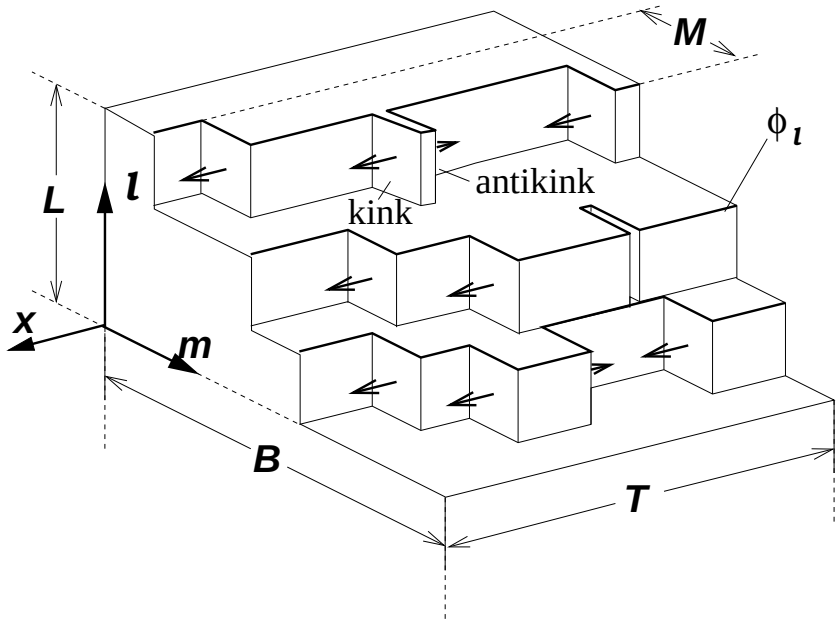

Figure 6.2: *A Gates-Westcott surface on a finite substrate. The deterministic motion is indicated.*

In the coordinates we chose one has $u_1, u_2 < 0$.

A surface with the above periodicity is specified by the L step lines in the rectangle $\{0, \dots, B-1\} \times [0, T]$ and the reference height at $(0,0)$, $H_0 \in \mathbb{Z}$. The periodicity is accounted for by periodic boundary conditions for $m \in \{0, \dots, B-1\}$ and twisted periodic boundary conditions for $x \in [0, T]$, i.e. the points $(m, 0)$ are identified with $\big((m-M) \bmod B, T\big)$. The height at time t can be reconstructed by the step line configuration on the twisted torus $\{0, \dots, B-1\} \times [0, T]$ together with the reference height $H_0(t)$. The increment $H_0(t) - H_0(0)$ is encoded in the number of step lines passing through $(0,0)$ in the time interval $[0, t]$. Note that we can equivalently think of L non-*intersecting* step lines $h_\ell(x,t)$ on the torus $\{0, \dots, N-1\} \times [0, T]$, $N = B + L$, twisted by $-M$. Let us note that the slope in the ϕ-formulation, (u_1, u_2), is related to the slope in the h-formulation,

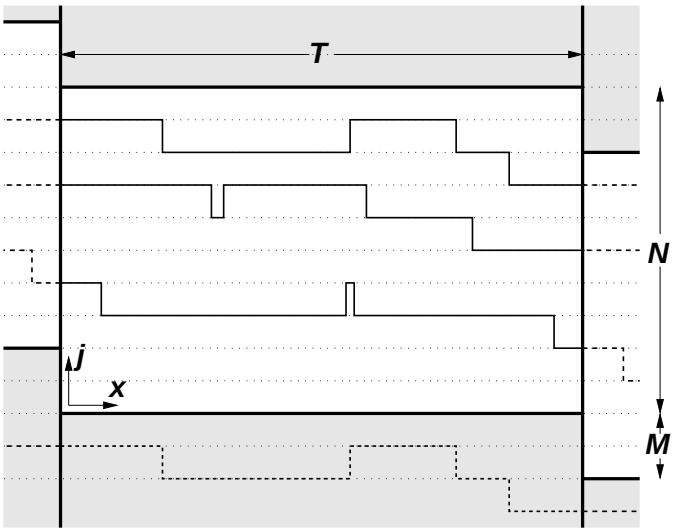

Figure 6.3: *The step lines of Figure 6.2 regarded as fermionic world lines.*

$(-\rho, -\sigma)$ as

$$\rho = \frac{|u_1|}{1+|u_1|}, \tag{6.2}$$

$$\sigma = \frac{u_2}{1+|u_1|}. \tag{6.3}$$

Let $y_j^{\ell,+} \in [0,T]$ be the position of the j-th antikink for step line ℓ, $j = 1, \dots, n_\ell$ and $y_j^{\ell,-} \in [0,T]$ be the position of the j-th kink, $j = 1, \dots, n_\ell + M$. We set $\mathbf{n} = (n_1, \dots, n_L)$, $|\mathbf{n}| = 2(n_1 + \cdots + n_L) + ML$, the total number of kinks and antikinks, and $\mathbf{h}_0 = (h_1(0), \dots, h_L(0))$. The twisted boundary conditions are reflected by the condition

$$\lim_{x \to T} (h_1(x), \dots, h_L(x)) = (h_1(0) - M, \dots, h_L(0) - M), \tag{6.4}$$

compare with Figure 6.3. The space of height line configurations Γ decomposes then as the disjoint union $\Gamma = \bigcup_{\mathbf{n},\mathbf{h}_0} \Gamma(\mathbf{n}; \mathbf{h}_0)$, where $\Gamma(\mathbf{n}; \mathbf{h}_0)$ is some subset of $[0,T]^{|\mathbf{n}|}$ as defined through the constraints already explained ($[0,T]^0$ is a single point). Furthermore for fixed $\mathbf{n}$ the $\Gamma(\mathbf{n}; h_0)$ are glued together in a way that is determined by the condition that (anti-)kinks leaving the interval $[0,T]$ reappear smoothly on the opposite side. Let w be the measure on Γ, such that $w \restriction \Gamma(\mathbf{n})$ is the $|\mathbf{n}|$-dimensional Lebesgue measure on $\Gamma(\mathbf{n})$. Then

$$\mu = Z^{-1} \left(\tfrac{\xi}{2}\right)^{|\mathbf{n}|/2} w \tag{6.5}$$

is the stationary measure for the GW dynamics with normalizing partition function Z.

To verify the stationarity of μ we first note that the Lebesgue measure on $\Gamma(\mathbf{n})$ is left invariant by the deterministic part of the dynamics. We make the ansatz $\mu \restriction \Gamma(\mathbf{n}) = p(|\mathbf{n}|) \cdot w \restriction \Gamma(\mathbf{n})$. At a configuration h with a total number of $|\mathbf{n}|$ kinks and antikinks there is a gain in probability with rate $2V_h\, p(|\mathbf{n}|+2)$ through the annihilation of kink-antikink pairs. Here $V_h = \sum_{\ell=1}^{L} \int_0^T \theta(h_{\ell+1}(x) - h_\ell(x))dx$, $\ell = L+1$ identified with $\ell = 1$, and $\theta(x) = 1$ for $x > 0$ and $\theta(x) = 0$ otherwise. It is the "number" of configurations immediately before the annihilation event which yields h. The loss in probability occurs with rate $\xi V_h\, p(|\mathbf{n}|)$ since V_h is also the "number" of configurations which arise from h by generating a kink-antikink pair. Equating gain and loss we obtain (6.5). For $\xi \neq 0$ the process is ergodic on Γ and therefore the stationary measure μ is unique. (Any configuration can be evolved to a reference configuration by properly adding kink-antikink pairs in the course of the deterministic evolution).

One defines the occupation variables at time t, $\eta_j(x)$, $j \in \{0, \dots, N-1\}$, $x \in [0, T]$, as

$$\eta_j(x) = \begin{cases} 1 & \text{if } h_\ell(x,t) = j \text{ for some } \ell, \\ 0 & \text{otherwise.} \end{cases} \tag{6.6}$$

In [97] the partition function and expectations with respect to μ are explicitly calculated for finite T, B and L, M. Then the infinite volume limit $B \to \infty$, $T \to \infty$ at fixed slope $\mathbf{u}$ is taken. Due to the twisted boundary conditions enforcing a tilt of the surface, $u_2 \neq 0$, the fermionic formulation has some extra complications which we are not discussing here. Implicitly it is shown there that a modification of the boundary conditions leads to the same result in the infinite volume limit and simplifies the calculations considerably.

6.3 The fermion picture and the infinite volume limit

We modify the state space Γ in such a way that instead of (6.4) periodic boundary conditions in the x-direction are enforced,

$$\lim_{x \to T} \{h_1(x), \dots, h_L(x)\} = \{h_1(0), \dots, h_L(0)\} \tag{6.7}$$

as sets. The relative order of the step lines is preserved in $[0, T]$. But the step lines are free to wind around the torus as x runs from 0 to T. Let us define the winding number W as the difference of total kink number and total antikink number divided by N. W is always an integer. If the winding number is L the

step lines wrap around the torus exactly one time and one has $h_\ell(T) = h_\ell(0)$. The definition of the measure μ is unchanged on sectors with constant winding number.

An average tilt of the lines is enforced by imposing an a priori distribution on the winding number W. We assign different weights to antikinks and kinks, η_+ and η_-, respectively. The weight for a kink/antikink pair is $\frac{\xi}{2}$, therefore

$$\eta_+\eta_- = \frac{\xi}{2}. \tag{6.8}$$

We set

$$\mu = Z^{-1}\eta_+^{|\mathbf{n}_+|}\eta_-^{|\mathbf{n}_-|}w, \tag{6.9}$$

with $|\mathbf{n}_+|$ the total number of antikinks and $|\mathbf{n}_-|$ the total number of kinks. This implicitly defines the distribution of the winding number $W = (|\mathbf{n}_+| - |\mathbf{n}_-|)/N$. The measure μ is stationary for the ensemble of tilted surfaces consisting of L step lines with (6.4) and the GW dynamics. The mean slope ρ is given by the line density L/N and the slope σ is given by the mean of the winding number $\langle W\rangle/T$. Therefore σ is a function of $\eta_\pm$, a relation which still has to be determined.

As in Chapter 5 we can write expectations with respect to μ as a path integral which can be rephrased in terms of fermionic expectations,

$$\begin{aligned}\mathbb{E}\big(\eta_{j_1}(x_1)\cdots\eta_{j_m}(x_m)\big) &= Z^{-1}\int_{\{h_\ell(0)\}=\{h_\ell(T)\}} \eta_+^{\sum_\ell\int_0^T\theta(\partial_x h_\ell(x))dx}\\ &\quad\times\eta_-^{\sum_\ell\int_0^T\theta(-\partial_x h_\ell(x))dx}\eta_{j_1}(x_1)\cdots\eta_{j_m}(x_m)dw\\ &= \mathrm{tr}\big(e^{-TH}\big)^{-1}\mathrm{tr}\big(e^{-x_1H}a_{j_1}^*a_{j_1}e^{-(x_2-x_1)H}a_{j_2}^*a_{j_2}\cdots\\ &\quad\times\cdots e^{-(x_m-x_{m-1})H}a_{j_m}^*a_{j_m}e^{-(T-x_m)H}\big),\end{aligned} \tag{6.10}$$

where the trace runs through the fermionic Fock space over $\{0,\dots,N-1\}$ containing L particles. The transfer matrix for the path integral becomes the non-hermitian "Hamiltonian"

$$H = -\sum_{j=0}^{N}\big(\eta_+a_{j+1}^*a_j + \eta_-a_j^*a_{j+1}\big). \tag{6.11}$$

Here $j = N$ is identified with $j = 0$ and the a_j^*, a_j are the generators and annihilators defining the CAR algebra over $\{0,\dots,N-1\}$. The single particle Hamiltonian corresponding to H is

$$h\psi(j) = -(\eta_+\psi_{j-1} + \eta_-\psi_{j+1}). \tag{6.12}$$

The complete set of eigenfunctions is given by $N^{-1/2}e^{ikj}$, $k \in \Lambda = \{-\pi + \frac{2\pi}{N}, \dots, \pi - \frac{2\pi}{N}, \pi\}$. The eigenvalues are

$$\varepsilon(k) = -\eta_s \cos(k) + i\eta_a \sin(k) \tag{6.13}$$

with $\eta_s = \eta_+ + \eta_-$, $\eta_a = \eta_+ - \eta_-$. We want to take the infinite volume limit.

First we send $T \to \infty$. Expectations with respect to the finite T density operator converge to expectations with respect to the ground state of H with L fermions, $|\omega_L\rangle$,

$$\lim_{T\to\infty} \mathrm{tr}\big(e^{-TH}\big)^{-1}\mathrm{tr}\big(e^{-TH}\ \cdot\ \big) = \langle\omega_L|\ \cdot\ |\omega_L\rangle \tag{6.14}$$

For technical reasons we require that $N + L$ must be an odd number, otherwise the ground state is twofold degenerated. The ground state $|\omega_L\rangle$ with L fermions is then given by

$$|\omega_L\rangle = a^*\big(-\tfrac{\pi(L-1)}{N}\big)a^*\big(-\tfrac{\pi(L-3)}{N}\big)\cdots a^*\big(\tfrac{\pi(L-1)}{N}\big)|0\rangle, \tag{6.15}$$

where $a^*(k) = N^{-1/2}\sum_{j=0}^{N-1} e^{ikj}a_j^*$ is the generator of a fermion in the eigenstate $k \in \Lambda$ and $|0\rangle$ is the empty state.

One has the discrete sine kernel in finite volume, $m, n \in \{0, \dots, N-1\}$

$$\begin{aligned} S_L(n,m) &\stackrel{\text{def}}{=} \langle\omega_L|a_m^*a_n|\omega_L\rangle = N^{-1}\sum_{k\in\Lambda,\,|k|\le\frac{\pi(L-1)}{N}} e^{ik(n-m)} \\ &= \frac{\sin\big(\frac{\pi L}{N}(n-m)\big)}{N\sin\big(\frac{\pi}{N}(n-m)\big)}. \end{aligned} \tag{6.16}$$

The extended kernel is

$$S_L(n,y;\,m,x) = \begin{cases} \sum_{|k|\le\frac{\pi(L-1)}{N}} e^{(y-x)\,\varepsilon(k)}e^{ik(n-m)} & \text{for } y \ge x, \\ -\sum_{|k|>\frac{\pi(L-1)}{N}} e^{(y-x)\,\varepsilon(k)}e^{ik(n-m)} & \text{for } y < x \end{cases} \tag{6.17}$$

and the expectation values for $T = \infty$ are given by

$$\mathbb{E}\big(\eta_{j_1}(x_1)\cdots\eta_{j_m}(x_m)\big) = \det\big(S_L(j_k,x_k,j_l,x_l)\big)_{1\le k,l\le m}, \tag{6.18}$$

valid for pairwise distinct (j_l, x_l), as discussed in Chapter 5.

Let us turn to the $N \to \infty$ limit. To guarantee a finite density of fermions ρ we have to set $L = [\rho N]$ or $L = [\rho N] + 1$, such that $N + L$ is odd. We obtain a quasifree state ω as the limit object of the ground state $|\omega_L\rangle$, defined by the discrete sine kernel

$$S(n,m) \stackrel{\text{def}}{=} \omega(a_m^*a_n) = \int_{-\pi\rho}^{\pi\rho}\frac{dk}{2\pi}e^{ik(n-m)} = \frac{\sin\big(\pi\rho\,(n-m)\big)}{\pi(n-m)}. \tag{6.19}$$

To determine arbitrary expectations one has to replace $S_L(n,y;\,m,x)$ in (6.18) by the extended sine kernel

$$S(n,y;\,m,x)=\begin{cases}\int_{-\pi\rho}^{\pi\rho}\frac{dk}{2\pi}e^{(y-x)\,\varepsilon(k)}e^{ik(n-m)} & \text{for } y\geq x,\\ -\int_{\pi\rho}^{2\pi-\pi\rho}\frac{dk}{2\pi}e^{(y-x)\,\varepsilon(k)}e^{ik(n-m)} & \text{for } y<x.\end{cases} \tag{6.20}$$

6.4 Slope, growth velocity, and two point correlations

The slope ρ is already explicitly incorporated in (6.20), it is the fermionic density, $\rho=\omega(a_i^*a_i)$, independently of i. We still have to find the relation between σ and $\eta_\pm$. To this end we calculate the drift of the lines. The operator for the rightward fermion current from x to $x+1$ is determined through the limit

$$\begin{aligned} j_i^+ &= \lim_{x\to 0}\tfrac{1}{x}(a_i^*a_ia_{i+1}a_{i+1}^*)e^{-xH}(a_{i+1}^*a_{i+1}a_ia_i^*)e^{xH}\\ &= (a_i^*a_ia_{i+1}a_{i+1}^*)\tfrac{\partial}{\partial x}\big(e^{-xH}(a_{i+1}^*a_{i+1}a_ia_i^*)e^{xH}\big)\Big|_{x=0}\\ &= a_i^*a_ia_{i+1}a_{i+1}^*[a_{i+1}^*a_{i+1}a_ia_i^*,H]\\ &= \eta_+a_{i+1}^*a_i \end{aligned} \tag{6.21}$$

by the fermion anticommutation rules. Analogously the operator for the leftward current from i to $i-1$, $j_i^-=\eta_-a_{i-1}^*a_i$. σ/ρ is the inclination of the step lines, or drift velocity of the fermions, therefore one has

$$\sigma=\omega(j^+-j^-)=(\eta_+-\eta_-)\pi^{-1}\sin(\pi\rho). \tag{6.22}$$

We want to impose the slopes (ρ,σ). By (6.8) and (6.22) we have to fix

$$\eta_+=\tfrac{1}{2}(\eta_s+\eta_a),\qquad \eta_-=\tfrac{1}{2}(\eta_s-\eta_a), \tag{6.23}$$

where $\eta_a=\frac{\pi\sigma}{\sin(\pi\rho)}$ and $\eta_s=\sqrt{2\xi+\eta_a^2}$ are the coefficients of the imaginary and real part in the dispersion relation (6.13), respectively.

The growth velocity $v(\rho,\sigma)$ of the surface perpendicular to the (j,x)-plane is given by the total number of kinks and antikinks, divided by the area TN, or the kink/antikink density in fermionic space-time. Therefore we have

$$v(\rho,\sigma)=\omega(j^++j^-)=\pi^{-1}\eta_s\sin(\pi\rho)=\tfrac{1}{\pi}\sqrt{2\xi\sin^2(\pi\rho)+\pi^2\sigma^2}. \tag{6.24}$$

This is the slope dependent growth velocity for the surface with non-intersecting step lines, therefore $\rho\in[0,1]$. In the original formulation with non-crossing step lines the area where (anti-)kinks contribute to the growth velocity is TB with

$B = N - \rho N$. In the infinite volume limit we thus obtain the stationary growth velocity for the Gate-Westcott model [97],

$$v_{\mathrm{GW}}(\mathbf{u}) = \tfrac{1+|u_1|}{\pi}\sqrt{2\xi \sin^2\bigl(\tfrac{\pi|u_1|}{1+|u_1|}\bigr) + \bigl(\tfrac{\pi|u_2|}{1+|u_1|}\bigr)^2}. \tag{6.25}$$

It is defined for all inclinations $u_1, u_2 \in \mathbb{R}$ by symmetry, compare Figure 6.4. Note that as expected, the growth velocity is everywhere saddlelike, except for

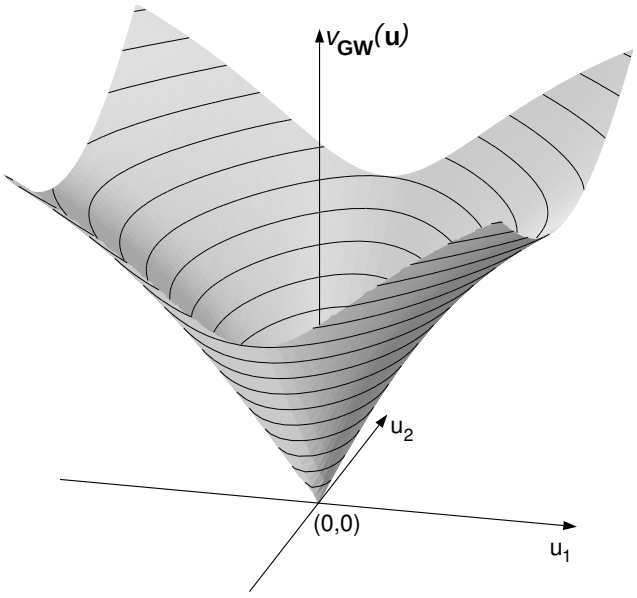

Figure 6.4: *The growth velocity of the Gates-Westcott model as a function of the surface tilt* $\mathbf{u}$.

the cusp at the origin.

We turn to the static height correlations for the surface with step lines $h_\ell(x)$. The corresponding height $H(x,n)$ is given by the reference height $H(0,0)$ and the number of step lines between $(0,0)$ and (x,n). We define the empirical antikink density

$$j_n^+(x) = \lim_{y\to 0} \tfrac{1}{y}\eta_n(x)\bigl(1-\eta_{n+1}(x)\bigr)\bigl(1-\eta_n(x+y)\bigr)\eta_{n+1}(x+y). \tag{6.26}$$

For a given realization of the surface it has delta peaks at the antikink positions. The empirical kink density is

$$j_n^-(x) = \lim_{y\to 0} \tfrac{1}{y}\eta_n(x)\bigl(1-\eta_{n-1}(x)\bigr)\bigl(1-\eta_n(x+y)\bigr)\eta_{n-1}(x+y). \tag{6.27}$$

It has delta peaks at the kink positions. There analogues as fermionic operators are given by (6.21) and following. The height $H(x,n)$ is determined as

$$H(x,n) = H(0,0) - \sum_{j=0}^{n-1} \eta_j(0) + \int_0^x \big(j_{n-1}^+(x') - j_n^-(x')\big)dx' \tag{6.28}$$

for $n \leq 0$ and accordingly for $n < 0$. For $y \in \mathbb{R}$ we set $H(x,y) = H(x, \lceil y \rceil)$, thus $H(x,y)$ is an integer valued function on $\mathbb{R}^2$. We are interested in the large scale behavior of the two point correlation function

$$C(n,x) = \mathbb{E}\big([H(n,x) - H(0,0) - n\rho - x\sigma]^2\big). \tag{6.29}$$

We look at the structure function

$$\begin{aligned} S(n,x) &= \mathbb{E}\big(\eta_n(x)\eta_0(0)\big) - \rho_2 = -S(n,x;\,0,0)S(0,0;\,n,x) \\ &= \int_{-\pi\rho}^{\pi\rho} \frac{d\kappa}{2\pi} \int_{\pi\rho}^{2\pi-\pi\rho} \frac{d\kappa'}{2\pi} e^{|x|(\varepsilon(\kappa)-\varepsilon(\kappa'))} e^{i\frac{x}{|x|}(\kappa-\kappa')n}. \end{aligned} \tag{6.30}$$

As in (3.51) the structure function is closely related to the second derivative of $C(x,t)$ with respect to x. In [97] the discrete analogue of (3.51) is derived,

$$C(n,x) = \int_{-\pi}^{\pi} \frac{dk}{2\pi} \frac{1}{1-\cos\,k} \big(\hat{S}(k,0) - e^{-ikn}\hat{S}(k,x)\big), \tag{6.31}$$

where $\hat{S}(k,x) = \sum_n e^{ikn} S(n,x)$ is the discrete Fourier transform of $S(n,x)$. For large n, x the asymptotic behavior

$$C(n,x) = \frac{1}{\pi^2} \ln(|n| + |x|) + \mathcal{O}(1) \tag{6.32}$$

is extracted there. Here we take advantage of translation invariance and Fourier transforms to refine the result considerably.

To this end we define the fermion propagator $G(n,x)$ by

$$S(n,y;\,m,x) = e^{-\pi\rho m} G(n-m, y-x) e^{\pi\rho x}. \tag{6.33}$$

The similarity transformation by $g(x) = e^{\pi\rho x}$ drops out when taking expectations (6.18). The Fourier transform of $G(n,x)$ in n and x is

$$\begin{aligned} G(k,\omega) &= \int dx \sum_n e^{i\omega x + ikn} G(n,x) \\ &= \int dx e^{i\omega x} \big(\chi(k)\theta(x) - \overline{\chi}(k)\theta(-x)\big) e^{(\epsilon(k)+\pi\rho)x} \\ &= \frac{1}{i\omega + E(k)}, \end{aligned} \tag{6.34}$$

where $\chi(k) = \chi_{-\pi\rho,\pi\rho]}(k)$, $\overline{\chi}(k) = 1 - \chi(k)$, and $E(k) = \epsilon(k) + \pi\rho$. Products of Fermi propagators in real space become convolutions in Fourier space. One has the following simple but very useful identity,

$$G(k,\omega)G(k+k',\omega+\omega') = \frac{G(k,\omega) - G(k+k',\omega+\omega')}{i\omega' + E(k+k') - E(k)}. \tag{6.35}$$

For the structure function (6.30) we obtain in Fourier space

$$\begin{aligned} S(k,\omega) &= \int \frac{d\omega'}{2\pi} \int \frac{dk'}{2\pi} G(k',\omega')G(k'-k,\omega'-\omega) \\ &= \int \frac{d\omega'}{2\pi} \int \frac{dk'}{2\pi} \frac{(i\omega' + E(k'))^{-1} - (i(\omega'-\omega) + E(k'-k))^{-1}}{-i\omega + E(k'-k) - E(k')} \end{aligned} \tag{6.36}$$

The transformation $\omega' \mapsto \omega - \omega'$, $k' \mapsto k - k'$ shows that $S(k,\omega)$ is real, since $E(-k) = \overline{E(k)}$. For fixed k' the ω' integration is performed by collecting poles in the upper halfplane (or, equivalently, in the lower one). The integral along a semicircle of radius R vanishes for $R \to \infty$, for the integrand decays as $|\omega'|^{-2}$. We obtain

$$\begin{aligned} S(k,\omega) &= \int \frac{dk'}{2\pi} \frac{\overline{\chi}(k') - \overline{\chi}(k'-k)}{-i\omega + E(k'-k) - E(k)} \\ &= \int \frac{dk'}{2\pi} \frac{\mathrm{Re}\big(E(k'-k) - E(k')\big)\big(\overline{\chi}(k') - \overline{\chi}(k'-k)\big)}{\big(\omega + \mathrm{Im}\big(E(k'-k) - E(k')\big)\big)^2 + \mathrm{Re}\big(E(k'-k) - E(k')\big)^2}. \end{aligned} \tag{6.37}$$

For the large scale behavior of $C(n,x)$ only the pole structure at $(k,\omega) = (0,0)$ is relevant. One gets

$$\epsilon^{-2} S(\epsilon k, \epsilon\omega) \longrightarrow \frac{1}{2\pi} \frac{2k^2\eta_s \sin(\pi\rho)}{\big(\omega - k\eta_a \cos(\pi\rho)\big)^2 + \big(k\eta_s \sin(\pi\rho)\big)^2} \tag{6.38}$$

for $\epsilon \to 0$. In the large scale limit one has as in (3.89) $C(k,\omega) \simeq 2k^{-2}S(k,\omega)$, for small k, ω. In real space this translates to

$$\begin{aligned} C(Ln,Lx) &= \frac{1}{\pi^2}\ln(CL) + \frac{1}{2\pi^2}\ln(\sin(\pi\rho)^2) \\ &\quad + \frac{1}{2\pi^2}\ln\big((n + \pi\sigma\cot(\pi\rho)x)^2 + (2\sin(\pi\rho)^2 + \pi^2\sigma^2)x^2\big) \\ &\quad + \mathcal{O}(L^{-1}). \end{aligned} \tag{6.39}$$

To calculate the constant C one would need to be able to control the rate of convergence in (6.38). We conjecture $C = 2e^{1+\gamma}$ by numerical comparison, $\gamma = 0.5772\cdots$ being Euler's constant.

The stationary distribution of a Gates-Westcott surface at given slope can be regarded as an equilibrium distribution with fugacity η_+ for antikinks, η_- for kinks. The corresponding free energy per area, the surface free energy $F(\rho,\sigma)$ has been determined in [97] with the result

$$f_\xi(\rho,\sigma) = \frac{1}{\pi}\sqrt{2\xi\sin^2\rho\pi + \sigma^2\pi^2} - \frac{\sigma}{2}\ln\frac{\sqrt{2\xi\sin^2\rho\pi+\sigma^2\pi^2}+\sigma\pi}{\sqrt{2\xi\sin^2\rho\pi+\sigma^2\pi^2}-\sigma\pi}. \quad (6.40)$$

Assuming that the height distribution becomes Gaussian on large scales, a calculation with the formal measure

$$dP(\{h(y,x)\}) \propto \exp(-\int f(\nabla h)dxdy) \quad (6.41)$$

yields in the Gaussian approximation for the fluctuations of $h(y,x)$ in Fourier space

$$\langle h_{k,\omega}h_{k',\omega'}\rangle \propto \frac{\delta(k+k')\delta(\omega+\omega')}{\binom{k}{\omega}^T f''(\rho,\sigma)\binom{k}{\omega}}, \quad (6.42)$$

where one has explicitely

$$f''_\xi(\rho,\sigma) = \frac{\pi}{\sqrt{2\xi(\sin\pi\rho)^2+\pi^2\sigma^2}}\begin{pmatrix} \frac{\pi^2\sigma^2}{(\sin\pi\rho)^2}+2\xi(\sin\pi\rho)^2 & -\pi\sigma\cot\pi\rho \\ -\pi\sigma\cot\pi\rho & 1\end{pmatrix}. \quad (6.43)$$

The quadratic form in the logarithm of (6.39) is just the inverse of (6.43).

CHAPTER 7

Models in higher dimensions

7.1 The isotropic PNG droplet

The PNG droplet is an instance of the polynuclear growth (PNG) model in a special geometry. To let a PNG droplet grow on a d–dimensional substrate, one starts with a single seed located at the origin of the substrate at zero height. The seed is a spike of unit height which expands laterally with constant speed. Above this circular (for $d \geq 3$ spherical) island new spikes nucleate with uniform rate forming further islands. Thus the droplet grows layer by layer. Two islands in the same layer coalesce upon touching but continue to enlarge in all directions. This ensures that each layer reached by the droplet is eventually filled without holes. Obviously we can choose the units of time and space in a way that the a lateral speed, as well as the nucleation rate equals one. Thus the isotropic PNG model has no adjustable parameters. Figure 7.1 shows the realization of a $(2+1)$-dimensional droplet $h(x,3)$, $x \in \mathbb{R}^2$.

Let $h(x,t) \in \mathbb{N}_0$ be the height of the droplet above $x \in \mathbb{R}^d$ at time $t \geq 0$. We have the initial and boundary conditions $h(x,t) = 0$, for $|x| > t$, $|\cdot|$ the Euclidean norm. Then

$$h(x,t) = \max\{h(x_j,t_j);\ j \in \mathbb{N} \text{ and } |x - x_j| \leq t - t_j,\ t > t_j\} + 1 \tag{7.1}$$

defines the height at (x,t) recursively in t, where $(x_j,t_j)_{j\in\mathbb{N}}$ is some enumeration of the nucleation events having density one in $\{(x,t) \in \mathbb{R}^{d+1}; |x| < t\}$ and density zero otherwise.

For an alternative description of the process $h(x,t)$, we define the partial order $\prec$,

$$(x',t') \prec (x,t) \qquad \text{iff } |x - x'| \leq t - t' \text{ and } t > t', \tag{7.2}$$

representing an ordered time-like relative position of two different space-time points. For a directed path from $(0,0)$ to (x,t) $\gamma : [0,1] \to \mathbb{R}^{d+1}$, with $\gamma(s') \prec \gamma(s)$, $0 \leq s' < s \leq 1$ we define the length $|\gamma|$ as the number of nucleation events passed in the image of γ. Then $h(x,t)$ can be alternatively defined as the longest directed path from $(0,0)$ to (x,t),

$$h(x,t) = \max_{\gamma} |\gamma|. \tag{7.3}$$

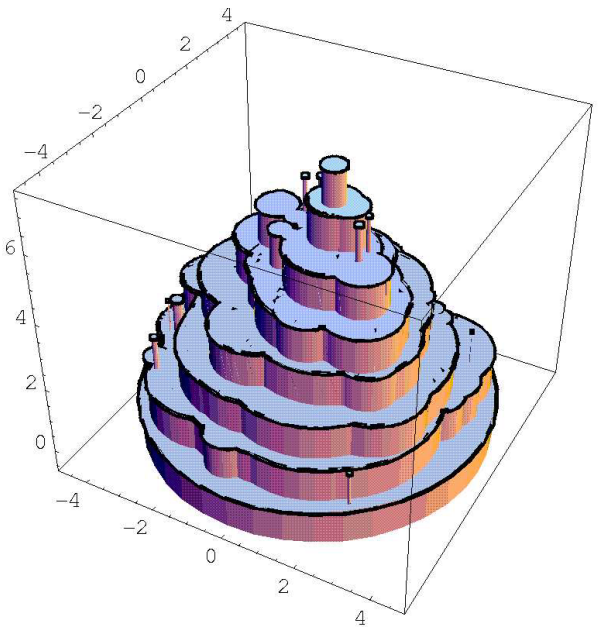

Figure 7.1: *A snapshot of a small isotropic PNG droplet in 2+1 dimensions.*

Physically if we assign to each path γ, regarded as a directed polymer chain, the energy $-|\gamma|$ then $h(x,t)$ has the interpretation of the ground state energy of a directed polymer in the random energy landscape made up by the nucleation events. By a superadditivity argument one obtains that $\mathbb{E}(h(x,t))$ is linearly bounded in t, which by monotonicity guarantees the existence of the limiting vertical growth speed $v_\infty = \lim_{t\to\infty} t^{-1}\mathbb{E}(h(0,t))$.

The model has an apparent Lorentz-type symmetry. The partial order $\prec$, as well as the Poisson statistics of nucleation events is invariant with respect to arbitrary Lorentz transformations of space-time where the speed of "light" is set to unity. In our restricted droplet geometry the height process h is still invariant for all special Lorentz transformations keeping fixed the origin $(0,0)$. Thus

$$h = h \circ L \quad \text{in distribution}, \tag{7.4}$$

where L is an arbitrary composition of spatial rotations around the origin and Lorentz boosts, L_c, with velocity $c \in \mathbb{R}^d$, $|c| < 1$, i.e.

$$L_c(x,t) = (x_\perp + x_\parallel \cosh\alpha + t\sinh\alpha, t\cosh\alpha - |x_\parallel|\sinh\alpha), \tag{7.5}$$

where $\tanh\alpha = |c|$ and $x = x_\perp + x_\parallel$ is the orthogonal decomposition of x with respect to c. We immediately derive that along a ray $\{x = ct; t \geq 0\}$, $|c| < 1$ the

distribution of h depends only on $|c|$ and, by Lorentz boosting, is given by

$$h(ct,t) = h\left(0, t\sqrt{1-|c|^2}\right). \tag{7.6}$$

If $h(0,t) \simeq v_d t + (a_d t)^{\beta_d}\chi^{\text{droplet}}$ asymptotically, the macroscopic shape of the droplet must be an ellipsoid, and the fluctuations transform according to (7.6) as

$$h(x,t) \simeq v_d\sqrt{t^2-|x|^2} + \left(a_d\sqrt{t^2-|x|^2}\right)^{\beta_d}\chi^{\text{droplet}}. \tag{7.7}$$

Since we are going to define the absolute scale of the droplet fluctuations, the distribution of χ^{droplet} implicitly through a conceptually even simpler growth model in the we need the (unknown) nonuniversal factor a, which for the isotropic PNG model depends only on the dimension. By Legendre transforming the deterministic part we immediately obtain the slope dependent growth velocity as

$$v(u) = \sqrt{v_d^2 + |u|^2}. \tag{7.8}$$

7.2 PNG models with general island shape

We generalize the isotropic PNG model to arbitrary convex island shapes. The spherical island shape is replaced by an arbitrary convex set $B \in \mathbb{R}^d$ containing the origin and with nonzero Lebesgue measure. Instead of the Euclidean norm on $\mathbb{R}^d$ one defines the quasi-norm

$$|x| = \inf\{\lambda\, 0;\, x \in \lambda B\}. \tag{7.9}$$

(7.1) with this quasi-norm defines the B-shaped PNG droplet, again with Poisson points of space-time density 1 lying in the forward "light-cone" of the origin, $\{(x,t) \in \mathbb{R}^{d+1}; |x| < t\}$. Convexity of the island shape B_c is preserved under Lorentz boosts L_c with $c \in B$, since $(B_c, \{1\}) = L_c\{(tB,t); t \geq 0\} \cap \mathbb{R}^d \times \{1\}$. Therefore we can focus on the height above the origin for a general B-shaped PNG droplet. We expect

$$h_B(0,t) \simeq v_B t + C_B t^{\beta_d}\chi_d^{\text{droplet}} \tag{7.10}$$

asymptotically in distribution. Rigorously there is not much known for general island shape B, only the case that B is a d-simplex due to a mapping to longest increasing subsequences of a tuple of random permutation has been studied in the mathematical literature as explained in more detail below.

First let us give an intuitive argument to guess v_B in the limit of high dimensions. For a sequence of d-dimensional island shapes B_d, $d \geq 1$ we start with a

flat substrate, $h(x,0) = 0$ with nucleations allowed everywhere in $\mathbb{R}^d$. The probability that $h(0,t) = 0$ at time t equals the probability that there have not been any nucleation events inside the backward light cone $\{(x,s) \in \mathbb{R}^{d+1}; |-x| < t-s\}$ of $(0,t)$, thus

$$\text{Prob}\{h(0,t) = 0\} = \exp\big(-t^{d+1}|B_d|/(d+1)\big), \tag{7.11}$$

with $|B_d|$ the d-dimensional Lebesgue measure of B_d. $1 - \text{Prob}\{h(0,t) = 0\}$ is the occupation ratio of the first layer. For large d, the occupation of the first layer is very close to zero until a critical time t_d, when it suddenly becomes occupied almost completely. t_d is not precisely defined for finite d, it is the time when the exponent in (7.11) becomes of order 1. Only after t_d nucleations take place almost completely in the second layer. Neglecting nucleations in the second layer before t_c and the tiny portion of not yet occupied regions in the first layer after t_d, the second layer is occupied almost completely only at $2t_d$ and so on, thus the growth velocity is expected to be $\approx 1/t_d$. If we define $t_d = \big(c(d+1)/|B_d|\big)^{1/(d+1)}$, i.e. when the exponent in (7.11) equals $-c$, $c > 0$, the limit $t_\infty = \lim_{d\to\infty} t_d$, if it exists, is obviously independent of c, and thus a promising candidate for $v_\infty = \lim_{d\to\infty} v_d$ is $1/t_\infty$. Let us give three examples. First for the **isotropic PNG model** one has $B_d = 2\pi^{d/2}/(d\Gamma(d/2))$, the volume of a d-dimensional unit sphere. This leads to the asymptotics $v_d \simeq \sqrt{2\pi e/d}$. Otherwise stated, if the radius of B_d is $\sqrt{d}$ instead of 1, on has $v_\infty = \sqrt{2\pi e}$. Second example is the **hypercube PNG model**, $B_d = [-1,1]^d$, which is investigated in the next section. The above reasoning leads to the conjecture $v_d \to 2$, as $d \to \infty$.

The third example is the **simplex PNG model**, where B_d is a d-dimensional simplex, taken as the simplex spanned by the endpoints of vectors of length d, forming a $(d+1)$-dimensional orthogonal basis whose body diagonal is aligned with the t-axis. Its Lebesgue measure is $|B_d| = d^d(d+1)/d!$ and thus by the Stirling formula one has $v_\infty = e$. Let us note that we chose the size of B_d in such a way that $h(0,t)$, with droplet initial conditions, equals in distribution the length of a directed polymer between two opposite corners of a hypercube $[0,t]^{d+1}$, filled with Poisson points of density 1. A third interpretation is the following. Take a d-tuple of independent random permutations, $(\pi_i)_{1\le i\le d}$, all of the same length N, where N itself is Poisson distributed with mean t^{d+1}. A subsequence $(j_l)_{1\le l\le k}$ of length k, $1 \le j_1 < \cdots < j_k \le N$, is called increasing if $\pi_i(j_l) < \pi_i(j_{l+1})$ for all $1 \le i \le d$ and $1 \le l < k$. Then again $h(0,t)$ equals in distribution the *length of a longest increasing subsequence* of such a tuple of random permutations. Bollobás and Winkler [22] analyzed $h(0,t)$ exactly in this formulation as a generalization of Ulam's problem [124], which corresponds to $d = 1$. They have shown that $v_d \le e$ for all $d \in \mathbb{N}$ and indeed $v_d \to e$ as $d \to \infty$.

Note that an arbitrary d-simplex can always be transformed to B_d as defined above by an affine transformation, thus knowing v_d for one d-simplex we know

it for every other d-simplex as well. In particular we are able to determine the macroscopic shape of a droplet modulo this single constant v_d. In the orthonormal frame, spanned by the edges of the forward light cone from the origin, with coordinates $(\xi_0, \ldots, \xi_d)$ one has

$$h(\xi_0, \ldots, \xi_d) \simeq v_d (\xi_0 \cdots \xi_d)^{\frac{1}{d+1}}. \tag{7.12}$$

The reason is that $h(\xi_0, \ldots, \xi_d)$ is determined by the Poisson points in a hypercuboid whose sides have lengths $\xi_0, \ldots, \xi_d$. A volume preserving linear transformation to a hyper-cube leaves invariant the Poisson point process and thus only the volume of the cuboid determines the height distribution. Legendre transforming in the same frame, and regarding ξ_0 as time direction leads to the growth velocity

$$v(u) = \left(\tfrac{v_d}{d+1}\right)^{d+1} (u_1 \cdots \mathrm{u}_d)^{-1}. \tag{7.13}$$

7.3 Monte Carlo simulations on a flat substrate

We let the PNG model grow from a flat substrate, a d–dimensional hyper cube of length L with periodic boundary conditions. Equivalently one can think of a substrate extended to infinity with spatially periodic noise. We mainly studied the height distribution $h_t = h(0,t)$, which by translation invariance can be determined via spatial and ensemble sampling. By the general KPZ theory we expect the scaling form

$$h_t \simeq v\, t + C\, t^{\beta} \chi^{\text{flat}} \tag{7.14}$$

with model dependent parameters v and C, and the dynamical roughness exponent β together with the universal distribution χ^{flat}, which (in the strong coupling regime) depend only on the substrate dimension d. In this simulation we recorded at different sampling times the first four moments of the height distribution, averaged spatially for each individual run and for a number of independent realizations.

A given surface configuration was encoded by the positions, creation times, and height levels of all nucleation events being created up to the current time, which are not yet covered completely by higher lying islands. To determine the height of a newly created nucleation event one has to determine from all the nucleation events in its backward light cone the highest level occurring. This has been down level-by-level with a dynamical KDB (k–dimensional binary) tree search algorithm adapted for periodic boundary conditions [107].

Since computer memory is restricted one has to get rid of nucleation events whose islands are already completely covered. This has been done by throwing

away all nucleation events of a lower lying level, if for a certain amount of time no new nucleation occurred in this level. If a level were removed to early there would be holes created in the surface. We determined the time to keep the levels empirically such that on the average not more then one nucleation event among 10^8 hits a hole.

To increase performance we did not use the Euclidean norm corresponding to spherical island shapes, but the maximum norm, $|x| = \max\{|x_i|\}$, corresponding to islands growing in the shape of d–dimensional hypercubes. The advantage is that the evaluation of the norm, clearly the most frequent operation, is less time consuming, and furthermore the KDB search is more efficient, since it bounds the substrate region to be searched for nucleation events by hyperplanes parallel to the island boundaries. The disadvantage of giving up isotropy and the Lorentz symmetry explained in the preceding section is acceptable, since we are mainly interested in universal quantities, roughness exponents and measures of the shape of the limiting distribution, like skewness and kurtosis.

System sizes are up to $L = 10^5$ for $d = 1$, $L = 1280$ for $d = 2$, $L = 128$ for $d = 3$, $L = 30$ for $d = 4$, and $L = 15$ for $d = 5$. Note that for times smaller than $L/2$ the evolution is not affected by the finiteness of the substrate, since the maximal lateral speed is 1. But also for larger times finite size effects are negligible for the recorded times, $t \leq 100$, since the correlation length grows laterally proportional to $t^{1/z}$ with $z = 2 - \alpha \in [1.5, 2]$, α the static roughness exponent. The computation time was several weeks on a modern work station for each dimension (besides the one-dimensional case where we spent much less time since the results are known in closed form as explained in Chapter 3

Figure 7.2 shows the mean height divided by the time and the extrapolated values of the growth velocities for each dimension $d = 1, \ldots, 5$. For the hypercube PNG model we expect $v_d \to 2$ as $d \to \infty$, compare with Section 7.2. The numerical values are are in accord with this conjecture and even imply monotone convergence from below. The numerical values for v_d are well fitted by the heuristic formula $v_d \approx 2 - 0.6\, d^{-1/2}$ (up to 1%).

To estimate the dynamical roughness exponent we plot in Figure 7.3 the truncated second moment of the height distribution, i.e. the quadratic height distribution width $\langle h_t^2 \rangle - \langle h_t \rangle^2$. The damped oscillations reflect the discrete nature of the height variable, taking only integer values. As can be seen from the vertical scale the width of the surface is only of order one and smaller for $d \geq 3$. This means, that the height distribution is concentrated mainly in only two or three levels.

For $d \leq 3$ we used the last decade of simulation data to fit the ansatz $w_t^2 \simeq c_d\, t^{2\beta_d}$ with the result $\beta_1 = 0.334(1)$, $c_1 = 0.502(4)$, (dotted line in the leftmost plot of Figure 7.4; the exact values are $\beta_1 = 1/3$ and $c_1 = \langle (\chi^{\mathrm{GOE}})^2 \rangle_c / 2^{1/3} = 0.50678$), $\beta_2 = 0.240(1)$, $c_2 = 0.2885(35)$, and $\beta_3 = 0.1665(20)$, $c_3 = 0.206(5)$. Figure 7.4 illustrates the results and gives an idea of the accuracy involved. We

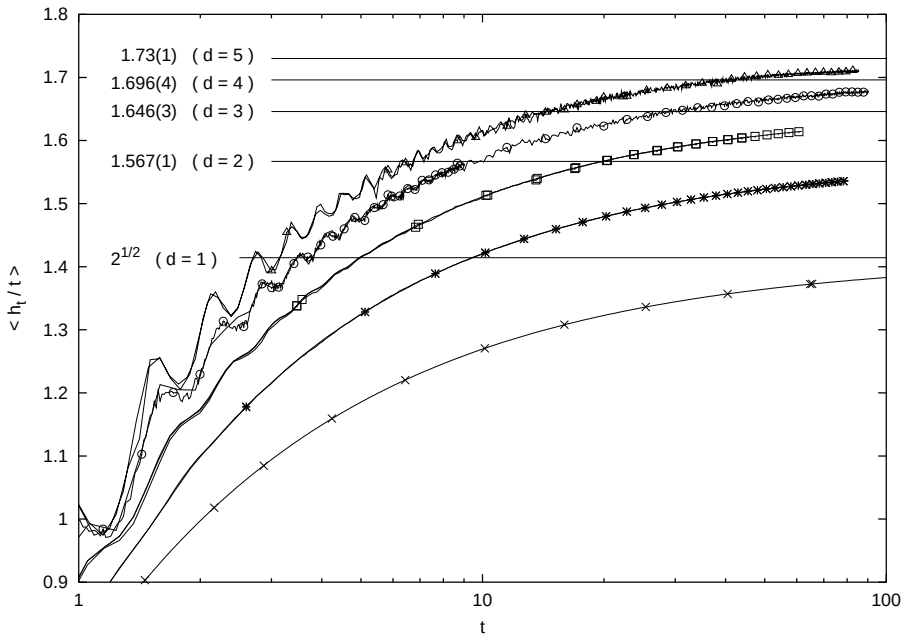

Figure 7.2: *The asymptotic growth velocity of the hypercube PNG model for* $d = 1, \ldots, 5$ *substrate dimensions.*

plot w_d^2/t^{β_d} semi-logarithmically against the time. The horizontal line indicates c_d, and the slope of the two guiding lines bounds the error in β_d for $d = 2, 3$.

Figure 7.5 shows the skewness and kurtosis of the height distribution for $d = 1, \ldots, 4$, calculated from our Monte Carlo data. For $d = 1$ also the exact result is shown, which converges to the skewness and kurtosis of χ^{GOE}, 0.2935 and 0.1652, respectively. For $d = 2$ the results for two substrate sizes $L = 1024$ and 1290 are superimposed. We estimate $0.40(3)$ and $0.30(5)$ for the skewness and kurtosis of χ^{flat} in two substrate dimensions. For $d = 3$ and $d = 4$ the results are less clear. We estimate $0.41(7)$ and $0.30(15)$, respectively, in three substrate dimensions and in the range of our data $0.20(15)$ and $0.15(40)$ in four substrate dimensions. The $d = 4$ results do not exclude convergence to a Gaussian distribution, where both skewness and kurtosis are zero, which would be expected if the upper critical dimension were already reached.

An alternative approach to determine the critical exponents, is to measure the static roughness of the surface. Starting from a flat substrate, the lateral correlation length ξ increases in time with the exponent $1/z = \beta/\alpha$. For distances below the correlation length one expects approximately stationary fluctuations, and one should be able to detect the scaling law for the second moment of height

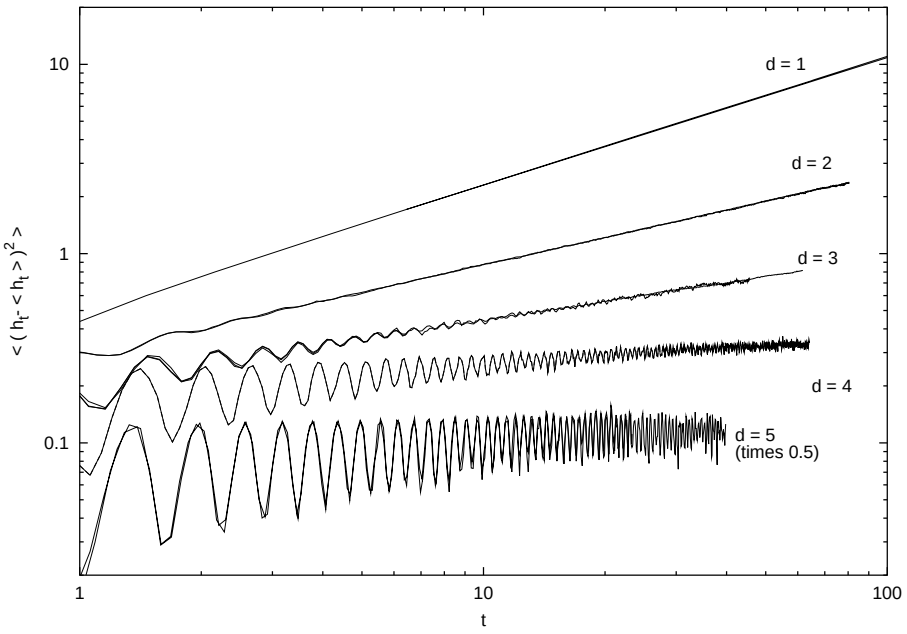

Figure 7.3: *The truncated second moments of the surface position h_t up to 5 substrate dimensions. The data for $d = 5$ are modified by a factor 0.5 to increase visibility.*

differences

$$\langle (h(x,t) - h(0,t))^2 \rangle \approx A\, x^{2\alpha}, \qquad x_m \ll |x| \ll \xi. \tag{7.15}$$

Here x_m is a microscopic cutoff length and is given by the microscopic dynamics. We assume it to be of the same size as the typical distance of nucleation events in a completely filled level, which is of order one. Already for $d = 2$ this leaves less then a decade for the validity of (7.15) since we where not able to prepare surfaces with a correlation length much larger than 10. If the system size is small enough to relax the surface to stationarity additional finite size effects yield even less reliable results. We indeed verified that our Monte Carlo data do not allow for a meaningful scaling fit.

On a finite substrate the correlation length can not exceed the system size L. After a time $t_{\text{stat}} \propto L^{\alpha/\beta}$ the correlation length is of the same order as L, and the whole surface statistic is close to stationarity. Since the quadratic surface width,

$$w^2 = \langle (h(0,t) - \overline{h(\cdot,t)})^2 \rangle, \tag{7.16}$$

with $\bar{\cdot}$ denoting spatial averaging for a given realization, is expected to scale with the exponent 2β in time for initial growth, the stationary surface width attained at

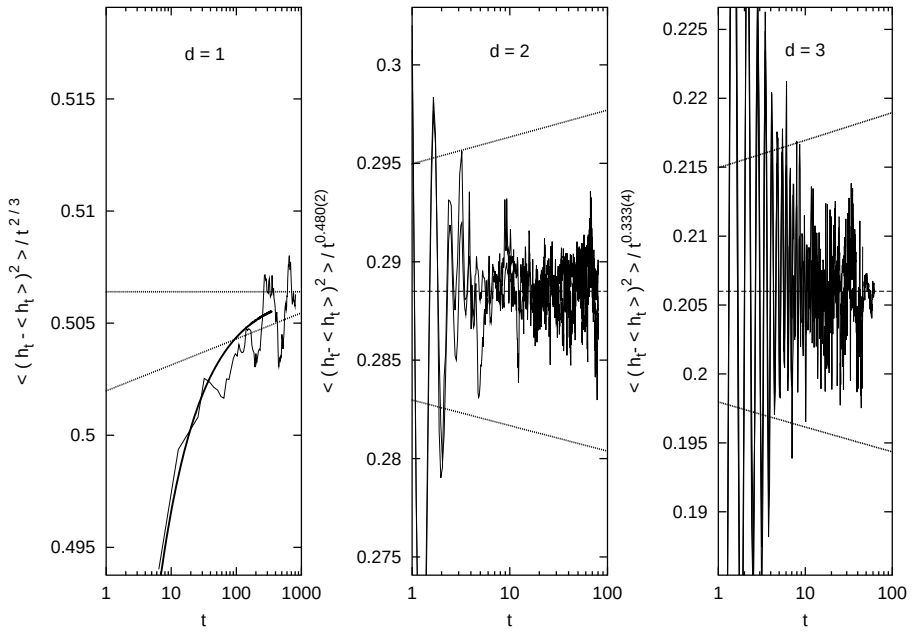

Figure 7.4: *Scaling plot of the surface width against the expected asymptotics. The left graph shows MC data compared to the exactly known solution in* 1 *substrate dimensions, relative to the exactly known scaling exponent* $2/3$*. The dotted line is a fit to the Monte Carlo data. For* 2 *dimensions (middle) the best fit for the dynamical exponent yields* $\beta = 0.240(1)$*, and for* 3 *dimensions (right) we obtain* $\beta = 0.1665(20)$*. The vertical scale is chosen to show a region of* $\pm 2.5\%$*,* $\pm 5\%$*, and* $\pm 10\%$ *around the converging value* $c_1 = 0.50678$*,* $c_2 = 0.2885$*, and* $c_3 = 0.206$*, respectively. The two guiding lines in the middle and right graph illustrate the error bounds for the dynamical exponents. Higher dimensional results are not shown since they do not allow for a meaningful fit.*

a time of order t_{stat} should scale as

$$w_L^2 \propto L^{2\alpha} \tag{7.17}$$

with the surface size L. In the simulations the surface at a given time is probed at only finitely many sample points. Thus the empirical estimate for the surface mean contains an error, which results in a small but systematic under–estimation of w^2. Since the heights of the sample points have no Gaussian distribution and furthermore are correlated uncontrollably we decided to avoid this error source and chose as a measure for the surface width the distribution of the height difference at two points on the surface at maximal distance, i.e.

$$\Delta h_L = h(x_L, t) - h(0, t), \tag{7.18}$$

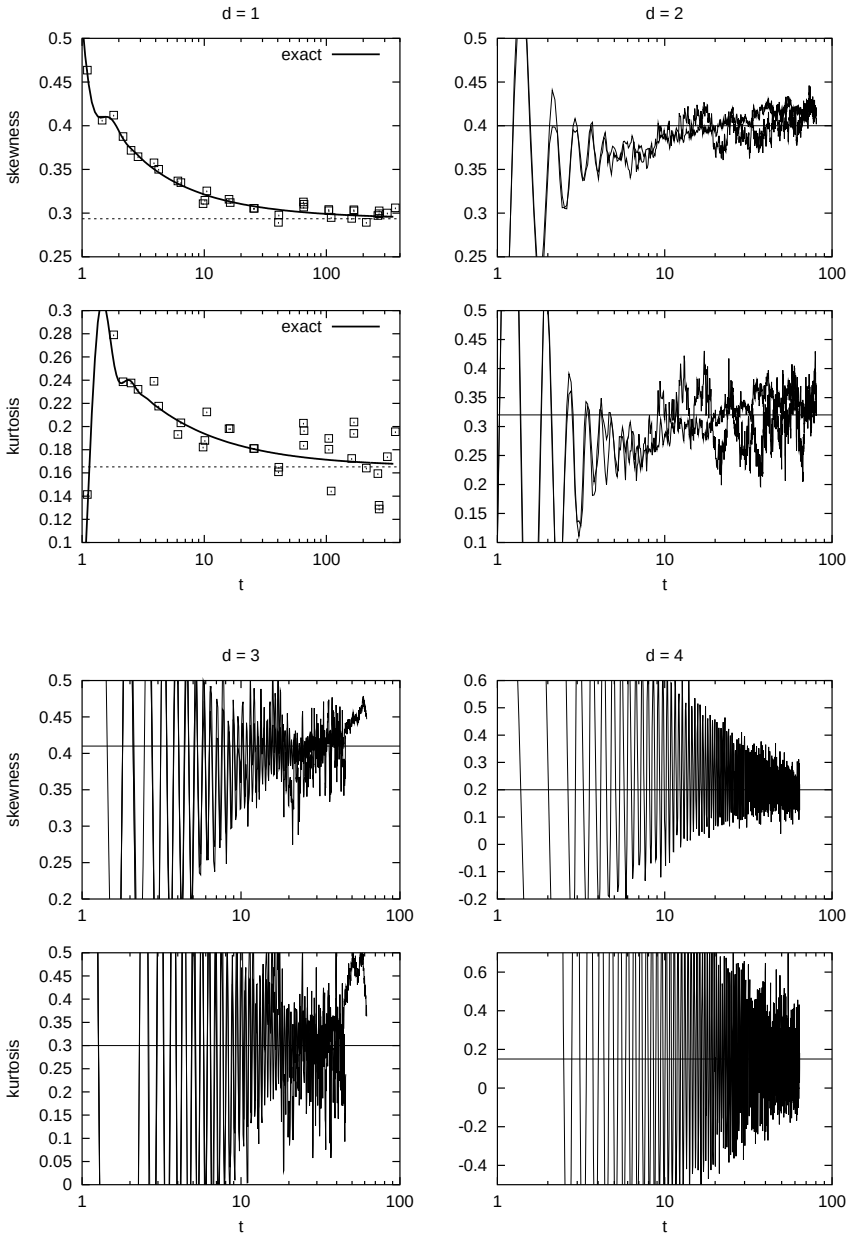

Figure 7.5: *Skewness and kurtosis of the height distributions for* $d = 1, \ldots, 4$*. The one-dimensional limits are* 0.2935 *and* 0.1652*, the skewness and kurtosis of* χ^{GOE}*. The dotted lines for* $d = 2$ *are at* 0.40 *and* 0.32*. The rough estimates for* $d = 3, 4$ *are* 0.41*,* 0.2 *for the skewness and* 0.30*,* 0.15 *for the kurtosis, respectively.*

with $x_L = (L/2, \ldots, L/2)$. This is clearly spatially invariant and does not depend

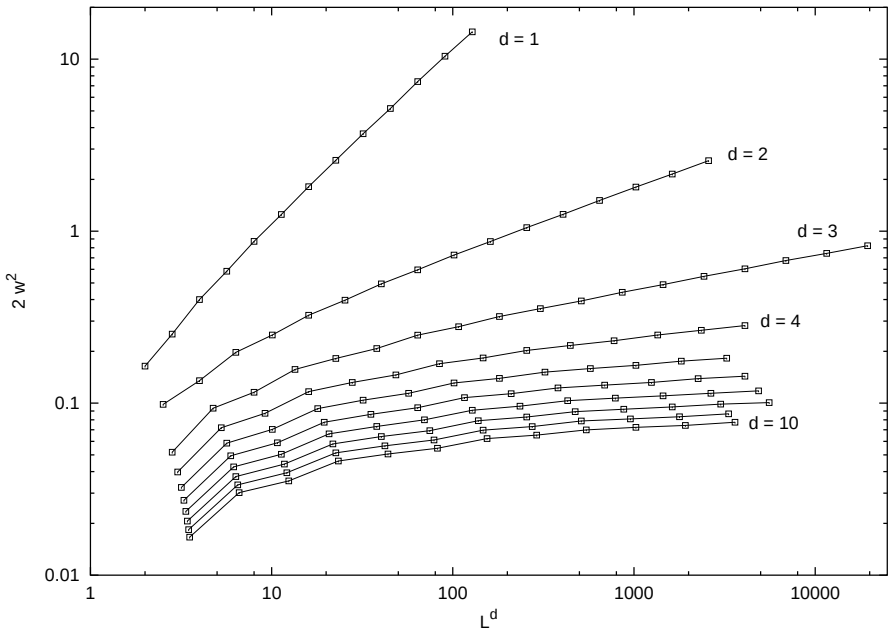

Figure 7.6: *The stationary surface width for a finite substrate of length L with periodic boundary conditions against the substrate area L^d, $d = 1$ to $d = 10$. System sizes are rather moderate, ranging from $L = 64$ for $d = 2$, $L = 32$ for $d = 3$ to only $L = 2.35$ for $d = 10$.*

on the number of sample points taken from one realization of a stationary surface. The disadvantage is, that we can not examine the surface skewness, an asymmetry in the distribution of $h - \overline{h}$, which has been recognized in dimensions $d \geq 2$ to persist even in the stationary state [32].

We observed that $\langle \Delta h_L^2 \rangle$ is always very close to $2w_L^2$, as expected if the two opposite sample points are only weakly correlated. Thus for brevity we write $2w^2$ for the quadratic surface width measured by the height difference at most distant points. In Figure 7.6 we plot this surface width against the area of the substrate for $d = 1, \ldots, 10$. In order to visualize the quality of scaling of these data according to (7.17) Figure 7.7 shows a finite size scaling of the data, i.e. the local slope of the log–log graphs in Figure 7.6 (divided by two) against $1/L$ such that if (7.17) holds the curves converge to the static roughness exponent α on the vertical axis at zero. The extrapolation of the curves yields for the first four dimensions, $\alpha_1 = 0.50(1)$, $\alpha_2 = 0.38(1)$, $\alpha_3 = 0.29(2)$, and $\alpha_4 = 0.18(3)$. The $d = 4$ estimate holds only if we assume that the corresponding curve remains convex but monotonically decreasing, when approaching 0. Otherwise $\alpha_4 = 0$ can not be excluded. For $d \geq 5$ a reasonable extrapolation is not possible at all.

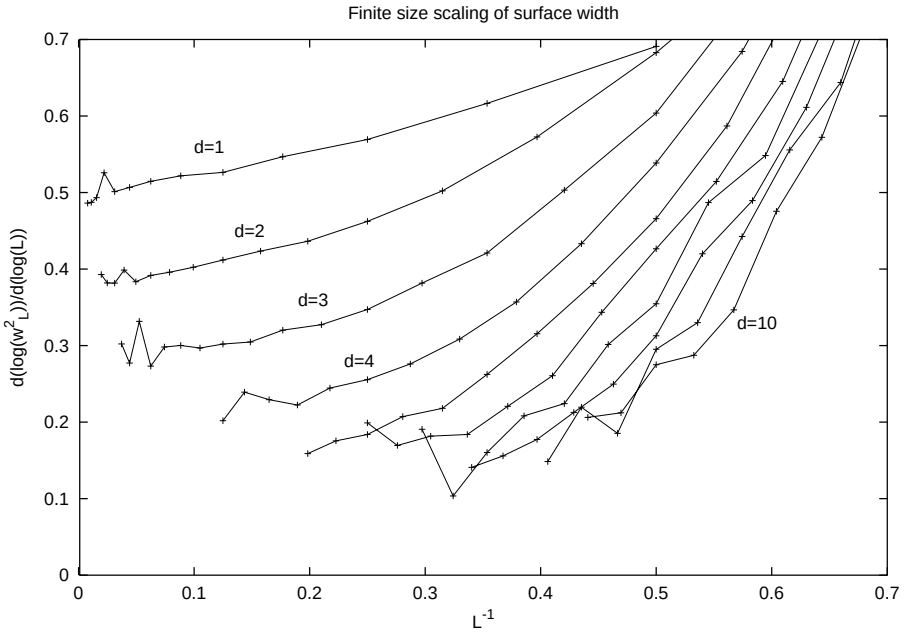

Figure 7.7: *Finite size scaling of the surface width. For $L \to \infty$, i.e. along the left vertical axis, the data are expected to converge to twice the static roughness exponent. Errorbars have not been recorded, but errors become larger upon approaching zero. We estimate from this data $\alpha = 0.50(1)$ for $d = 1$, $\alpha = 0.38(1)$ for $d = 2$, and $0.29(2)$ for $d = 3$. For $d = 4$ one can extract $\alpha = 0.18(3)$ if one assumes that the curve stays convex but decreasing when approaching 0. But note that this is excluded if $d = 4$ is the upper critical dimension implying $\alpha = 0$. For higher dimensions the data are not conclusive at all.*

7.4 2+1 dimensional triangle PNG droplet

In a second project we simulated the triangle PNG droplet. We regard this model as the conceptually simplest of all growth models since it can be mapped to the longest commonly increasing subsequence problem of random permutations as described in section 7.2. Therefore we propose to define the absolute scale of the limiting droplet distribution for curved KPZ growth by means of the simplex model. Thus we define

$$\chi_d^{\text{droplet}} = \lim_{s\to\infty} s^{-\beta_d}\big(h(s) - v_d s\big), \tag{7.19}$$

as a limit of distributions, if this definition makes sense, i.e. if the dynamical scaling exponent $\beta_d > 0$ is well defined (the existence of v_d being shown in [22] for $d \in \mathbb{N}$). For $d = 1$ this definition coincides with the GUE Tracy-Widom distribu-

tion χ_{GUE}, compare with Chapter 4. We concentrated on the $d = 2$ case, since we did not expect good statistical results in higher dimensions with the algorithms and the computer power available. For $d = 2$ we shall give strong numerical support that χ_2^{droplet} indeed is well defined with $\beta = 0.2408(12)$.

The principle used for the Monte-Carlo simulation is very simple. We fill a cube of length L with Poisson points of density one. The points are ordered with respect to one coordinate axis. To get the height of a point one has to find the height of the highest point in its backward light cone, which is just a cuboid, and add 1. The height function $h(s)$, $s \in [0, L]^3$, is then defined as the maximal height of the points in the backward light cone of s.

To save memory and to obtain a complexity of the algorithm of order L^3 we actually split the large cube into smaller cubes which are processed in lexicographical order. If a cube is processed, the height function restricted to its three distal (further away from the origin) faces forms a $(1 + 1)$–dimensional PNG height function on each face. The points on the face which generate this height function (projections of bulk points) are passed to the corresponding nearest neighbor cube as boundary points. Thus each cube has boundary points at his proximal (closer to the origin) faces, with associated height, which are treated as bulk points belonging to the cuboid. Once the boundary points at the proximal faces are known, the height of all points inside the cuboid can be determined as described above without any reference to points lying outside. Also the height at $s \in \mathbb{R}^3$, $h(s)$, can be determined by processing only the cuboid containing s.

The distribution of $h_s = h(s, s, s)$ is then determined by recording the height of all points with coordinates (s_1, s_2, s_3) lying in the "mass shell" $s \le (s_1 s_2 s_3)^{1/3} < s + 1/1024$. Our largest L was 1200 but we recorded h_s only up to $s = 1024$. We managed to process about 50000 points/sec and consumed the equivalent of nearly one year on a modern work station. We simulated cubes with different lengths L, in order to improve the statistics for smaller s. The distributions for each s contain up to $2 \cdot 10^8$ events for s around 200, $5 \cdot 10^6$ at $s \approx 400$, and still $5 \cdot 10^5$ at $s = 1000$, roughly approximated by $4 \cdot 10^7 \exp(-s/220)$.

The upper half of Figure 7.8 shows the mean height $\langle h_s \rangle$ divided by s in order to extract the asymptotic growth velocity. A nonlinear fit for the ansatz

$$\langle h_s \rangle = v\, s + c\, s^{\beta} + k, \tag{7.20}$$

motivated by the behavior for one substrate dimension, yields

$$\begin{aligned} v &= 2.3640(3), \\ c &= -2.85(1) \\ \beta &= 0.2404(6), \\ k &= 2.16(2). \end{aligned} \tag{7.21}$$

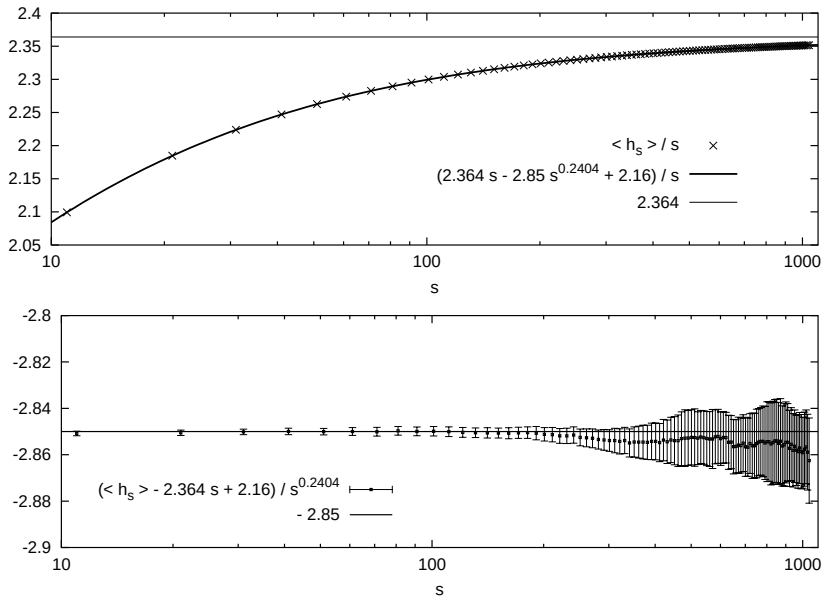

Figure 7.8: *The upper graph shows the average height of the* $(2+1)$*–dimensional triangle PNG droplet at times* $t = \sqrt{3}s$*, above the origin, divided by* s*, a fitted curve, and the asymptotic speed* 2.364*, errorbars much smaller than the symbols and omitted. The lower graph shows the deviations of the first moments of* $\langle h_s \rangle$ *from the fitted curve on the scale of the expected limiting distribution with errorbars.*

The result for the growth velocity is consistent with and even somewhat more precise than the estimate $v \in [2.363, 2.366]$ of Breimer et al. [27], who exclusively concentrated in our terms on the mean growth velocity of the simplex PNG model in dimensions $d = 1, \ldots, 5$.

The lower graph of Figure 7.8 shows the shifted and scaled mean in order to extract the first moment of the limiting distribution $c = \langle \chi^{\text{droplet}} \rangle$.

Figure 7.9 shows the scaling of the truncated second moment of h_s. The theoretically predicted exponent $2\beta = 1/2$ [80] is taken out, to emphasize the significance of the deviation from this conjecture. The scaling ansatz

$$\langle h_s^2 \rangle - \langle h_s \rangle^2 = c_2 \, s^{2\beta} \tag{7.22}$$

in the range $30 \leq s \leq 1024$ yields $c_2 = 0.475(2)$ and $\beta = 0.241(1)$.

Also the third and forth moments scale as expected. In Figure 7.10 the skewness and kurtosis of the height distributions for different s are shown. From this data we estimate the corresponding quantities for χ_2^{droplet} in two substrate dimensions as $0.323(5)$ and $0.21(4)$, respectively.

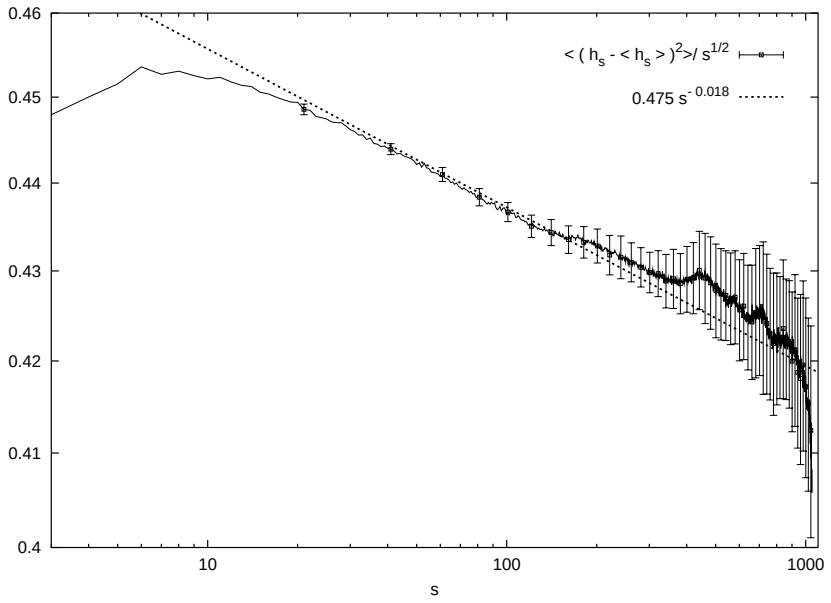

Figure 7.9: *The quadratic width of the height distribution divided by* $s^{1/2}$.

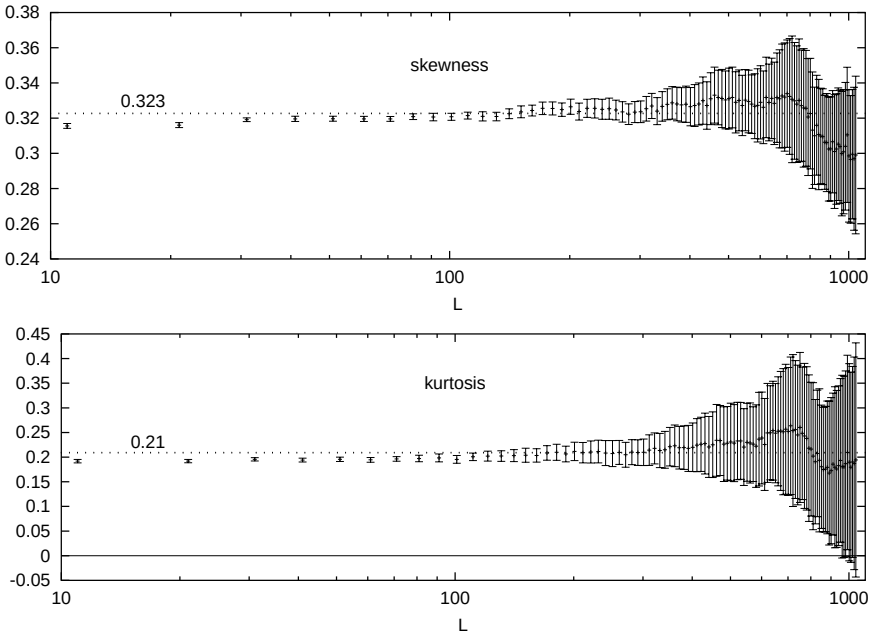

Figure 7.10: *Skewness and kurtosis of the height distributions.*

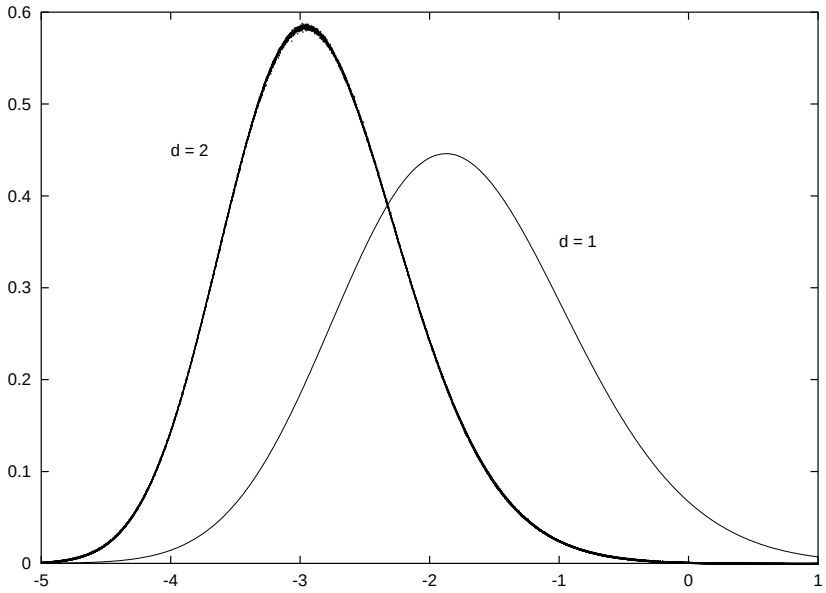

Figure 7.11: *The droplet probability distributions for one and two dimensional substrate dimensions.*

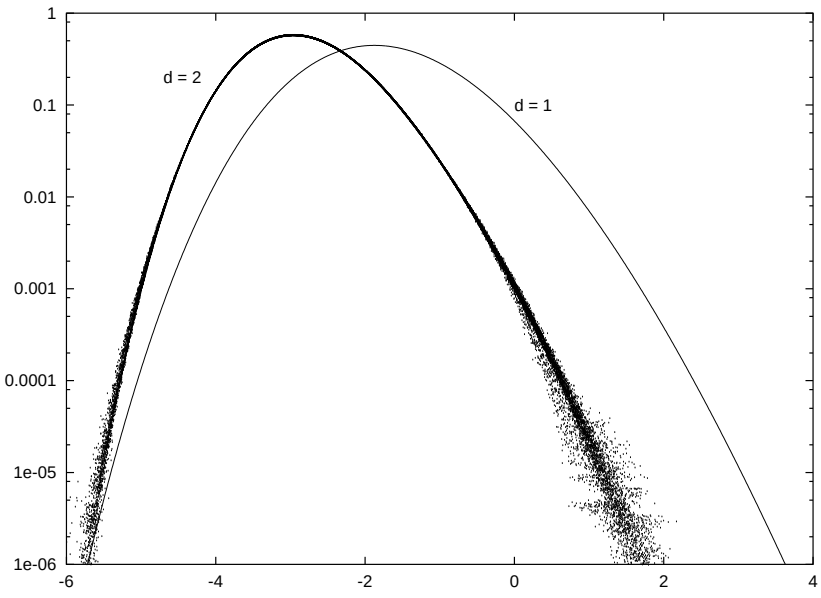

Figure 7.12: *The same distributions as in Figure 7.11 on a semi logarithmic scale.*

Finally Figures 7.11 and 7.12 show the limiting probability distribution of χ_2^{droplet} itself, in comparison to the same random variable in one substrate dimension, the Tracy-Widom-GUE distribution. The $d = 2$ line is obtained as the shifted and scaled superposition of the empirical distributions for $100 \leq s \leq 800$.

7.5 Summary of the numerical results

Let us collect the numerical results obtained in Sections 7.3 and 7.4. For the hypercube PNG model with flat initial conditions we determined on an effectively infinite substrate the asymptotic growth velocity v_d and the prefactor for the algebraic increase in the variance C_d which are nonuniversal quantities. The universal quantities recorded are the dynamical scaling exponent β_d, the skewness and kurtosis of the universal height distribution χ_d^{flat}, and, by means of the stationary surface width as a function of the substrate size the static roughness exponent α_d. The scaling relation $\alpha_d(1 + 1/\beta_d) = 2$ due to Gallilean invariance of the KPZ

	$d = 1$	$d = 2$	$d = 3$	$d = 4$	$d = 5$
v_d	$2^{1/2}$	$1.567(1)$	$1.646(3)$	$1.696(4)$	$1.73(1)$
C_d	$0.502(4)$	$0.2885(35)$	$0.206(5)$	-	-
χ_d^{flat}					
skewness	0.2935(exact)	$0.40(3)$	$0.41(7)$	$0.20(15)$	-
kurtosis	0.1652(exact)	$0.32(5)$	$0.15(40)$	-	-
β_d	$0.334(1)$	$0.240(1)$	$0.1665(20)$	-	-
$2\beta_d/(1+\beta_d)$	$0.501(2)$	$0.3871(13)$	$0.2855(30)$	-	-
α_d	$0.50(1)$	$0.38(1)$	$0.29(2)$	$0.18(3)$	-
$\alpha_d(1+1/\beta_d)$	$2.00(5)$	$1.96(6)$	$2.03(14)$	-	-

Table 7.1: *Nonuniversal and universal quantities from the hypercube PNG model.*

equation is just a check for consistency since its validity is beyond any doubt. Since β_d has much less uncertainty we included in the table a guess for α_d from the values for β_d assuming the scaling relation to hold.

Let us compare the scaling exponents with values found in the literature. In $d = 2$ almost all numerical studies agree more or less on $\beta_2 = 0.240(1)$ [120, 3, 4]. A more recent study by Marinari et al. [85], measuring α_d in a similar way as we did, predicts (again assuming the scaling relation) $\beta_2 = 0.2445(25)$. Nevertheless it seems to be widely agreed upon that β_2 obtained from Monte-Carlo simulations is bounded away from the value $\frac{1}{4}$ conjectured by theoretical considerations of Lässig [80]. Only Chin and den Nijs [32] claim consistency with $\alpha_2 = \frac{2}{5}$ ($\beta = \frac{1}{4}$) ascribing deviations from it to persisting finite-size effects.

χ_d^{droplet}	$d=1$	$d=2$
mean	-1.77109	$-2.85(1)$
variance	0.81320	$0.475(2)$
skewness	0.2241	$0.323(5)$
kurtosis	0.09345	$0.21(4)$

Table 7.2: *characteristics of the distributions* $\chi_d^{droplet}$ *for* $d = 1, 2$.

In $d = 3$ [120] and [3] consistently obtain $\beta_3 = 0.180(5)$. [85] has a more precise guess, $\beta_3 = 0.185(1)$ from $\alpha_3 = 0.3135(15)$. This differs considerably from our result $\beta_3 = 0.1665(20)$, itself being consistent with Lässig's theoretical prediction $\beta_3 = \frac{1}{2k}$ for some $k \in \mathbb{N}$ [80], obviously with $k = 3$.

At $d = 4$ many theoretical studies locate the upper critical dimension of the KPZ-theory [81, 34]. Thus they expect $\beta_d = 0$ for $d \geq 4$. From the numerical side the existence of an upper critical dimension is heavily disputed [28, 86, 2]. Most accurate measurements obtained are $\beta_4 = 0.15(1)$ in [3] and $\beta_4 = 0.146(2)$ in [85]. Critics would assign these nonzero values for β_4 to finite size effects, since simulated system sizes are quite small. Our own results are not very decisive in this question. The estimated value $\alpha_4 = 0.18(3)$, leading to $\beta_4 = 0.10(2)$ is obtained only under the assumption that the curve approximated in Fig. 7.6 for $d = 4$ is actually convex.

In Section 7.4 we determined for the triangle PNG model its specific growth velocity $v = 2.3640(3)$ and the dynamical scaling exponent $\beta_2 = 0.2408(12)$ in agreement with the result from the hyper-cube PNG model. The limiting height distribution χ_2^{droplet} has been recorded. We collect the results for mean, variance, skewness and kurtosis in Table 7.2 for $d = 1$ from the GUE Tracy-Widom distribution and for $d = 2$ from our Monte-Carlo simulations for the triangle PNG model. To our knowledge this is the first time that this droplet distribution, or, in the language of directed polymers, point-to-point distribution for $d = 2$ itself has been investigated.

APPENDIX A

Orthogonal polynomial identities

We collect identities for orthogonal polynomials on the unit circle used in Chapter 3. For the reader who is new to the subject we sketch the proofs.

Let $f(\theta)$ be a non-negative integrable function on $[-\pi, \pi]$. Define the inner product for polynomials p, q,

$$\langle p, q\rangle = (2\pi)^{-1} \int_{-\pi}^{\pi} \overline{p(e^{i\theta})} q(e^{i\theta}) f(\theta) d\theta. \tag{A.1}$$

If $f(\theta)$ has the form $f(\theta) = F(e^{i\theta})$, with the function $F(z)$ being analytic on the unit circle, the inner product can be written as a contour integral around 0,

$$\langle p, q\rangle = \oint \overline{p}(z^{-1}) q(z) \frac{F(z)dz}{2\pi i z}, \tag{A.2}$$

where $\overline{p}(z) = \overline{p(\overline{z})}$. We are interested in the determinant of the Toeplitz matrix $T_n\big(f(\theta)\big) = (\langle z^k, z^l\rangle)_{0\le k,l<n}$

$$D_n = \det T_n\big(f(\theta)\big). \tag{A.3}$$

We orthogonalize recursively the monomials z^n, $n \ge 0$, to obtain orthogonal polynomials with respect to the weight function $f(\theta)$,

$$\pi_n(z) = z^n - \sum_{k=0}^{n-1} \frac{\langle z^n, \pi_k\rangle}{\langle \pi_k, \pi_k\rangle} \pi_k(z). \tag{A.4}$$

By definition the polynomials are monic, i.e. $\pi_n(z) = z^n + \mathcal{O}(z^{n-1})$, there quadratic norm is denoted as N_n, thus

$$\langle \pi_m, \pi_n\rangle = \delta_{m,n} N_n. \tag{A.5}$$

To abbreviate we write $p_n = \pi_n(0)$. The reciprocal polynomials $\pi_n^*(z)$ are defined as

$$\pi_n^*(z) = z^n \overline{\pi}(z^{-1}). \tag{A.6}$$

As easily seen, they are orthogonal to all polynomials of degree $\leq n$ with vanishing constant term,

$$\langle \pi_n^*, z^k \rangle = 0 \quad \text{for } 1 \leq k \leq n \quad \text{and} \quad \langle \pi_n^*, 1 \rangle = N_n. \tag{A.7}$$

Therefore $\langle \pi_n^*, \pi_k^* \rangle = N_n$ for all k and

$$\langle \pi_n^*, \pi_k \rangle = p_k N_n \quad \text{for } 0 \leq k \leq n. \tag{A.8}$$

We have the following identities:

Proposition 1.1

$$D_n = \prod_{k=0}^{n-1} N_k, \tag{A.9}$$

$$N_n = N_0 \prod_{k=1}^{n} (1 - |p_k|^2). \tag{A.10}$$

$$N_n \sum_{k=0}^{n-1} \frac{\pi_k(a)\overline{\pi_k(b)}}{N_k} = \frac{\pi_n^*(a)\overline{\pi_n^*(b)} - \pi_n(a)\overline{\pi_n(b)}}{1 - a\bar{b}}, \tag{A.11}$$

$$\pi_n(z) = z\,\pi_{n-1}(z) + \overline{p_n}\,\pi_{n-1}^*(z), \tag{A.12}$$

$$\pi_n^*(z) = z\,p_n\,\pi_{n-1}(z) + \pi_{n-1}^*(z), \tag{A.13}$$

$$\pi_n(1) = \prod_{k=1}^{n} (1 - \overline{p_k}). \tag{A.14}$$

$$\pi_n^*(-1) = \prod_{k=1}^{n} (1 + (-1)^k p_k) \tag{A.15}$$

Proof: The proofs can be found scattered in [118] with slightly different notation. We recapitulate them here in a concise form. First the orthogonal polynomials can be written explicitly as a determinant,

$$\pi_n(w) = D_n^{-1} \det \begin{pmatrix} \langle 1,1 \rangle & \langle 1,z \rangle & \cdots & \langle 1,z^n \rangle \\ \langle z,1 \rangle & \langle z,z \rangle & \cdots & \langle z,z^n \rangle \\ \vdots & \vdots & & \vdots \\ \langle z^{n-1},1 \rangle & \langle z^{n-1},z \rangle & \cdots & \langle z^{n-1},z^n \rangle \\ 1 & w & \cdots & w^n \end{pmatrix} \tag{A.16}$$

To check one notes that $\pi_n(z)$ is orthogonal to z^k, $0 \leq k < n$ and has the proper leading coefficient.

To relate N_n with the Toeplitz determinants we adopt the notation $D_{n,k\,l}$ for the (k,l)-minor of D_n, i.e. the determinant of the Toeplitz matrix with k-th row and l-th column removed, and $D_{n,k\,l,k'l'}$ the minor with k-th, k'-th row and l-th, l'-th column removed. One has by expanding the determinants

$$\begin{aligned} D_{n-1}^2 N_n &= D_{n-1}^2 \langle \pi_n, \pi_n \rangle = \sum_{i,j=0}^{n} (-1)^{n+i} D_{n,n\,i} \langle z^i, z^j \rangle (-1)^{n+j} D_{n,n\,j} \\ &= \sum_{i=0}^{n} (-1)^{i+n} D_{n,n\,i} \langle z^i, z^n \rangle D_{n,n\,n} \\ &\quad + \sum_{j=0}^{n-1} \sum_{i=0}^{n} \sum_{0 \le k \le n,\, k \ne i} \langle z^k, z^j \rangle (-1)^{i+j+k+\theta(k-i)} D_{n,n\,i,j\,k} \langle z^i, z^j \rangle D_{n,n\,j} \\ &= D_n D_{n-1}, \end{aligned} \tag{A.17}$$

with $\theta(n) = 0$ for $n \le 0$ and $\theta(n) = 1$ otherwise. The last equality holds, since $D_{n,n\,n} = D_{n-1}$ and in the sum over i, k, $i \ne k$ the terms with i and k interchanged have opposite sign. Thus $D_n = N_n D_{n-1}$, $D_0 = 1$ and (A.9) follows.

To get (A.10) we set

$$P_n(w,z) = \sum_{k=0}^{n} N_k^{-1} \pi_k(w) \overline{\pi_k(z)}. \tag{A.18}$$

Using bra and ket notation, $P_n = \sum_{k=0}^{n} |\pi_k\rangle N_k^{-1} \langle \pi_k|$ is just the projector onto polynomials with degree not higher than n. Obviously

$$\langle \pi_k, P_n(\cdot, 0) \rangle = p_n, \tag{A.19}$$

which by (A.8) identifies $P_n(w,0) = N_n^{-1} \pi_n^*(w)$. For $w = 0$ this implies

$$P_n(0,0) = \sum_{k=0}^{n} N_k^{-1} |p_k|^2 = N_n^{-1}, \tag{A.20}$$

yielding (A.10).

To obtain the Christoffel-Darboux formula (A.11) remember that $P_{n-1}(w,z)$ is the projector onto polynomials of degree less than n. On the other hand we have for an arbitrary polynomial $p(z)$ of degree less than n, with $z = e^{i\theta}$,

$$\begin{aligned} &\int_{-\pi}^{\pi} \frac{\pi_n^*(w)\overline{\pi_n^*(z)} - \pi_n(w)\overline{\pi_n(z)}}{1 - w\overline{z}} p(z) f(\theta) d\theta \\ &= p(w) \int_{-\pi}^{\pi} \frac{\pi_n^*(w)\overline{\pi_n^*(z)} - \pi_n(w)\overline{\pi_n(z)}}{1 - w\overline{z}} f(\theta) d\theta \\ &\quad + \int_{-\pi}^{\pi} \left(\pi_n^*(w)\overline{\pi_n^*(z)} - \pi_n(w)\overline{\pi_n(z)} \right) \frac{p(z) - p(w)}{1 - w\overline{z}} f(\theta) d\theta. \end{aligned} \tag{A.21}$$

The last integral vanishes, since writing $p(z) - p(w) = (z-w)r(z)$ one has $\langle \pi_n^*, zr(z)\rangle = 0$ by (A.7) and $\langle \pi_n, zr(z)\rangle = 0$ by (A.5). This shows that the quotient of $(1-w\overline{z})^{-1}\big(\pi_n^*(w)\overline{\pi_n^*(z)} - \pi_n(w)\overline{\pi_n(z)}\big)$ and $P_{n-1}(w,z)$ is independent of z. The same argument for $\overline{p(w)}$ with w and z interchanged implies that it is also independent of z. To get the proportionality factor c we set $w = z = 0$ and obtain by (A.20)

$$c = \frac{1-|p_n|^2}{(N_{n-1})^{-1}} = N_n, \tag{A.22}$$

which proves (A.11).

If we compare only the highest order $\overline{b^n}$ in (A.11) we get

$$-a\tfrac{N_n}{N_{n-1}}\pi_{n-1}(a) = \pi_n^*(a)\overline{p_n} - \pi_n(a). \tag{A.23}$$

Taking the reciprocal polynomials and solving for $\pi_n^*(a)$ one obtains (A.12). (A.13) is just the reciprocal of (A.12). Finally (A.14) and (A.15) follow by induction from (A.12) and (A.13) with $z = \pm 1$ while noting that $\pi_n(1) = \pi_n^*(1)$ and $\pi_n(-1) = (-1)^n\pi_n^*(1)$. $\square$

For the special weight function $f(\theta) = e^{-2v\,\cos(\theta)}$ one can derive a nonlinear recursion relation for the p_n's, and a system of linear differential equations for $\pi_n(z), \pi_n^*(z)$. The recursion relation for p_n turns out to be the discrete Painlevé II equation. It has been derived in the context of orthogonal polynomials for the first time in [94], and later on more or less independently in [62, 123, 9, 24]. The differential equations for the orthogonal polynomials appear here for the first time in the given explicit form. They are implicitly derived in [9] in the context of the Riemann-Hilbert formulation of orthogonal polynomials.

Proposition 1.2 *For the orthogonal polynomials with respect to the weight function $f(\theta) = e^{-2v\,\cos(\theta)}$ one has*

$$p_{n+1} = -\frac{\frac{n}{v}p_n}{1-p_n^2} - p_{n-1} \quad \text{for } n > 0. \tag{A.24}$$

The orthogonal polynomials satisfy the differential equations

$$\begin{aligned} \pi_n{}'(z) &= \big(\tfrac{n-p_{n+1}p_n v}{z} + \tfrac{v}{z^2}\big)\pi_n(z) + \big(\tfrac{p_{n+1}v}{z} - \tfrac{p_n v}{z^2}\big)\pi_n^*(z) \\ \pi_n^{*\prime}(z) &= \big(-\tfrac{p_{n+1}v}{z} + p_n v\big)\pi_n(z) + \big(-v + \tfrac{p_{n+1}p_n v}{z}\big)\pi_n^*(z). \end{aligned} \tag{A.25}$$

Proof: Following essentially [94] we have, still for a general differentiable weight

function,

$$\begin{aligned} n(N_n - N_{n-1}) &= N_n + (n-1)N_n - nN_{n-1} \\ &= \langle z\,\pi_{n-1}, \pi_n\rangle + \langle z^2\pi'_{n-1}, \pi_n\rangle - \langle \pi_{n-1}, \pi'_n\rangle \\ &= -\oint z\tfrac{d}{dz}\big(z^{-1}\overline{\pi_{n-1}}(z^{-1})\pi_n(z)\big)\frac{F(z)}{2\pi i z}dz \\ &= \oint \overline{\pi_{n-1}}(z^{-1})\pi_n(z)\frac{F'(z)}{F(z)}\frac{F(z)}{2\pi i z}dz. \end{aligned} \tag{A.26}$$

We are interested here in the special case when $f(\theta) = e^{2v\cos\theta}$, equivalently $F(z) = e^{v(z+z^{-1})}$. Its log-derivative is $v(1-z^{-2})$ and we obtain

$$N_n - N_{n-1} = -\tfrac{v}{n}\langle z^2\pi_{n-1}, \pi_n\rangle. \tag{A.27}$$

Note that now all the polynomials are real, thus we can omit the conjugation bars. We write $\pi_n(z) = z^n + a_n z^{n-1} + \cdots$. Order z^{n-1} in (A.12) yields the recursion relation $a_n = a_{n-1} + p_n\, p_{n-1}$, and we obtain

$$\begin{aligned} \tfrac{n}{v}(N_n - N_{n-1}) &= -\langle z^{n+1} + a_{n-1}z^n, \pi_n\rangle. \\ &= -\langle \pi_{n+1} - a_{n+1}z^n, \pi_n\rangle - a_{n-1}N_n \\ &= (a_{n+1} - a_{n-1})N_n \\ &= (p_{n+1}p_n + p_n p_{n-1})N_n. \end{aligned} \tag{A.28}$$

Since $N_n = N_{n-1}(1-p_n^2)$ we arrive at (A.24).

Proving eqs. (A.25) is an elementary but tedious induction. One just has to check that they are valid for $n = 0$ and that

$$\begin{aligned} &\pi'_n - (\pi_{n-1} + z\pi'_{n-1} + p_n\pi^{*\prime}_{n-1}) \\ &\quad = z^{-1}\big(np_n + (1-p_n^2)(p_{n+1}+p_{n-1})v\big)\pi^*_{n-1} = 0, \\ &\pi^{*\prime}_n - (p_n\pi_{n-1} + zp_n\pi'_{n-1} + \pi^{*\prime}_{n-1}) \\ &\quad = -\big(np_n + (1-p_n^2)(p_{n+1}+p_{n-1})v\big)\pi_{n-1} = 0, \end{aligned} \tag{A.29}$$

when applying (A.25) for n and $n-1$. □

APPENDIX B

Taylor expansion method for Painlevé II

The key object in determining the scaling function $g_1^{\text{dyn}}(y) = g(y)$, of Section 3.3 is the Hastings-McLeod solution [61] to Painlevé II, $u(s)$, which is the unique solution to

$$u'' = 2u^3 + su \tag{B.1}$$

with asymptotic boundary conditions (3.10) and (3.11). Tracy and Widom [121, 123] integrate (B.1) numerically with conventional differential equation solvers using the known asymptotics at $s = \pm\infty$. The precision achieved with this technique does not suffice for our purposes, since we need $u(s)$ as starting values (3.76) for the differential equations (3.75). We develop here a different method to obtain $u(s)$, in principle with arbitrary precision. Next the functions $a(s, y)$ and $b(s, y)$ have to be determined, which directly leads to values for the distribution functions $F_y(s)$. They have to be further integrated with respect to s in order to obtain their variance, which is the desired scaling function $g(y)$. The Taylor expansion method to be explained intrinsically produces not only function values at a point but also higher derivatives. Therefore we obtain $f(y)$ not by numerically differentiating $g(y)$ but rather by direct calculation via the knowledge of $\partial_y^2 F_y(s)$.

In a first step, to obtain reliable approximations to the Hastings-McLeod solution, we need a good guess of $u(s)$ at some finite s_0 by using asymptotic expansions around $\pm\infty$. It turns out that the left asymptotics is not well suited to this purpose, since, when integrated along s, the error of an approximation from an optimally truncated asymptotic power series at large negative s always blows up to order 1 near $s = 0$ on an exponential scale. Approximations of the right asymptotics on the other hand allow a, in principle, arbitrary precision on any given finite interval.

For $s \to \infty$ the deviations of $u(s)$ from the Airy function can be expanded in an alternating asymptotic power series with exponentially small prefactor,

$$u_{\text{right},n}(s) = -\text{Ai}(s) - \frac{e^{-3\zeta}}{32\pi^{3/2}s^{7/4}} \sum_{k=0}^{n} \frac{(-1)^k a_k}{\zeta^k}, \tag{B.2}$$

with the abbreviation $\zeta = \frac{2}{3}s^{3/2}$. The coefficients are $a_0 = 1$, $a_1 = \frac{23}{24}$, $a_2 = \frac{1493}{1152}$, ..., and can be obtained via the recursion relation

$$a_n = \mathrm{Ai}_n^{(3)} + \tfrac{3}{4}n\,a_{n-1} - \tfrac{1}{8}(n-\tfrac{1}{6})(n-\tfrac{5}{6})a_{n-2} \quad \text{for } n \geq 0 \tag{B.3}$$

with initial conditions $a_{-1} = a_{-2} = 0$.

$$\mathrm{Ai}_n^{(3)} = \sum_{0\leq k\leq l\leq n} \mathrm{Ai}_{n-l}\mathrm{Ai}_{l-k}\mathrm{Ai}_k. \tag{B.4}$$

are the coefficients in the asymptotic expansion of $\mathrm{Ai}(x)^3$ and

$$\mathrm{Ai}_n = \frac{(6n-1)(6n-5)}{72n}\mathrm{Ai}_{n-1}, \qquad \mathrm{Ai}_0 = 1 \tag{B.5}$$

are the coefficients of the asymptotic expansion of the Airy function itself [1],

$$\mathrm{Ai}(s) \sim \frac{e^{-\zeta}}{2\sqrt{\pi}s^{1/4}} \sum_{n\geq 0} \frac{(-1)^n}{\zeta^n}\mathrm{Ai}_n. \tag{B.6}$$

Empirically we observe that for $s_0 \gg 0$ the optimal truncation in (B.2) is $n \approx \frac{4}{3}s_0^{3/2}$ leading to an exponentially improved precision

$$\left|\frac{u_{\text{right},n}(s_0) - u(s_0)}{u(s_0)}\right| \approx \exp(-\tfrac{8}{3}s_0^{3/2}). \tag{B.7}$$

We use the notions accuracy for the absolute error of an approximation and precision for its relative error. Linear perturbation around the true solution tells us that the precision of the approximate solution decreases rapidly when integrating in the positive direction, such that $u_{\text{right},n}(s)/u(s) - 1$ is of order one at $s \approx 3^{2/3}s_0 = 2.08s_0$, but the accuracy is still $\approx \exp(-2s_0^{3/2})$. In the negative direction the accuracy decreases but the precision of the approximation stays roughly constant down to $s = 0$. For negative values of s, accuracy and precision are similar, since $u(s)$ is approximately of order 1. Accuracy is lost completely at about $-2s_0$, but at $-2^{1/3}s_0 = -1.26s_0$ still half of the accuracy, $\exp(-1.33s_0^{3/2})$, is retained. What remains is to integrate (B.1) with initial values $u(s_0) = u_{\text{right},n}(s_0)$, $u'(s_0) = u'_{\text{right},n}(s_0)$, $n = [\frac{4}{3}s_0^{3/2}]$.

To solve initial value problems for ordinary differential equations highly sophisticated iteration schemes are available, like Runge-Kutta, Adams-Bashford and multi-step methods. For arbitrary high (but fixed) precision results, all these methods become ineffective, since the step size is a decreasing function of the required precision goal for the solution and tends to become ineffectively small. The only remaining choice is to Taylor expand the solution at a given point. The step

size is limited by the radius of convergence only and the precision is controlled by the error made in truncating the Taylor series at some order, compare [17] for a thorough discussion.

$u(s)$ is expanded at s_0 as

$$u(s) = \sum_{n\geq 0} u_n (s - s_0)^n. \tag{B.8}$$

For the Painlevé II equation the expansion coefficients u_n at s_0 are determined by $u_0 = u(s_0)$, $u_1 = u'(s_0)$ and

$$u_{n+2} = \frac{2u_n^{(3)} + s_0\, u_n + u_{n-1}}{(n+2)(n+1)}, \tag{B.9}$$

where $u_n^{(k)} = \sum_{j=0}^{n} u_{n-j} u_j^{(k-1)}$ are the expansion coefficients of $u(s)^k$ at s_0, $u_n^{(1)} = u_n$. We include the factorial into the expansion coefficients instead of taking the bare Taylor coefficients, in order to reduce the workload from multiplications by binomials when multiplying two expansions numerically.

Numerically we find that the Hastings-McLeod solution does not have any pole in a strip $|\mathrm{Im}(s)| < 2.9$. To have a safety margin we choose a step size one for the extrapolation of the expansion (B.8).

We take the starting values $u(s_0)$, $u'(s_0)$ from (B.2) at $s_0 = 100$. The coefficients of the functions $U(s)$, $V(s)$, see (3.15) and (3.76), when expanded around s_0 are given by

$$U_{n+1} = \frac{u_n}{n+1}, \quad V_{n+2} = \frac{u_n^{(2)}}{(n+2)(n+1)}, \quad n \geq 0, \tag{B.10}$$

and $V_1 = u_0^4 - u_1^2 + s_0 u_0^2$, leaving unspecified the yet unknown integration constants U_0 and V_0. By means of the recursion relation (B.9) one determines the values of u, u', U, and V at $s = s_0 \pm 1$, with these new values at $s = s_0 \pm 2$ and so on. The precision of the integration is in principle only limited by the error in the initial conditions at s_0. In practice the numerical errors from iterating (B.9) and from truncating (B.8) are easily controlled such that they can be neglected compared to the initial uncertainty. The precision of the approximated values is of order 1 at $s = 200$ (with an accuracy of $\approx 10^{-870}$) and we a posteriori assign to $U(s_0)$ and $V(s_0)$ values, such that $U(200) = V(200) = 0$. The arithmetic computing is done with the C++-based multiprecision package `MPFUN++` [31]. At the end of this first step we have at our disposal the values for u, u', U, V at the integers in the interval $[-20, 200]$. For the convenience of the interested reader let us just

state the results at $s = 0$ up to 50 digits,

$$\begin{aligned} u(0) &= \texttt{-0.36706155154807842774779211317561096151219205361 3139}, \\ u'(0) &= \texttt{0.29537210544755005455700704731023798822723379873 5629}, \\ U(0) &= \texttt{0.33696069793055139359788442696096484388599388662 8226}, \\ V(0) &= \texttt{0.03110598530631235366595910087756700056422416895478 38}, \end{aligned}$$

which might be used as starting values for a quick conventional integration of Painlevé II to reproduce parts of our results with much less effort but also less precision.

The next step is to determine $a(s,y)$, $b(s,y)$ at $s_0 \in \{-20,\ldots,200\}$ in the interval $y \in [-9,9]$ employing (3.75) and (3.76). Setting

$$\begin{aligned} a(s,y) &= \sum_{m,n\geq 0} a_{m,n}(s-s_0)^m(y-y_0)^n, \\ b(s,y) &= \sum_{m,n\geq 0} b_{m,n}(s-s_0)^m(y-y_0)^n, \end{aligned} \tag{B.11}$$

(3.75) becomes a recursion relation for the expansion coefficients,

$$\begin{aligned} a_{m,n+1} &= \frac{1}{n+1}\sum_{k=0}^{m}\big(u_k^{(2)}a_{m-k,n} - (k+1)u_{k+1}b_{m-k,n} - u_k b_{m-k,n-1}\big), \\ b_{m,n+1} &= \frac{1}{n+1}\Big(b_{m,n-2} - b_{m-1,n} \\ &\quad + \sum_{k=0}^{m}\big(-u_k^{(2)}b_{m-k,n} + (k+1)u_{k+1}a_{m-k,n} - u_k a_{m-k,n-1}\big)\Big), \end{aligned} \tag{B.12}$$

$n \geq 0$, allowing one to determine $a_{0,n}$, $b_{0,n}$, $n \geq 0$ upon the knowledge of $a_{0,0}$, $b_{0,0}$. We integrate along $\pm y$ with an extrapolation step size of $\frac{1}{8}$. From (3.74) one obtains the recursions

$$\begin{aligned} a_{m+1,n} &= \frac{1}{m+1}\sum_{k=0}^{m} u_k b_{m-k,n} \\ b_{m+1,n} &= \frac{1}{m+1}\Big(-b_{m,n-1} + \sum_{k=0}^{m} u_k a_{m-k,n}\Big). \end{aligned} \tag{B.13}$$

The expansion coefficients $g_{m,n}$ of $g(s,y)$ at (s_0,y_0), are determined from (3.77) as

$$g_{m,n} = (n+1)\big(a^-_{m,n}a_{m,n+1} - b^-_{m,n}b_{m,n+1}\big) \tag{B.14}$$

where $a^-_{m,n}$, $b^-_{m,n}$ are the corresponding expansion coefficients of a and b at $(s_0, -y_0)$.

To finally determine $g(y)$ and its derivatives we write

$$\begin{aligned} g^{(n)}(y_0) &= \frac{d^n}{dy_0^n} \sum_{s_0 \in \mathbb{Z}} \int_{s_0}^{s_0+1} (s - y_0^2)^2 \frac{d^2}{ds^2} \big(g(s, y_0) F_{\text{GUE}}(s) \big) ds \\ &= \sum_{s_0 \in \mathbb{Z}} n! \sum_{m \geq 1} c_{m,n}. \end{aligned} \tag{B.15}$$

$c_{m,n}$ are the expansion coefficients of $(s, y) \mapsto \int_{s_0}^{s} (r - y^2)^2 \frac{d^2}{dr^2} \big(g(r, y) F_{\text{GUE}}(r) \big) dr$ at (s_0, y_0),

$$c_{m,n} = (m-2)(gF)_{m-1,n} - 2m(gF)_{m,n-2} + \tfrac{m(m+1)}{m-1} (gF)_{m+1,n-4}. \tag{B.16}$$

Here

$$(gF)_{m,n} = \sum_{k=0}^{m} F_k g_{m-k,n} \tag{B.17}$$

are the expansion coefficients of $g(s, y) F_{\text{GUE}}(s)$ and $F_n = -\sum_{k=1}^{n} \frac{k}{n} V_k F_{n-k}$ are the expansion coefficients of F_{GUE}. Numerically the sum over s_0 in (B.15) is truncated to values inside $[-15, 200]$, since outside contributions turn out to be negligible at the chosen precision goal. After accomplishing this program we keep values for $g(y)$ at $y \in \frac{1}{128}\mathbb{Z} \cap [-9, 9]$ and for $g^{(n)}(y)$, $n = 0, \ldots, 4$, at $y \in \frac{1}{8}\mathbb{Z} \cap [-9, 9]$ with an accuracy of about 100 digits (a table in ASCII format is available online at [103]). For interpolating these values we deliberately used the `Interpolation`-function of the Mathematica® package yielding best results due to the high precision data with an interpolation order of 57.

BIBLIOGRAPHY

[1] M. Abramowitz and I. A. Stegun, editors. *Pocketbook of Mathematical Functions*. Verlag Harri Deutsch, Thun - Frankfurt am Main, 1984. 86, 128

[2] T. Ala-Nissila. Comment on "Upper critical dimension of the Kardar-Parisi-Zhang equation". *Phys. Rev. Lett.*, 80(4):887–887, 1998. 20, 120

[3] T. Ala-Nissila, T. Hjelt, J. M. Kosterlitz, and O. Venäläinen. Scaling exponents for kinetic roughening in higher dimensions. *J. Stat. Phys.*, 72(1/2):207–225, 1993. 4, 23, 23, 119, 120, 120

[4] T. Ala-Nissila and O. Venäläinen. Scaling exponents for driven two-dimensional surface growth. *J. Stat. Phys.*, 76(3/4):1083–1088, 1994. 4, 119

[5] D. Aldous and P. Diaconis. Hammersley's interacting particle process and longest increasing subsequences. *Probab. Th. Rel. Fields*, 103:199–213, 1995. 34

[6] D. Aldous and P. Diaconis. Longest increasing subsequences: from patience sorting to the Baik-Deift-Johansson theorem. *Bull. Amer. Math. Soc.*, 36:413, 1999. 38, 40, 40

[7] J. Amar and F. Family. Universality in surface growth: Scaling functions and amplitude ratios. *Phys. Rev. A*, 45(8):5378–5393, 1992. 4, 23

[8] S. Assing. A pregenerator for Burgers equation forced by conservative noise. *Commun. Math. Phys.*, 225:611–623, 2002. 26

[9] J. Baik. Riemann-Hilbert problems for last passage percolation. *math.PR/0107079*, 2001. 41, 50, 52, 53, 124, 124

[10] J. Baik, P. Deift, and K. Johansson. On the distribution of the length of the longest increasing subsequence of random permutations. *J. Amer. Math. Soc.*, 12:1119, 1999. 5, 38, 39, 40, 42

[11] J. Baik and E. M. Rains. Limiting distributions for a polynuclear growth model with external sources. *J. Stat. Phys.*, 100(3–4):523–541, 2000. 47, 50, 53, 53, 72

[12] J. Baik and E. M. Rains. Algebraic aspects of increasing subsequences. *Duke Math. J.*, 109(1):1–65, 2001. 40, 44, 44, 45, 50, 53, 53, 67

[13] J. Baik and E. M. Rains. The asymptotics of monotone subsequences of involutions. *Duke Math. J.*, 109(2):205–281, 2001. 45, 53

[14] J. Baik and E. M. Rains. Symmetrized random permutations. In P. Bleher and A. Its, editors, *Random Matrix Models and Their Applications*, volume 40 of *MSRI*, pages 1–19, 2001. 43, 44, 45

[15] P. Bak, C. Tang, and K. Wiesenfeld. Self-organized criticality: An explanation of the $1/f$ noise. *Phys. Rev. Lett.*, 59:381–384, 1987. 2

[16] A. L. Barabási and H. E. Stanley. *Fractal concepts in surface growth*. Cambridge University Press, Cambridge, 1995. 2

[17] D. Barton, I. M. Willers, and R. V. M. Zahar. Taylor series methods for ordinary differential equations - An evaluation. In J. Rice, editor, *Mathematical Software*, pages 369–390. Academic Press, New York, 1971. 129

[18] H. v. Beijeren, R. Kutner, and H. Spohn. Excess noise for driven diffusive systems. *Phys. Rev. Lett.*, 54(18):2026–2029, 1985. 4, 47, 55

[19] C. Bennett, M. Büttiker, R. Landauer, and H. Thomas. Kinematics of the forced and overdamped Sine-Gordon soliton gas. *J. Stat. Phys.*, 24(3):419–442, 1981. 32

[20] L. Bertini and G. Giacomin. Stochastic Burgers and KPZ equations from particle systems. *Commun. Math. Phys.*, 183:571–607, 1997. 26

[21] J. Bhattacharjee. Upper critical dimension of the Kardar-Parisi-Zhang equation. *J. Phys. A: Math. Gen.*, 31(5):L93–L96, 1998. 20

[22] B. Bollobás and W. P. The longest chain among random points in Euclidean space. *Proc. Amer. Math. Soc.*, 103(2):347–353, 1988. 106, 114

[23] E. Bolthausen. A note on the diffusion of directed polymers in a random environment. *Comm. Math. Phys.*, 123(4):529–534, 1989. 20

[24] A. Borodin. Discrete gap probabilities and discrete Painlevé equations. *Duke Math. J.*, 117(3):489–542, 2003. 41, 124

[25] A. Borodin and A. Okounkov. A Fredholm determinant formula for Toeplitz determinants. *Integr. Equat. Oper. Th.*, 37(4):386–396, 2000. 85

[26] O. Bratteli and D. Robinson. *Operator Algebras and Quantum Statistical Mechanics 2.* Springer-Verlag, New York, 1997. 82

[27] E. Breimer, M. Goldberg, B. Kolstad, and M. Magdon-Ismail. On the height of a random set of points in a d-dimensional unit cube. *Exp. Math.*, 10(4):583–597, 2001. 116

[28] C. Castellano, A. Gabrielli, M. Marsili, M. Munoz, and L. Pietronero. High dimensional behavior of the Kardar-Parisi-Zhang growth dynamics. *Phys. Rev. E*, 58(5):R5209–R5212, 1998. 120

[29] C. Castellano, M. Marsili, M. A. Munoz, and L. Pietronero. Scale invariant dynamics of surface growth. *Phys. Rev. E*, 59:6460–6475, 1999. 4, 23

[30] C. Castellano, M. Marsili, and L. Pietronero. Non-perturbative renormalization of the KPZ growth dynamics. *Phys. Rev. Lett.*, 80:3527–3530, 1998. 23, 23

[31] S. Chatterjee. MPFUN++, a C++-based multiprecision system. `http://www.cs.unc.edu/Research/HARPOON/mpfun++/`, 2000. 129

[32] C.-S. Chin and M. den Nijs. Stationary state skewness in two dimensional Kardar-Parisi-Zhang type growth. *Phys. Rev. E*, 59(3):2633–2641, 1999. 20, 113, 119

[33] F. Colaiori and M. A. Moore. Stretched exponential relaxation in the mode-coupling theory for the Kardar-Parisi-Zhang equation. *Phys. Rev. E*, 63:057103, 2001. 55, 56

[34] F. Colaiori and M. A. Moore. Upper critical dimension, dynamic exponent, and scaling functions in the mode-coupling theory for the Kardar-Parisi-Zhang equation. *Phys. Rev. Lett.*, 86:3946–3949, 2001. 4, 20, 120

[35] F. Colaiori and M. A. Moore. Numerical solution of the mode-coupling equations for the Kardar-Parisi-Zhang equation in one dimension. *Phys. Rev. E*, 65:017105, 2002. 4, 4, 47, 55, 55, 55, 56

[36] A. De Masi and E. Presutti. *Mathematical methods for hydrodynamic limits*, volume 1501 of *Lecture Notes in Mathematics*. Springer-Verlag, Berlin, 1991. 20

[37] P. A. Deift and X. Zhou. A steepest descent method for oscillatory Riemman-Hilbert problems; asymptotics for the MKdV equation. *Ann. Math.*, 137:295–368, 1993. 42

[38] B. Derrida and C. Appert. Universal large deviation function of the Kardar-Parisi-Zhang equation in one dimension. *J. Stat. Phys.*, 94:1–30, 1999. 4

[39] B. Derrida and J. L. Lebowitz. Exact large deviation function in the asymmetric exclusion process. *Phys. Rev. Lett.*, 80:209–213, 1998. 4

[40] D. Dhar. An exactly solved model for interfacial growth. *Phase Transitions*, 9(1):51, 1987. 4, 19

[41] F. J. Dyson. A Brownian-motion model for the eigenvalues of random matrices. *J. Math. Phys.*, 3:1191–1198, 1962. 76

[42] S. F. Edwards and D. R. Wilkinson. The surface statistics of a granular aggregate. *Proc. R. Soc. London, Ser. A*, 381:17, 1982. 3, 25

[43] F. Family and T. Vicsek, editors. *Dynamics of fractal surfaces*. World Scientific, Singapore, 1991. 2

[44] H. C. Fogedby. Scaling function for the noisy Burgers equation in the soliton approximation. *Europhys. Lett.*, 56(4):492–498, 2001. 4, 4, 47

[45] H. C. Fogedby. Towards a strong coupling theory for the KPZ equation. *Physica A*, 314:182, 2002. 4

[46] D. Forster, D. R. Nelson, and M. J. Stephen. Large-distance and long-time properties of a randomly stirred fluid. *Phys. Rev. A*, 16:732–749, 1977. 4

[47] F. C. Frank. Nucleation-controlled growth on a one-dimensional growth of finite length. *J. Cryst. Growth*, 22(3):223–236, 1974. 31

[48] E. Frey and U. C. Täuber. Two-loop renormalization-group analysis of the Burgers-Kardar-Parisi-Zhang equation. *Phys. Rev. E*, 50(2):1024–1045, 1994. 4, 24

[49] E. Frey, U. C. Täuber, and T. Hwa. Mode-coupling and renormalization group results for the noisy Burgers equation. *Phys. Rev. E*, 53(5):4424–4438, 1996. 4, 4, 47, 47, 55

[50] D. J. Gates and M. Westcott. Stationary states of crystal growth in three dimensions. *J. Stat. Phys.*, 81:681–715, 1995. 14, 89, 91

[51] I. M. Gessel. Symmetric functions and p-recursiveness. *J. Comb. Theory A*, 53:257–285, 1990. 40

[52] N. Goldenfeld. Kinetics of a model for nucleation-controlled polymer crystal growth. *J. Phys. A*, 17:2807–2821, 1984. 31

[53] J. Gravner, C. A. Tracy, and H. Widom. Limit theorems for height fluctuations in a class of discrete space and time growth model. *J. Stat. Phys.*, 102:1085–1132, 2001. 66

[54] J. Gravner, C. A. Tracy, and H. Widom. Fluctuations in the composite regime of a disordered growth model. *Commun. Math. Phys.*, 229:433–458, 2002. 66

[55] J. Gravner, C. A. Tracy, and H. Widom. A growth model in a random environment. *Ann. Probab.*, 30:1340–1368, 2002. 66, 67

[56] L.-H. Gwa and H. Spohn. Bethe solution for the dynamical-scaling exponent of the noisy Burgers equation. *Phys. Rev. A*, 46:844–854, 1992. 4, 19

[57] L.-H. Gwa and H. Spohn. Six-vertex model, roughened surfaces, and an asymmetric spin Hamiltonian. *Phys. Rev. Lett*, 68:725–728, 1992. 4

[58] T. Halpin-Healy. Directed polymers in random media: probability distributions. *Phys. Rev. A*, 44(6):R3415–R3418, 1991. 23

[59] T. Halpin-Healy and Y.-C. Zhang. Kinetic roughening phenomena, stochastic growth, directed polymers and all that. *Phys. Rep.*, 254:215–414, 1995. 3

[60] J. M. Hammersley. A few seedlings of research. In *Proc. Sixth Berkeley Symp. Math. Statist. and Probability*, volume 1, pages 345–394. University of California Press, 1972. 34, 38

[61] S. P. Hastings and J. B. McLeod. A boundary value problem associated with the second Painlevé transcendent and the Korteweg-de Vries equation. *Arch. Rat. Mech. Anal.*, 73:31–51, 1980. 38, 127

[62] M. Hisakado. Unitary matrix models and Painlevé III. *Mod. Phys. Letts A*, 11:3001–3010, 1996. 41, 124

[63] T. Hwa and E. Frey. Exact scaling function of interface growth dynamics. *Phys. Rev. A*, 44(12):R7873–R7876, 1991. 47, 47

[64] J. Imbrie and T. Spencer. Diffusion of directed polymers in a random environment. *J. Stat. Phys.*, 52(3–4):609–626, 1988. 20

[65] M. E. H. Ismail and N. S. Witte. Discriminants and functional equations for polynomials orthogonal on the unit circle. *J. Approx. Th.*, 110:200–228, 2001. 52

[66] H. Jeong, B. Kahng, and D. Kim. Dynamics of a toom interface in three dimensions. *Phys. Rev. Lett.*, 71(5):747–749, 1993. 89

[67] K. Johansson. Discrete orthogonal polynomial ensembles and the plancherel measure. *Commun. Math. Phys.*, 209(2):437–476, 2000. 65

[68] K. Johansson. Shape fluctuations and random matrices. *Comm. Math. Phys.*, 209:437–476, 2000. 5, 19, 61, 62

[69] K. Johansson. Discrete polynuclear growth and determinantal processes. *math.PR/0206208*, 2002. 63, 74, 76, 76, 77

[70] M. Kardar, G. Parisi, and Y. Z. Zhang. Dynamic scaling of growing interfaces. *Phys. Rev. Lett.*, 56:889–892, 1986. 2, 17, 20, 23, 23, 24, 89

[71] J. M. Kim. Phase transition of directed polymer in random potentials on 4+1 dimensions. *Phys. A*, 270:335–341, 1999. 4, 23

[72] J. M. Kim, M. A. Moore, and A. J. Bray. Zero-temperature directed polymers in a random potential. *Phys. Rev. A*, 44(4):2345–2351, 1991. 4, 23

[73] C. Kipnis and C. Landim. *Scaling limits of interacting particle systems*, volume 320 of *Grundlehren der mathematischen Wissenschaften*. Springer-Verlag, Berlin, 1999. 20

[74] J. Krug. Scaling relation for a growing interface. *Phys. Rev. A*, 36(11):5465–5466, 1987. 22

[75] J. Krug. Origins of scale invariance in growth processes. *Adv. Phys.*, 46:139–282, 1997. 3

[76] J. Krug and J. Garcia. Asymmetric particle systems on $\mathbb{R}$. *J. Stat. Phys.*, 99(1–2):31–55, 2000. 34

[77] J. Krug, P. Meakin, and T. Halpin-Healy. Amplitude universality for driven interfaces and directed polymers in random media. *Phys. Rev. A*, 45(2):638–653, 1992. 4, 4, 23, 43

[78] J. Krug and H. Spohn. Kinetic roughening of growing surfaces. In C. Godrèche, editor, *Solids far from equilibrium*. Cambridge University Press, Cambridge, 1991. 3, 12, 19, 22, 23

[79] M. Lässig. On the renormalization of the Kardar-Parisi-Zhang equation. *Nucl. Phys. B*, 448:559–574, 1995. 4, 19, 24

[80] M. Lässig. On growth, disorder, and field theory. *J. Phys. C*, 10(44):9905–9950, 1998. 3, 4, 20, 23, 23, 24, 116, 119, 120

[81] M. Lässig and H. Kinzelbach. Upper critical dimension of the Kardar-Parisi-Zhang equation. *Phys. Rev. Lett.*, 78(5):903–906, 1997. 20, 23, 25, 120

[82] M. Liggett, Thomas. *Interacting particle systems*. Springer Verlag, Berlin, Heidelberg, New York, 1985. 70

[83] M. Liggett, Thomas. *Stochastic interacting systems: contact, voter and exclusion processes*. Springer Verlag, Berlin, Heidelberg, New York, 1999. 70

[84] B. Logan and L. Shepp. A variational problem for random young tableaus. *Advances in Math.*, 26:206–222, 1977. 38

[85] E. Marinari, A. Pagnani, and G. Parisi. Critical exponents of the KPZ equation via multi-surface coding numerical simulations. *J. Phys. A: Math. Gen.*, 33(46):8181–8192, 2000. 4, 119, 120, 120

[86] E. Marinari, A. Pagnani, G. Parisi, and Z. Rácz. Width distributions and the upper critical dimension of Kardar-Parisi-Zhang interfaces. *Phys. Rev. E*, 65:026136, 2002. 4, 4, 20, 120

[87] P. Meakin. The growth of rough surfaces and interfaces. *Phys. Rep.*, 235:189–289, 1993. 3

[88] P. Meakin. *Fractals, scaling and growth far from equilibrium*. Number 5 in Cambridge Nonlinear Science Series. Cambridge University Press, Cambridge, 1998. 2

[89] E. Medina, T. Hwa, M. Kardar, and Y.-C. Zhang. Burgers equation with correlated noise: Renormalization-group analysis and applications to directed polymers and interface growth. *Phys. Rev. A*, 39(3053–3075), 1989. 22

[90] M. L. Mehta. *Random matrices, 2nd ed.* Academic Press, San Diego, 1991. 38

[91] M. Myllys, J. Maunuksela, M. Alava, J. Merikoski, and J. Timonen. Kinetic roughening in slow combustion of paper. *Phys. Rev. E*, 64(036101):1–12, 2001. 47

[92] T. Nattermann and L.-H. Tang. Kinetic surface roughening. I. The Kardar-Parisi-Zhang equation in the weak coupling regime. *Phys. Rev. A*, 45(10):7156–7161, 1992. 3, 25

[93] G. Parisi. *Statistical field theory*. Addison Wesley, New York, 1988. 3

[94] V. Periwal and D. Shevitz. Unitary-matrix models as exactly solvable string theories. *Phys. Rev. Lett.*, 64(12):1326–1329, 1990. 41, 124, 124

[95] M. Piza. Directed polymers in a random environment: some results on fluctuations. *J. Stat. Phys.*, 89(3–4):581–603, 1997. 20

[96] M. Plischke, Z. Rácz, and D. Liu. Time-reversal invariance and universality of two-dimensional growth models. *Phys. Rev. B*, 35(7):3485–3495, 1986. 29

[97] M. Prähofer and H. Spohn. An exactly solved model of three dimensional surface growth in the anisotropic KPZ regime. *J. Stat. Phys.*, 88:999, 1997. 7, 14, 94, 98, 99, 101

[98] M. Prähofer and H. Spohn. Statistical self-similarity of one-dimensional growth processes. *Physica A*, 279(1–4):342–352, 2000. 7, 40

[99] M. Prähofer and H. Spohn. Universal distributions for growth processes in one dimension and random matrices. *Phys. Rev. Lett.*, 84(21):4882–4885, 2000. 5, 7, 43, 47

[100] M. Prähofer and H. Spohn. Current fluctuations for the totally asymmetric simple exclusion process. In S. Vladas, editor, *In and out of equilibrium*, volume 51 of *Progress in Probability*, pages 185–204. Birkhauser Boston, 2002. 7, 74

[101] M. Prähofer and H. Spohn. Exact scaling functions for one-dimensional stationary KPZ growth. *cond-mat/0212519*, 2002. 7

[102] M. Prähofer and H. Spohn. Scale invariance of the PNG droplet and the Airy process. *J. Stat. Phys.*, 108(5–6):1071–1106, 2002. iii, iv, 7, 22, 63, 76, 76, 77, 81, 82, 83, 87, 87

[103] M. Prähofer and H. Spohn. The scaling function $g(y)$. http://www-m5.ma.tum.de/KPZ/, 2002. 131

[104] E. M. Rains. Increasing subsequences and the classical groups. *Electron. J. Combin.*, 5(1):R12, 1998. 40, 44

[105] E. M. Rains. A mean identity for longest increasing subsequence problems. *math.CO/0004082*, 2000. 51

[106] R. Rajesh and D. Dhar. An exactly solvable anisotropic directed percolation model in three dimensions. *Phys. Rev. Lett.*, 81(8):1646–1649, 1998. 5, 59, 60, 70

[107] J. T. Robinson. The k-d-b-tree: A search structure for large multidimensional dynamic indexes. In Y. E. Lien, editor, *Proceedings of the 1981 ACM SIGMOD International Conference on Management of Data, Ann Arbor, Michigan, April 29 - May 1, 1981*, pages 10–18. ACM Press, 1981. 107

[108] H. Rost. Non-equilibrium behavior of a many particle system: density profile and local equilibrium. *Z. Wahrsch. Verw. Gebiete*, 58:41, 1981. 59

[109] P. G. Saffman and G. I. Taylor. The penetration of a fluid into a medium of Hele-Shaw cell containing a more viscous liquid. *Proc. R. Soc. London, Ser. A*, 245:312–329, 1958. 2

[110] M. Schreckenberg, A. Schadschneider, K. Nagel, and N. Ito. Discrete stochastic models for traffic flow. *Phys. Rev. E*, 51(4):2939–2949, 1995. 63, 70

[111] T. Seppäläinen. A microscopic model for the Burgers equation and longest increasing subsequences. *Electronic J. Prob.*, 1(5):1–51, 1996. 34

[112] T. Seppäläinen. Hydrodynamic scaling, convex duality, and asymptotic shapes of growth models. *Markov Process. Related Fields*, 4:1–26, 1998. 20, 34

[113] T. Seppäläinen. Diffusive fluctuations for one-dimensional totally asymmetric interacting random dynamics. *Commun. Math. Phys.*, 229(1):141–182, 2002. 34, 35

[114] A. Soshnikov. Determinantal random point fields. *Russ. Math. Surv.*, 55:923–975, 2000. 83

[115] T. Spencer. A mathematical approach to universality in two dimensions. *Physica A*, 279(1-4):250–259, 2000. 5

[116] H. Spohn. *Large scale dynamics of interacting particles*. Springer-Verlag, Heidelberg und Berlin, 1991. 20

[117] H. Spohn. Interface motion in models with stochastic dynamics. *J. Stat. Phys.*, 71:1081–1132, 1993. 16

[118] G. Szegö. *Orthogonal polynomials*. American Mathematical Society Providence, Rhode Island, 1967. 41, 41, 122

[119] L.-H. Tang. Steady–state scaling function of the (1+1)–dimensional single–step model. *J. Stat. Phys.*, 67:819–826, 1992. 4, 47, 47

[120] L.-H. Tang, B. M. Forrest, and D. E. Wolf. Kinetic surface roughening. II. Hypercube stacking models. *Phys. Rev. A*, 45(10):7162–7179, 1992. 4, 23, 23, 28, 30, 30, 62, 119, 120

[121] C. A. Tracy and H. Widom. Level spacing distribution and the Airy kernel. *Commun. Math. Phys.*, 159:151–174, 1994. 38, 76, 127

[122] C. A. Tracy and H. Widom. On orthogonal and symplectic matrix ensembles. *Commun. Math. Phys.*, 177:727–754, 1996. 43, 44, 45

[123] C. A. Tracy and H. Widom. private communication, 1999. 41, 124, 127

[124] S. M. Ulam. *Modern Mathematics for the Engineer*, ed. E. F. Beckenbach, volume II, chapter 11, pages 261–277. McGraw-Hill, New York, Toronto, London, 1961. 36, 106

[125] A. M. Vershik and S. V. Kerov. Asymptotics of the plancherel measure of the symmetric group and the limiting form of Young tables. *Soviet Math. Dokl.*, 18:527–531, 1977. 38

[126] T. Vicsek. *Fractal growth phenomena, 2nd edition*. World Scientific, Singapore, 1992. 2

[127] G. Viennot. Une forme géométrique de la correspondence de Robinson-Schensted. In D. Foata, editor, *Combinatoire et représentation du groupe symétrique*, volume 579 of *Lecture Notes in Mathematics*, pages 29–58. Springer-Verlag, Berlin, 1977. 75

[128] W. Werner. Random planar curves and Schramm-Loewner evolutions. *math.PR/0303354*, 2003. 2

[129] T. A. Witten and L. M. Sander. Diffusion-limited aggregation, a kinetic critical phenomenon. *Phys. Rev. Lett.*, 47:1400–1403, 1981. 2

[130] D. E. Wolf. Kinetic roughening of vicinal surfaces. *Phys. Rev. Lett.*, 67:1783–1786, 1991. 3, 15, 17, 19, 26, 89, 90

[131] T. Wu, B. McCoy, C. Tracy, and E. Barouch. The spin-spin correlation function of the 2-dimensional Ising model: exact results in the scaling region. *Phys. Rev. B*, 13:316–374, 1976. 4

[132] G. Wulff. Zur Frage der Geschwindigkeit des Wachstums und der Auflösung der Kristallflächen. *Z. Kristallogr. Mineral.*, 34:449–530, 1901. 12